UNIVERSITY OF OKLAHOMA

GRADUATE COLLEGE

OPTIMIZING THERMAL CONDUCTIVITY IN FUNCTIONALIZED MACROMOLECULES

A DISSERTATION

SUBMITTED TO THE GRADUATE FACULTY

in partial fulfillment of the requirements for the

Degree of

DOCTOR OF PHILOSOPHY

By

ABDELLAH AIT MOUSSA
Norman, Oklahoma
2012

Downloaded from SHAREOK. Persistent Handle URL: https://hdl.handle.net/11244/320237

OPTIMIZING THERMAL CONDUCTIVITY IN FUNCTIONALIZED MACROMOLECULES

A DISSERTATION APPROVED FOR THE
HOMER L.DODGE DEPARTMENT OF PHYSICS AND ASTRONOMY

BY

Dr. Kieran Mullen, Chair

Dr. John Furneaux

Dr. Dimitrios Papavassiliou

Dr. Greg Parker

Dr. Michael Santos

© Copyright by ABDELLAH AIT MOUSSA 2012
All rights reserved.

To My Wife and Kids

Mikieala. J and Eryka. K Ait Moussa

Acknowledgments

First, I wish to express my gratitude to my research advisor, Professor Kieran Mullen, for teaching me a great deal of Physics, for his guidance and unconditional support during all these years of graduate school, and for being an excellent mentor. I am grateful for having had the opportunity to work with him.

I also wish to thank Professor Alberto Storiolo and his research group in the chemical engineering department at the University of Oklahoma for the numerous discussions, and general advice, in particular I would like to acknowledge the help of Deepthi Konathan for her support and guidance. I wish to also thank Jason Glass and Professor Evan Lemley from the University of Central Oklahoma for their help and support in running the multiple simulations used in this work.

Finally, I am forever indebted to my wife for her understanding, endless patience and encouragement when it was most required.

Table of Contents

Acknowledgments **iv**

Abstract **xv**

Introduction **1**

1 Langevin Equations **8**

1.1 Introduction 8

1.2 Development 9

1.2.1 Classical interpretation of the noise 14

1.2.2 Quantum mechanical interpretation of the noise 20

1.3 Conclusion 26

2 Using Normal Modes to Calculate and Optimize Thermal Conductivity in Functionalized Macromolecules **28**

2.1 Introduction 28

2.2 The Analytical Technique 28

2.2.1 Site Displacement 28

2.2.2 Thermal Heat Flux 33

2.2.3 Participation Ratio 37

2.3 Application 37

2.3.1 One Dimensional Chain 37

2.3.2 Two Dimensional Sheet of Graphene 40

2.3.2.1 Numerical results of thermal heat flux in functionalized graphene 41

2.3.2.2 Effect of changing the length of the chains on the thermal conduction 42

2.4 Conclusion 43

3 Normal Mode Analysis with Thermal Colored Noise 47

3.1 Introduction 47

3.2 Analytical Technique 47

3.2.1 Classical noise 48

3.2.2 Quantum noise 54

3.3 Application 58

3.3.1 One dimensional linear chain 58

3.3.1.1 Heat flux: Classical noise 58

3.3.1.2 Heat flux: Quantum noise 59

3.3.1.3 Heat capacity of the chain 60

3.3.2 Two dimensional Sheet of Graphene 60

3.3.2.1 Heat flux 61

3.3.3 Improving the thermal conductivity of functionalized graphene 62

3.3.3.1 Effect of changing the length of the chains on the thermal conduction 63

3.3.3.2 Effect of branching the chains on the thermal conduction 64

3.3.3.3 Effect of changing the chains site masses and strength of their interactions 65

3.4 Conclusion 68

4 Classical Langevin Equations with Thermal Colored Noise, Numerical Solution 76

4.1 Introduction 76

4.2 Development 76

4.3 Program structure diagram 87

4.4 Application 88
4.4.1 One dimensional linear chain; Classical approximation . . 88
4.4.2 Two Dimensional Sheet of Pristine Graphene 89
4.4.3 Two Dimensional Sheet of functionalized graphene 90
4.5 Conclusion 92

5 Classical Langevin Equations with Time and Space Correlated Noise 96

5.1 Introduction 96
5.2 Development 96
5.2.1 Solving Langevin equations with spatial correlated noise . 108
5.3 Application 112
5.3.1 One dimensional linear chain 112
5.3.2 Two dimensional Sheet of functionalized Graphene 114
5.4 Conclusion 115

6 Conclusion 117

References 119

A Thermal Properties 123

A.1 Flux: White Noise 123
A.2 Flux: Colored Noise 124
A.3 Flux: Space/Time Correlated Noise 125
A.4 Heat Capacity 127

B Force Field 128

B.1 The Tersoff-Brenner potential 128
B.2 The NERD potential 129
B.3 Force Field for perfluoralkanes molecules 132

C Estimating the noise parameters **134**

List of Tables

1 Physical properties 2

3.1 Ratio of the temperature drop across the chain graphene interface $k_B(T_+ - T_-)$ as a function of chain length (N). k_B is the Boltzmann constant, T_+ and T_- are respectively the temperatures of the hot and cold heat bath. 68

3.2 **Configuration (b)**: Ratio of thermal conductance of branched λ_b and unbranched functional groups, λ_{nb}. Br@(branched at), Brsize (branched size), #SPC (number of sites per chain). The subscripts 54 and 96 refer to the size of the graphene sheet 69

3.3 **Configuration (c)**: Ratio of thermal conductance of branched and λ_b and unbranched functional groups λ_{nb}. Br@(branched at), Brsize (branched size), #SPC (number of sites per chain). The subscripts 54 and 96 refer to the size of the graphene sheet 70

3.4 Ratio of the thermal conductances of functionalized graphene with fluorinated alkanes (λ_f) and that of functionalized graphene with alkanes with the same chain length (λ_s). 71

4.1 Ratio of the average kinetic energy $\langle m\ v^2 \rangle$ and $k_B T_+$ as a function of chain length (N), k_B is the Boltzmann constant, T_+ is the temperatures of the hot bath. 92

B.1 TB parameters for Carbon 130

B.2 Intramolecular potential energy parameters 132

B.3 Intramolecular potential energy parameters 133

List of Figures

0.1 Conceptual diagram of single-walled carbon nanotube (SWCNT) (A) and multiwalled carbon nanotube (MWCNT) (B) delivery systems showing typical dimensions of length, width, and separation distance between graphene layers in MWCNTs [28]. 3

0.2 Representative simulation snapshots for GS of 54 carbon atoms in n-octane at 300 K. Red and yellow spheres represent CH_2 and CH_3 groups of n-octane, respectively. Visual inspection suggests that pristine GS (left) aggregate yielding pancake stacks. When the GS are functionalized they remain well dispersed in n-octane after 120 ns of simulation (right) [9] 4

1.1 Pictorial representation of a system described by the Hamiltonian H_s interacting with two heat bath described by the Hamiltonian H_L and H_R. 8

2.1 A pictorial representation of a linear chain of $N = 4$ mutually coupled oscillators in interaction with two thermal reservoirs working at different temperatures. Here $T_1 = T_+$ and $T_N = T_-$. 38

2.2 $\left(D_h = \frac{K}{a}\sum_{ij} S'_{ij}\right)$, and $\left(D_c = \frac{K}{a}\sum_{ij} S_{ij}\right)$ as a function of time (t) for a chain of 4 atoms. As expected these factors converge to the same value, This means that in the steady state regime the total heat flux j is proportional to the temperature difference of the hot and cold baths. 39

2.3 A pictorial representation of a functionalized sheet of graphene. The number of atoms in the graphene sheet is 36, The alkane chains are n-pentane. The end of the chains interact with two thermal reservoirs working at different temperatures. 40

2.4 (a) Time evolution of (D_h/λ_g) and (D_c/λ_g) eq.2.42. As expected (D_h/λ_g) and (D_c/λ_g) converge to the same value, This means that in the steady state regime the total heat flux is proportional to the temperature difference of the hot and cold baths. 42

2.5 The ratio of the Thermal conductance of functionalized graphene λ_f to the thermal conductance of graphene λ_g as a function of chain length. 43

2.6 Pictorial representation of a high participation ratio mode ($P = 0.86$) (a), and a low participation ratio mode ($P = 0.13$). 44

2.7 Number of modes with increasing participation ratios for functionalized graphene configurations with five, six and eight chain sites. 45

3.1 $e^{-|t|/\tau}$ as a function of t for different values of the parameter τ. The solid line ($\tau = 0.04$), the dashed line ($\tau = 0.1$) 49

3.2 A pictorial representation of a linear chain of $N = 6$ mutually coupled oscillators in interaction with two thermal reservoirs working at different temperatures. Here $T_H = T_+$ and $T_C = T_-$. 58

3.3 (D_h), and (D_c) as a function of time (t) for a chain of 6 atoms with the correlation time $\tau = 0.5$ $(\sqrt{k/m})$. As expected these factors converge to the same but opposite values. 59

3.4 Thermal conductance versus temperature for a chain of 6 atoms with the correlation time $\tau = 0.5$ $(\sqrt{k/m})$. As expected increases with temperature to final reach its classical limit. 60

3.5 Heat capacity (C_v) as a function of temperature of the linear 1D chain of coupled harmonic oscillators of size N=6, where k is the Boltzmann constant, and $\hbar$ is Planck constant. 61

3.6 A pictorial representation of a functionalized sheet of graphene. The number of atoms in the graphene sheet is 54, The alkane chains are n-pentane. The end of the chains interact with two thermal reservoirs working at temperatures T_+ and T_-. 62

3.7 Ratio of the thermal conductance of the functionalized graphene configuration and that of pristine graphene as a function of temperature, where k is the Boltzmann constant, and $\hbar$ is Planck constant. 63

3.8 The ratio of the Thermal conductances of functionalized graphene λ_f and graphene λ_g as a function of chain length N. (solid disk): heating one site, (solid triagle): heating two sites, (empty square): heating three sites, (solid square): heating four sites. 65

3.9 Ratio of the average temperature profile ($T =< m\ v^2 >$) between the hot and cold baths and kT_+ for the graphene configuration in fig.3.8, k is the Boltzmann constant, T_+ is the temperature of the heat bath. . . 66

3.10 Number of normal modes versus participation ratio (PR). (solid triangle): functionalized graphene with chains of length (N=6), (empty square): functionalized graphene with chains of length (N=5). 67

3.11 Pictorial representation of a branched and unbranched sheets of graphene. The number of atoms in the graphene sheet is 54. The end of the chains interact with two thermal reservoirs working at different temperatures. 73

3.12 Number of normal modes versus participation ratio (PR). (solid triangle): non branched N=5 (fig.3.11(a)), (empty square): double branched N=5 (fig.3.11(b)). 74

3.13 Number of normal modes versus participation ratio (PR). (solid triangle): not branched N=5 (fig.3.11(a)), (empty square): triple branched N=5 (fig.3.11(c)). 74

3.14 Pictorial representation of a graphene sheet of 54 carbon atoms functionalized with two organic chains of size $N = 6$. 74

3.15 Quantum optimized structure of perfluorohexane. The dark spheres represent the carbon atoms, the green sphere are the fluorine atoms. The helical C-C-C-C twist angle of 16.8^o corresponds to a dihedral angle of 163.2^o and to a projected 1-5 27^o [30]. 75

4.1 A pictorial representation of a linear chain of $N = 6$ mutually coupled oscillators in interaction with two thermal reservoirs working at different temperatures. Here $T_1 = T_+$ and $T_N = T_-$. 89

4.2 Numerical results of heat Flux $J_i = (1/2)k(x_{i+1} - x_i)(\dot{x}_{i+1} + \dot{x}_{ii})$ for a linear chain of $N = 6$ mutually coupled oscillators in interaction with two thermal reservoirs working at different temperatures ($k_B T_- = 1\ (Ka^2)$ and $T_+ = 2\ (Ka^2)$), ($\tau = 0.1\ \sqrt{K/m}$). The curves represent the heat flux across the different sections of the chain 90

4.3 Analytical results of heat Flux $J_i = (1/2)k(x_{i+1} - x_i)(\dot{x}_{i+1} + \dot{x}_{ii})$ for a linear chain of $N = 6$ mutually coupled oscillators in interaction with two thermal reservoirs working at different temperatures (($k_B T_- = 1\ (Ka^2)$ and $T_+ = 2\ (Ka^2)$), ($\tau = 0.1\ \sqrt{K/m}$). 91

4.4 A pictorial representation pristine graphene. The number of atoms in the graphene sheet is 54. 92

4.5 Time variation of the ratio of the numerical average heat flux (J_{num}) throughout the graphene configuration shown in fig.4.4 and the heat flux of pristine graphene from the normal mode analysis (J_{nm}). ($k_B T_+ = 0.008\ (eV)$ and $k_B T_- = 0.007\ (eV)$), ($\tau = 0.50$) and ($\gamma = 1$). 93

4.6 A pictorial representation of a functionalized sheet of graphene. The number of atoms in the graphene sheet is 54, The alkane chains are n-pentane. The end of the chains interact with two thermal reservoirs working at different temperatures T_+ and T_-. 94

4.7 Time variation of the ratio of the numerical average heat flux (J_{num}) throughout the graphene configuration shown in fig.4.6 and the heat flux of the same configuration calculated from the normal mode analysis (J_{nm}). ($k_B T_h = 0.008\ (eV)$ and $k_B T_c = 0.007\ (eV)$), ($\tau = 0.50$) and ($\gamma = 1$). 94

4.8 Ratio of the time variation of the average temperature $T = \langle m\ v^2 \rangle$ across the alkanes/graphene interface and $k_B\ T_h$. 95

5.1 Pictorial representation of the system described by the Hamiltonian H_s where p sites on each side interact with two heat bath described by the Hamiltonian H_L and H_R. 97

5.2 A pictorial representation of a linear chain of six ($N = 6$) mutually coupled oscillators interacting with two thermal reservoirs working at different temperatures. Here $T_R = T_+$ and $T_L = T_-$. 113

5.3 ratio of the thermal conductance of the chain with spatial noise (λ_s) and the thermal conductance of the same chain with colored noise (λ_t) as a function of the number sites in contact with each heat bath (p). . 113

5.4 A pictorial representation of a functionalized sheet of graphene. The number of atoms in the graphene sheet is 54, The alkane chains are n-pentane. The end of the chains interact with two thermal reservoirs working at different temperatures T_+ and T_-. 115

5.5 Ratio of the thermal conductance of functionalized graphene with space correlated noise λ_s and colored noise λ_t for size chains from $N = 5$ to $N = 7$. The last two sites of each chain are in contact with heat baths. 116

5.6 The ratio of the Thermal conductances of functionalized graphene λ and that of graphene λ_g as a function of chain length N. (solid square): heating one site, (solid triagle): heating two sites 116

Abstract

The quest for high thermal conductivity materials has lead to nano-composites incorporating macromolecular materials with excellent thermal conductivity, such as carbon nanotubes and graphene nano-ribbons, in a matrix of poorer thermal conductivity. To minimize the interface thermal resistance the stiff, incorporated materials can be chemically functionalized with various side chains, this however may disrupt the overall thermal conductivity of the fillers. We report here an efficient theoretical method using normal modes to calculate the thermal conductivity of such systems and show how the participation ratio of these modes can be used to evaluate different choices for functionalization. We use this method to examine how effective different organic chains improve the heat flux through a graphene nano-sheet, also to identify the configuration of the functional groups that best conduct heat to the macromolecule. To confirm the efficiency of our model, we compare results from simulations including non-linear corrections to results from the normal mode analysis conducted on identical systems. Finally, we investigate the effect of space correlated noise on the overall results of optimization.

Introduction

Structured composites attract enormous attention for several reasons, including the promise to enhance the properties of the parent polymers (mechanical properties, permeability, thermal and electrical conductivity, etc), while maintaining the typical polymer light weight. Carbon-based nanocomposites (material with fillers with at least one dimension less than 100 nm) promise multi-functional properties, e.g., electrical and thermal conductivities in addition to enhanced mechanical strength. Increased effectiveness is expected for high-aspect ratio fillers, such as carbon nanotubes, graphene sheets/ribbons.

The thermal conductivity of single wall carbon nanotubes (SWCNTs), fig.0.1, at room temperature is about 6000 W/mK and that of multi-wall carbon nanotubes (MWCNTs) is about 3000 W/mK [7, 13, 4]. Graphene also displays a number of remarkable properties including extremely high electron mobility (up to $\sim 2 \times 10^5$ cm^2/Vs [24, 6]), and extremely high thermal conductivity (ranging from $(4.84 \pm 0.44) \times 10^3$ to $(5.30 \pm 0.48) \times 10^3$ $Wm^{-1}K^{-1}$)[2]. The thermal conductivity of single and few-layer graphene depends strongly on the size and thickness of the flakes. A-side-by side comparison of some of the physical properties of graphene and other materials is shown in tab.1.

The outstanding thermal performance of these composites suggests their use in thermal management applications in electronics and optoelectronics [21, 39, 5, 11]. However, the incorporation of CNTs and graphene into polymers has not produced high thermal conductivity composites because of the constituents' interface thermal resistance. This "Kapitza resistance" occurs at the boundary of two dissimilar materials [17, 18] and produces a temperature drop across the interface that is proportional to the heat flux. The effect is large when the two materials have a large difference in elasticity so that there is only a weak

Table 1: Physical properties

Mechanical properties

	Young modulus (TPa)	Tensile strength (GPa)
SWCNT	1 - 5	13 - 53
MWCNT	0.2 - 0.95	11 - 150
Graphene	1	80
Stainless steel	0.186 - 0.214	0.38 - 1.55

Thermal properties

	Thermal conductivity (W/(m K))	Phonon mean free path (μm)	Speed of sound (m/s)
SWCNT	6000	0.5 - 1.5	2×10^4
MWCNT	3000	0.22	-
Graphene	4.84×10^3 - 5.30×10^3	0.775	1.5×10^4
Stainless steel	401	-	-

Electrical properties

	Resistivity $\Omega\ cm$	Mobility $cm^2\ V^{-1}\ s^{-1}$
CNT	$0.34\ 10^{-4}$	10^5
Graphene	10^-6	2×10^5
Stainless steel	7.2×10^{-5}	-

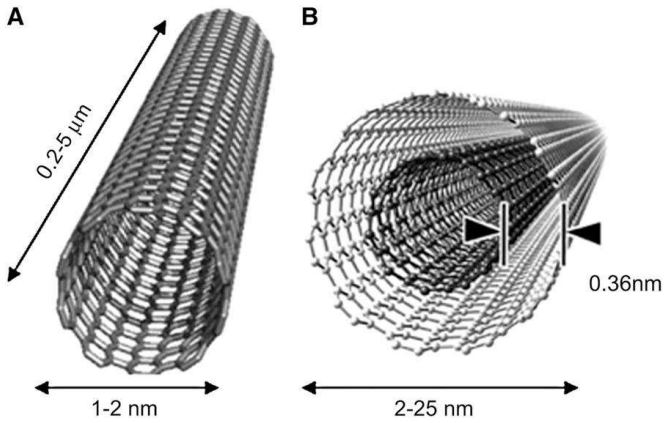


Figure 0.1: Conceptual diagram of single-walled carbon nanotube (SWCNT) (A) and multiwalled carbon nanotube (MWCNT) (B) delivery systems showing typical dimensions of length, width, and separation distance between graphene layers in MWCNTs [28].

coupling of phonon modes at the interface. If this resistance could be minimized then polymer composites could be used in radiators and other heat exchangers replacing heavier, costlier metallic components.

To this end, in the graphene system, two strategies have been proposed. The first is based on the fabrication of graphene strips with reduced lateral size, (known as graphene nanoribbons (GNRs)[35]). GNRs with width(s) from several tens of nanometers down to 2 nm have been fabricated either by plasma etching [19] or by means of chemical treatment of graphite [20]. Alternatively, chemical functionalization of graphene-based materials [38] is a promising strategy and does not require aggressive ribbon width reduction. It may even enhance the mechanical strength of the composites because of the potential of these side groups to bond to the matrix. In addition, functionalized graphene tends to aggregate less than do nonfunctionalized graphene when dispersed in aqueous or organic solutions fig.0.2. In spite of all these advantages, functionalization may induce severe disruption of the otherwise good conducting properties of graphene. Optimizing the thermal conduction to the graphene appears then to be a major challenge, and constructing models to simulate the heat conduction to the graphene tend

to be helpful.

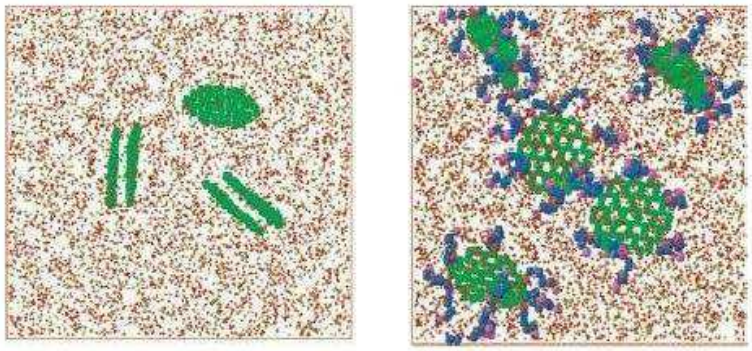


Figure 0.2: Representative simulation snapshots for GS of 54 carbon atoms in n-octane at 300 K. Red and yellow spheres represent CH_2 and CH_3 groups of n-octane, respectively. Visual inspection suggests that pristine GS (left) aggregate yielding pancake stacks. When the GS are functionalized they remain well dispersed in n-octane after 120 ns of simulation (right) [9]

The interactions between a system of fewer degrees of freedom, such as a small sheet of graphene, and a heat bath with many degrees of freedom such a bath of polymers, can be simulated through molecular dynamics (MD). Alternatively, the effect of the solvent can be approximated by the inclusion of a set of drag and random terms in the particles equations of motion, the resulting dynamics is known as Langevin dynamics, and their principal advantage over MD simulation is the reduction in the time required for computation which eventually allows one to perform longer simulations. Langevin dynamics will be used throughout this thesis to analyze heat transport in carbon based materials and graphene in particular. The origin of the drag force comes from the impulse produced by the multiple collisions of the particle and the rest of the molecules in the fluid, in this scenario some of the particle's momentum is transferred to the fluid causing it to slow down, also the extend to how the particle's history affects its future motion. The noise is a stochastic or random force, the properties of which are given only in the average. This force is supposed to come from occasional impacts of the particle and the molecules of the surrounding medium. It is then not surprising to

find that there is a fundamental relation between friction and noise. If the system approaches equilibrium at long times, the fluctuation-dissipation theorem is used to relate these forces to each other. Particularly, if the friction at any time t is proportional to the velocity at the same time, the noise in the classical limit, is delta-function correlated or "white". ("White" means that the Fourier transform of the correlation function of the noise, or its spectral density, is independent of frequency). The Langevin equations in this case are called "Markovian". This is usually the case when the forces of impact between the particle and the rest of the molecules of the fluid are varying extremely rapidly over the time of any observation. Real problems however are often not Markovian, the friction at time t can depend on the history of the velocity $v(t')$ for times t' that are earlier than t. That is, the friction may have a 'memory'. In this case, the friction coefficient is replaced by a memory function $K(t)$, sometimes called an aftereffect function. Problems of this kind are called non-Markovian.

Classical molecular dynamics simulation and classical Langevin dynamics can only produce classical results, the validity of which are justified at high temperatures but doubtful in the low temperature limit. Recall that the Debye temperature for carbon based material such as graphene is high and temperatures of $300K$ are considered low. Because of this, the heat capacity, thermal conductivity and other properties are much less than their classical values. In situations such as these, one can in fact restore, the classical Langevin dynamics by using quantum heat baths derived from Bose-Einstein statistics, such treatment is known as a classical approximation to the quantum Langevin equations. its advantage, over its classical counterpart is that it predicts the expected behavior of the system at low temperatures and produces the classical results at high temperatures. This thesis is structured as follow

- **Chapter 1: Langevin Equations**

In this chapter, we derive the generalized Langevin equations for a system interacting with two langevin heat baths. The heat baths are modeled in this approach as infinite numbers of coupled harmonic oscillators. In the first half of the analysis, we treat the oscillators in the heat baths as classical particles that are canonically distributed according to Boltzmann statistics. In the second half of the analysis the oscillators in the baths are treated as quantum particles canonically distributed with respect to the free oscillators Hamiltonian according to Bose-Einstein statistics.

- **Chapter 2: Using Normal Modes to Calculate and Optimize Thermal Conductivity in Functionalized Macromolecules**

  In this chapter we introduce a new technique to calculating thermal conductivity of functionalized molecules in general and use graphene nanosheets as a case study. We show by linearizing the interatomic interactions, and by numerically calculating the normal modes, that the total heat flux, throughout the functionalized macromolecule is a function of the temperature difference of the hot and cold baths. Even more interestingly, we show that we can control the heat transport throughout the system by varying the functionalized chains.

- **Chapter 3: Langevin Equations with Thermal Colored Noise**

  This chapter is an extension the analysis developed in chapter 2, where now we include means to suppress high frequency modes through an exponentially correlated noise. We incorporate quantum driving forces that are temperature dependent to mimic the effect of Bose-Einstein suppression of high energy modes. We also investigate ways to improve the thermal conductivity to the graphene

- **Chapter 4: Langevin Equations with Thermal Colored Noise, Nu-**

merical Solution

In this chapter we solve the classical Langevin equations numerically for a system in contact with Langevin heat baths. The results of these technique are used to foresee the extent to which the normal mode approach developed in chapters 2 and 3 is capable of predicting the best configurations to optimizing heat throughout the the functionalized graphene.

- **Chapter 5: Classical Langevin Equations with Time and Space Correlated Noise**

  In this chapter we consider the dynamics of interacting particles which are driven by correlated (not-independent) noise sources. We investigate the effect of spatial correlations in the noise on the dynamical correlations in the relative motion of the system particles.

- **Chapter 6: Conclusions**

Chapter 1

Langevin Equations

1.1 Introduction

The interactions between a system of fewer degrees of freedom and a heat bath with many degrees of freedom can be approximated in the system's equations of motion by the inclusion of apparently random and drag terms [40, 23, 8]. In this chapter, we shall derive the generalized Langevin equations for a system described by the Hamiltonian H_s interacting with two Langevin heat baths described by the Hamiltonians H_R and H_L respectively as shown in fig.1.1. The heat baths are modeled in this approach as infinite numbers of coupled harmonic oscillators. The randomness in the interactions between the heat bath and system originates from the unknown initial conditions of the oscillators in the bath. In the first half of the derivation, we treat the oscillators in the heat baths as classical particles that are canonically distributed according to Boltzmann statistics. In the second half, the oscillators in the baths are treated as quantum particles canonically distributed with respect to the free oscillators Hamiltonian according to Bose-Einstein statistics.

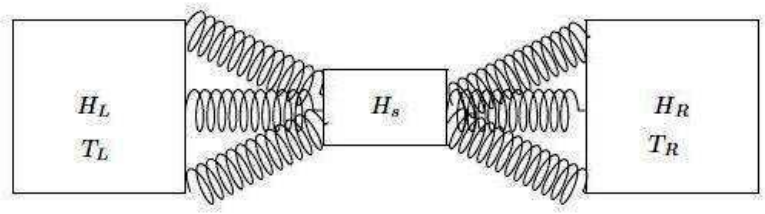


Figure 1.1: Pictorial representation of a system described by the Hamiltonian H_s interacting with two heat bath described by the Hamiltonian H_L and H_R.

1.2 Development

Consider a system made of N particles the first and last of which interact with two harmonic oscillator baths fig.1.1. The interactions among the particles in the system are described by the potential $U(q_{s_1}, ..., q_{s_N})$ where q_{s_i} refer to the position of the i^{th} particle in the system. If p_{s_i} is the momentum the i^{th} particle in the system, the Hamiltonian of the system is of the form

$$H_s = \sum_{1}^{N} \frac{p_{s_i}^2}{2m_{s_i}} + U(q_{s_1}, ..., q_{s_N}) \tag{1.1}$$

In the independent oscillator model of the heat bath, the particle is surrounded by a large (eventually infinite) number of heat bath particles, each attached to it by a spring. The Hamiltonian of the left and right oscillator baths are of the form

$$H_R = \sum_{1}^{N_R} \frac{p_{R_i}^2}{2m_{R_i}} + \frac{1}{2} m_{R_i} \omega_{R_i}^2 \left(q_{R_i} - \frac{\lambda_{R_i}}{m_{R_i}\omega_{R_i}^2} q_{s_1} \right)^2 \tag{1.2}$$

$$H_L = \sum_{1}^{N_L} \frac{p_{L_i}^2}{2m_{L_i}} + \frac{1}{2} m_{L_i} \omega_{L_i}^2 \left(q_{L_i} - \frac{\lambda_{L_i}}{m_{L_i}\omega_{L_i}^2} q_{s_N} \right)^2 \tag{1.3}$$

where the $p_{R_1}, ..., p_{R_{N_R}}$, $p_{L_1}, ..., p_{L_{N_L}}$, $q_{R_1}, ..., q_{R_{N_R}}$, $q_{L_1}, ..., q_{L_{N_L}}$ are respectively the momenta and displacements of the oscillators in the right and left heat baths, $\omega_{R_1}, ..., \omega_{R_{N_R}}$, $\omega_{L_1}, ..., \omega_{L_{N_L}}$, $m_{R_1}, ..., m_{R_{N_R}}$, $m_{L_1}, ..., m_{L_{N_L}}$ are respectively the oscillator frequencies and masses, and $\lambda_{R_1}, ..., \lambda_{R_{N_R}}$, and $\lambda_{L_1}, ..., \lambda_{L_{N_L}}$, are respectively the coupling constants with the right and left heat baths.

The Hamiltonian of the entire system and baths is

$$H = H_s + H_R + H_L \tag{1.4}$$

Let us now focus on the heat baths. The equations of motion are

$$\begin{aligned}
\dot{q}_{R_i} &= \frac{p_{R_i}}{m_{R_i}} \\
\dot{p}_{R_i} &= -m_{R_i}\omega_{R_i}^2(q_{R_i} - \frac{\lambda_{R_i}}{m_{R_i}\omega_{R_i}^2}q_{s_1}) \\
\dot{q}_{L_i} &= \frac{p_{L_i}}{m_{L_i}} \\
\dot{p}_{L_i} &= -m_{L_i}\omega_{L_i}^2(q_{L_i} - \frac{\lambda_{L_i}}{m_{L_i}\omega_{L_i}^2}q_{s_N})
\end{aligned} \tag{1.5}$$

Introducing the vectors

$$\begin{aligned}
\vec{S}_{b_R}(t) &= \left(q_{R_1}, ..., q_{R_{N_R}}, p_{R_1}, ..., p_{R_{N_R}}\right) \\
\vec{S}_{b_L}(t) &= \left(q_{L_1}, ..., q_{L_{N_L}}, p_{L_1}, ..., p_{L_{N_L}}\right) \\
\vec{S}_s(t) &= (q_{s_1}, ..., q_{s_N}, p_{s_1}, ..., p_{s_N})
\end{aligned} \tag{1.6}$$

Eq.1.5 becomes of the form

$$\begin{aligned}
\dot{\vec{S}}_{b_R}(t) &= \begin{pmatrix} \widetilde{0} & \widetilde{M_R^{-1}} \\ -\widetilde{K_R} & \widetilde{0} \end{pmatrix} \vec{S}_{b_R}(t) + \begin{pmatrix} \widetilde{0} & \widetilde{0} \\ \widetilde{\lambda_R}^t & \widetilde{0} \end{pmatrix} \cdot \vec{S}_s(t) \\
\dot{\vec{S}}_{b_L}(t) &= \begin{pmatrix} \widetilde{0} & \widetilde{M_L^{-1}} \\ -\widetilde{K_L} & \widetilde{0} \end{pmatrix} \vec{S}_{b_L}(t) + \begin{pmatrix} \widetilde{0} & \widetilde{0} \\ \widetilde{\lambda_L}^t & \widetilde{0} \end{pmatrix} \cdot \vec{S}_s(t)
\end{aligned} \tag{1.7}$$

where $\widetilde{M}^{-1}$ is a diagonal matrix with elements $1/m_i$. $\widetilde{K}$ is also diagonal with elements $K_{ij} = \delta_{ij} m_i {\omega_i}^2$, $\widetilde{\lambda}_{R_{ij}} = \delta_{i1}\lambda_j$, and $\widetilde{\lambda}_{L_{ij}} = \delta_{iN}\lambda_j$, δ_{ij} is the Kronecker delta function

If we define

$$\widetilde{A} = \begin{pmatrix} \widetilde{0} & \widetilde{M^{-1}} \\ -\widetilde{K} & \widetilde{0} \end{pmatrix} \tag{1.8}$$

then the solution to eq.1.7 for each bath is of the form eq.1.9

$$\vec{S}_b(t) = \exp(t\ \widetilde{A}) \cdot \vec{S}_b(0) + \int_0^t dt'\ \exp((t-t')\ \widetilde{A}) \cdot \begin{pmatrix} \widetilde{0} & \widetilde{0} \\ \widetilde{\lambda}^t & \widetilde{0} \end{pmatrix} \cdot \vec{S}_s(t') \tag{1.9}$$

Integration by parts leads to another form, where we assumed that $\vec{S}_s(0) = 0$

$$\begin{aligned} \vec{S}_b(t) = -\widetilde{A}^{-1} \cdot \begin{pmatrix} \widetilde{0} & \widetilde{0} \\ \widetilde{\lambda}^t & \widetilde{0} \end{pmatrix} \cdot \vec{S}_s(t) + \exp(t\ \widetilde{A}) \cdot \vec{S}_b(0) + \\ \int_0^t dt'\ \exp((t-t')\ \widetilde{A}) \cdot \widetilde{A}^{-1} \cdot \begin{pmatrix} \widetilde{0} & \widetilde{0} \\ \widetilde{\lambda}^t & \widetilde{0} \end{pmatrix} \cdot \frac{d}{dt}\left(\vec{S}_s(t')\right) \end{aligned} \tag{1.10}$$

Now we turn our attention to the system. The equations of motion for the system are

$$\dot{q}_{s_i} = \frac{p_{s_i}}{m_{s_i}}$$

$$\dot{p}_{s_i} = -\frac{\partial U}{\partial q_{s_i}} + \delta_{i1} \sum_{j=1}^{N_R} \lambda_{R_j} \left(q_{R_j} - \frac{\lambda_{R_j}}{m_{R_j}\omega_{R_j}^2} q_{s_i} \right) + \delta_{iN} \sum_{j=1}^{N_L} \lambda_{L_j} \left(q_{L_j} - \frac{\lambda_{L_j}}{m_{L_j}\omega_{L_j}^2} q_{s_i} \right) \tag{1.11}$$

which can also be expressed in the form

$$\dot{\vec{S}}_s(t) = \vec{f}(\vec{S}_s(t)) + \begin{pmatrix} \widetilde{0} & \widetilde{0} \\ \widetilde{\lambda_R} & \widetilde{0} \end{pmatrix} \cdot \vec{S}_{b_R}(t) - \widetilde{\eta}_R \cdot \vec{S}_s(t) + \begin{pmatrix} \widetilde{0} & \widetilde{0} \\ \widetilde{\lambda_L} & \widetilde{0} \end{pmatrix} \cdot \vec{S}_{b_L}(t) - \widetilde{\eta}_L \cdot \vec{S}_s(t) \tag{1.12}$$

where

$$\vec{f}(\vec{S}_s(t)) = \left(0, ..., 0, -\frac{\partial U}{\partial q_{s_1}}, ..., -\frac{\partial U}{\partial q_{s_N}}\right) \tag{1.13}$$

and

$$\widetilde{\eta}_R = \begin{pmatrix} \widetilde{0} & -\widetilde{M}^{-1} \\ \delta_{i1} \sum_{j=1}^{N_R} \frac{\lambda_j^2}{m_j\ \omega_j^2} & \widetilde{0} \end{pmatrix}$$

$$\widetilde{\eta}_L = \begin{pmatrix} \widetilde{0} & -\widetilde{M}^{-1} \\ \delta_{iN} \sum_{j=1}^{N_L} \frac{\lambda_j^2}{m_j\ \omega_j^2} & \widetilde{0} \end{pmatrix} \tag{1.14}$$

Substituting $\vec{S}_b$ with its expression from eq.1.10 leads to

$$
\begin{aligned}
\dot{\vec{S}}_s(t) = \vec{f}(\vec{S}_s(t)) - \left[\begin{pmatrix} \widetilde{0} & \widetilde{0} \\ \widetilde{\lambda_R} & \widetilde{0} \end{pmatrix} \cdot \widetilde{A}_R^{-1} \cdot \begin{pmatrix} \widetilde{0} & \widetilde{0} \\ \widetilde{\lambda_R}^t & \widetilde{0} \end{pmatrix} + \widetilde{\eta}_R \right] \cdot \vec{S}_s(t) \\
+ \begin{pmatrix} \widetilde{0} & \widetilde{0} \\ \widetilde{\lambda_R} & \widetilde{0} \end{pmatrix} \cdot \exp(t\ \widetilde{A}_R) \cdot \vec{S}_{b_R}(0) + \\
\int_0^t dt' \begin{pmatrix} \widetilde{0} & \widetilde{0} \\ \widetilde{\lambda_R} & \widetilde{0} \end{pmatrix} \cdot \exp((t-t')\ \widetilde{A}_R) \cdot \widetilde{A}_R^{-1} \cdot \begin{pmatrix} \widetilde{0} & \widetilde{0} \\ \widetilde{0} & \widetilde{\lambda_R}^t \end{pmatrix} \cdot \vec{S}_s(t') \\
- \left[\begin{pmatrix} \widetilde{0} & \widetilde{0} \\ \widetilde{\lambda_L} & \widetilde{0} \end{pmatrix} \cdot \widetilde{A}_L^{-1} \cdot \begin{pmatrix} \widetilde{0} & \widetilde{0} \\ \widetilde{\lambda_L}^t & \widetilde{0} \end{pmatrix} + \widetilde{\eta}_L \right] \cdot \vec{S}_s(t) \\
+ \begin{pmatrix} \widetilde{0} & \widetilde{0} \\ \widetilde{\lambda_L} & \widetilde{0} \end{pmatrix} \cdot \exp(t\ \widetilde{A}_L) \cdot \vec{S}_{b_L}(0) + \\
\int_0^t dt' \begin{pmatrix} \widetilde{0} & \widetilde{0} \\ \widetilde{\lambda_L} & \widetilde{0} \end{pmatrix} \cdot \exp((t-t')\ \widetilde{A}_L) \cdot \widetilde{A}_L^{-1} \cdot \begin{pmatrix} \widetilde{0} & \widetilde{0} \\ \widetilde{0} & \widetilde{\lambda_L}^t \end{pmatrix} \cdot \vec{S}_s(t')
\end{aligned}
\tag{1.15}
$$

The matrix elements of the second and fifth terms in eq.1.15 are all equal to zero, accordingly the previous equation simplifies to

$$\dot{\vec{S}}_s(t) = \vec{f}(\vec{S}_s(t)) + \begin{pmatrix} \widetilde{0} & \widetilde{0} \\ \widetilde{\lambda_R} & \widetilde{0} \end{pmatrix} \cdot \exp(t\ \widetilde{A}_R) \cdot \vec{S}_{b_R}(0) +$$

$$\int_0^t dt' \begin{pmatrix} \widetilde{0} & \widetilde{0} \\ \widetilde{\lambda_R} & \widetilde{0} \end{pmatrix} \cdot \exp((t-t')\ \widetilde{A}_R) \cdot \widetilde{A}_R^{-1} \cdot \begin{pmatrix} \widetilde{0} & \widetilde{0} \\ \widetilde{0} & \widetilde{\lambda_R}^t \end{pmatrix} \cdot \vec{S}_s(t')$$

$$+ \begin{pmatrix} \widetilde{0} & \widetilde{0} \\ \widetilde{\lambda_L} & \widetilde{0} \end{pmatrix} \cdot \exp(t\ \widetilde{A}_L) \cdot \vec{S}_{b_L}(0) + \tag{1.16}$$

$$\int_0^t dt' \begin{pmatrix} \widetilde{0} & \widetilde{0} \\ \widetilde{\lambda_L} & \widetilde{0} \end{pmatrix} \cdot \exp((t-t')\ \widetilde{A}_L) \cdot \widetilde{A}_L^{-1} \cdot \begin{pmatrix} \widetilde{0} & \widetilde{0} \\ \widetilde{0} & \widetilde{\lambda_L}^t \end{pmatrix} \cdot \vec{S}_s(t')$$

This is the equation of motion for $\vec{S}_s(t)$, it is expressed in terms of its own history from 0 to t and the bath variables enter only through their initial values.

1.2.1 Classical interpretation of the noise

If we assume that the bath particles act as classical particles, we can identify the terms that acts as a noise source for each heat bath. We introduce the driving forces for each bath as

$$\vec{F}_R(t) = \begin{pmatrix} \widetilde{0} & \widetilde{0} \\ \widetilde{\lambda}_R^t & \widetilde{0} \end{pmatrix} \cdot \exp(t\ \widetilde{A}_R) \cdot \vec{S}_{b_R}(0)$$

$$\vec{F}_L(t) = \begin{pmatrix} \widetilde{0} & \widetilde{0} \\ \widetilde{\lambda}_L^t & \widetilde{0} \end{pmatrix} \cdot \exp(t\ \widetilde{A}_L) \cdot \vec{S}_{b_L}(0) \tag{1.17}$$

The forces defined in eq.1.17 depend explicitly on the initial positions and momenta of the oscillators in the baths, interpreted here as classical particles. These are not known, moreover, their number could be very large so that explicit specification of the initial conditions in the bath becomes impossible. One solution would be to treat $\vec{F}(t)$ as a stochastic process. The properties of this process can be obtained from the explicit expression for the random force since the stochastic nature of the force originates from the unknown initial positions and momenta of the particles in the bath. To this end, we consider an ensemble of initial bath variables $\vec{S}_b(0)$ drawn at random from the Boltzmann distribution eq.1.18:

$$P(\vec{S}_b(0)) = \frac{e^{-\beta H_{bo}}}{Z} \tag{1.18}$$

where $\beta = \dfrac{1}{k_B T}$, T is the temperature of the bath, k_B is the Botltzmann constant, and H_{bo} is the free Hamiltonian of the bath.

$$H_{bo} = \sum_1^N \frac{p_i^2}{2m_i} + \frac{1}{2} m_i \omega_i^2 q_i^2 \tag{1.19}$$

The partition function Z is

$$Z = \int \left(\prod_i dS_{b_i} \right) \; e^{-\beta H_{bo}} \tag{1.20}$$

In this ensemble the mean of $\vec{S}_b(0)$ is

$$\langle \vec{S}_b(0) \rangle = \frac{\int \left(\prod_i dS_{b_i} \right) \; \vec{S}_b(0) \; e^{-\beta H_{bo}}}{\int \left(\prod_i dS_{b_i} \right) \; e^{-\beta H_{bo}}} = 0 \tag{1.21}$$

The dispersion of $\vec{S}_b(0)$ can be found in a similar way $\langle \vec{S}_b(0) \cdot \vec{S}_b(0)^t \rangle$, where the superscript t stands for transpose. The component of $\vec{S}_b(0) \cdot \vec{S}_b(0)^t$ are of the form $S_{b_i}(0) S_{b_j}(0)$ The average of which turns out to be of the form

$$\langle S_{b_i}(0) S_{b_j}(0)) \rangle = \delta_{ij} \frac{k_B T}{m_i \omega_i^2} = k_B T K_{ij}^{-1} \tag{1.22}$$

which can also be written in a compact form as

$$\begin{aligned} \langle \vec{S}_{b_R}(0) \cdot \vec{S}_{b_R}(0)^t \rangle &= k_B T_R \widetilde{K}_R^{-1} \\ \langle \vec{S}_{b_L}(0) \cdot \vec{S}_{b_L}(0)^t \rangle &= k_B T_L \widetilde{K}_L^{-1} \end{aligned} \tag{1.23}$$

From the above relations we derive the statistics of the noise

$$\langle \vec{F}(t) \rangle = 0$$

$$\langle \vec{F}(t)\vec{F}(t')^t \rangle = \langle \begin{pmatrix} \widetilde{0} & \widetilde{0} \\ \widetilde{\lambda} & \widetilde{0} \end{pmatrix} \cdot \exp(t\ \widetilde{A}) \cdot \left(\vec{S}_b(0) \cdot \vec{S}_b(0)^t \right) \cdot \exp(t'\ \widetilde{A})^t \cdot \begin{pmatrix} \widetilde{0} & \widetilde{0} \\ \widetilde{\lambda} & \widetilde{0} \end{pmatrix}^t \rangle \tag{1.24}$$

One can easily prove that

$$\widetilde{A} = \begin{pmatrix} \widetilde{0} & \widetilde{I} \\ -\widetilde{I} & 0 \end{pmatrix} \cdot \left(\vec{S}_b(0) \cdot \vec{S}_b(0)^t \right)^{-1} \tag{1.25}$$

$$\begin{aligned} &\left(\vec{S}_b(0) \cdot \vec{S}_b(0)^t \right) \cdot \left[\exp \left(t \begin{pmatrix} \widetilde{0} & \widetilde{I} \\ -\widetilde{I} & 0 \end{pmatrix} \cdot \left(\vec{S}_b(0) \cdot \vec{S}_b(0)^t \right)^{-1} \right) \right]^t = \\ &\exp \left(-t \begin{pmatrix} \widetilde{0} & \widetilde{I} \\ -\widetilde{I} & 0 \end{pmatrix} \cdot \left(\vec{S}_b(0) \cdot \vec{S}_b(0)^t \right)^{-1} \right) \cdot \left(\vec{S}_b(0) \cdot \vec{S}_b(0)^t \right) \end{aligned} \tag{1.26}$$

Substituting this in eq.1.24 bring the noise correlation to

$$\langle \vec{F}(t)\vec{F}(t')^t \rangle = k_B T_{R/L} \begin{pmatrix} \widetilde{0} & \widetilde{0} \\ \widetilde{\lambda} & \widetilde{0} \end{pmatrix} \cdot \exp((t-t')\ \widetilde{A}) \cdot \langle \left(\vec{S}_b(0) \cdot \vec{S}_b(0)^t \right) \rangle \cdot \begin{pmatrix} \widetilde{0} & \widetilde{0} \\ \widetilde{\lambda} & \widetilde{0} \end{pmatrix}^t$$

$$= k_B T_{R/L} \widetilde{L}(t-t') \tag{1.27}$$

where

$$\widetilde{L}(t-t') = \begin{pmatrix} \widetilde{0} & \widetilde{0} \\ \widetilde{\lambda} & \widetilde{0} \end{pmatrix} \cdot \exp((t-t')\ \widetilde{A}) \cdot \langle \left(\vec{S}_b(0) \cdot \vec{S}_b(0)^t \right) \rangle \cdot \begin{pmatrix} \widetilde{0} & \widetilde{0} \\ \widetilde{\lambda} & \widetilde{0} \end{pmatrix}^t \tag{1.28}$$

or

$$\widetilde{L}(t-t') = - \begin{pmatrix} \widetilde{0} & \widetilde{0} \\ \widetilde{\lambda} & \widetilde{0} \end{pmatrix} \cdot \exp((t-t')\ \widetilde{A}) \cdot \widetilde{A}^{-1} \cdot \begin{pmatrix} \widetilde{0} & \widetilde{0} \\ \widetilde{0} & \widetilde{\lambda}^t \end{pmatrix} \tag{1.29}$$

Eq.1.29 is known as the memory function, it describes the effect of the history of the particle on its future. Using this result, the equations of motion Eq.1.16 become the final Langevin equations for the system particles and expressed as

$$\dot{\vec{S}}_s(t) = \vec{f}(\vec{S}_s(t)) + \int_0^t dt' \ \widetilde{L}_R(t-t') \cdot \vec{S}_s(t-t') \\ + \int_0^t dt' \ \widetilde{L}_L(t-t') \cdot \vec{S}_s(t-t') + \vec{F}_R(t) + \vec{F}_L(t) \tag{1.30}$$

Now by writing

$$\exp((t) \ \widetilde{A}) = \sum_n \frac{t^n \widetilde{A}^n}{n!} = \sum_n \frac{t^{2n} \widetilde{A}^{2n}}{(2n)!} + \sum_n \frac{t^{2n+1} \widetilde{A}^{2n+1}}{(2n+1)!} \tag{1.31}$$

The elements of $\widetilde{A}^{2n+1}$ are all off diagonal and do not contribute to the expression of $\widetilde{L}(t-t')$. The elements of $\widetilde{A}^{2n}$ are along the diagonal and contribute to the expression of $\widetilde{L}(t-t')$ as

$$\widetilde{L}(t-t') = \delta_{i,j}\delta_{i,N+1} \sum_j \frac{\lambda_{R_j}^2}{m_{R_i}\omega_{R_i}^2} \cos(\omega_{R_j} t) \\ + \delta_{i,j}\delta_{i,2N} \sum_j \frac{\lambda_{L_j}^2}{m_{L_i}\omega_{L_i}^2} \cos(\omega_{L_j} t) \tag{1.32}$$

Which reduces for each bath to the from

$$K(t) = \sum_i \frac{{\lambda_i}^2}{m_i {\omega_i}^2} \cos(\omega_i t) \tag{1.33}$$

If we treat the frequency distribution as continuous, then we can replace the sum in eq.1.33 by an integral as in eq.1.34, and the memory function eq.1.33 becomes eq.1.35, where the oscillators are assumed to have unit mass.

$$\sum \to N \int_0^{+\infty} g(\omega) \ d\omega \tag{1.34}$$

$$K(t) = \int_0^{+\infty} \frac{N\ \lambda^2(\omega)}{\omega^2}\ g(\omega)\cos(\omega t)\ d\omega \tag{1.35}$$

If now $N\ \lambda^2(\omega)\ g(\omega) \propto \omega^2$ for all frequencies then eq.1.35 becomes the Dirac delta function eq.1.36 and the noise is white. This is usually the case when the forces of impact between the particle and the rest of the molecules of the fluid are varying extremely rapidly over the time of any observation.

$$K(t) \propto \int_0^{+\infty} \cos(\omega t)\ d\omega \propto \delta(t) \tag{1.36}$$

If $N\ \lambda^2(\omega)\ g(\omega) \propto \omega^2/(1+\tau^2\ \omega^2)$ for all frequencies then eq.1.35 becomes an exponentially decaying function of time eq.1.37 and the noise is colored.

$$K(t) \propto \int_{-0}^{+\infty} \frac{1}{1+\tau^2\ \omega^2}\cos(\omega t)\ d\omega \propto \frac{1}{\tau}\ e^{-t/\tau} \tag{1.37}$$

1.2.2 Quantum mechanical interpretation of the noise

Due to a very high Debye temperature for carbon based materials [37], $300K$ is considered a low temperature. Accordingly, the classical Langevin equations developed in the previous section may not be suitable. It is however still possible to account for some of these effects if one decides to adopt a quasi-classical approximation where the system is still treated classically, the noise however is interpreted quantum mechanically. In this section we develop the quantum correlation relation that will be used later in this quasi-classical approximation. To this end, we introduce the noise sources for each bath as in eq.1.17.

In the quantum mechanical interpretation of the noise (eq.1.17) we assume that the oscillators in the thermal heat bath are canonically distributed with

respect to the free oscillator Hamiltonian according to Bose-Einstein statistics [10]. The operators $\hat{p}_{b_i}$ and $\hat{q}_{b_i}$ satisfy the commutation relations eq.1.38.

$$[\hat{q}_{b_i}, \hat{p}_{b_j}] = i\hbar\delta_{ij} \qquad [\hat{q}_{b_i}, \hat{q}_{b_j}] = [\hat{p}_{b_i}, \hat{p}_{b_j}] = 0 \tag{1.38}$$

The expectation value of any operator F with respect to the canonical ensemble at temperature T is defined by

$$< F >= T_r\{Fe^{-\beta H_o}\}/T_r\{e^{-\beta H_o}\} \tag{1.39}$$

where the trace operation (T_r) is in the space of the eigenfunctions of the free oscillator Hamiltonian operator H_o

$$H_o = \frac{1}{2}\sum_i \frac{\hat{p}_{b_i}^2}{m_i} + \frac{1}{2}\sum_i \omega_i^2 \hat{q}_{b_i}^2 \tag{1.40}$$

We introduce the operators

$$\begin{aligned} a_s &= \frac{\hat{p}_{b_s} - i\omega_s \hat{q}_{b_s}}{\sqrt{2\hbar\omega_s}} \\ a_s^\dagger &= \frac{\hat{p}_{b_s} + i\omega_s \hat{q}_{b_s}}{\sqrt{2\hbar\omega_s}} \end{aligned} \tag{1.41}$$

The commutation relation between these two operators follows from eq.1.38 as

$$[a_s, a_r^\dagger] = \delta_{sr} \qquad [a_s, a_r] = [a_s^\dagger, a_r^\dagger] = 0 \tag{1.42}$$

We can solve for $\hat{q}_{b_s}$ and $\hat{p}_{b_s}$ from the definitions in eq.1.41 as

$$\hat{q}_{b_s} = i\sqrt{\frac{\hbar}{2\omega_s}}(a_s - a_s^\dagger)$$

$$\hat{p}_{b_s} = \sqrt{\frac{\hbar\omega_s}{2}}(a_s + a_s^\dagger) \tag{1.43}$$

Inserting these expressions in the Hamiltonian eq.1.40 and using the relations eq.1.42 we get

$$H_o = \sum_s \hbar\omega_s(a_s^\dagger a_s + \frac{1}{2}) \tag{1.44}$$

The operator $a_s^\dagger a_s$ is the number operator for the sth mode; its eigenvalues are the nonnegative integers. The operator a_s is the step down (annihilation) operator, and the operator $a_s^\dagger$ is the step-up (creation) operator; they have matrix elements only between eigen-states of the number operator which differ by unity.

The expectation value of $a_s^\dagger a_r$ is of the form [10]

$$\begin{aligned}\langle a_s^\dagger a_r\rangle &= \delta_{sr} T_r\{a_s^\dagger a_r e^{-\beta H_o}\}/T_r\{e^{-\beta H_o}\} \\ &= \delta_{sr}\frac{\sum_{n=0}^{\infty} n\exp[-\frac{\hbar\omega_s}{kT}(n+\frac{1}{2})]}{\exp[-\frac{\hbar\omega_s}{kT}(n+\frac{1}{2})]} \\ &= \frac{\delta_{sr}}{\exp[-\frac{\hbar\omega_s}{kT}(n+\frac{1}{2})]-1} = \frac{1}{2}\delta_{sr}[\coth(\frac{\hbar\omega_s}{2kT})-1]\end{aligned} \tag{1.45}$$

similarly

$$\langle a_s^\dagger a_r \rangle = \frac{1}{2}\delta_{sr}[\coth(\frac{\hbar\omega_s}{2kT}) + 1] \tag{1.46}$$

From these results we obtain the following pair correlations

$$\begin{aligned}
\langle \hat{q}_{b_j} \hat{p}_{b_i} \rangle &= -\langle \hat{p}_{b_i} \hat{q}_{b_j} \rangle = \frac{1}{2} i\hbar\delta_{ij} \\
\langle \hat{q}_{b_j} \hat{q}_{b_i} \rangle &= \frac{\hbar}{2\omega_i}\delta_{ij} \coth(\frac{\hbar\omega_i}{2kT}) \\
\langle \hat{p}_{b_j} \hat{p}_{b_i} \rangle &= \frac{\hbar\omega_i}{2}\delta_{ij} \coth(\frac{\hbar\omega_i}{2kT})
\end{aligned} \tag{1.47}$$

Finally the noise correlation

$$\begin{aligned}
\langle \vec{F}(t)\vec{F}(t')^t \rangle &= \langle \begin{pmatrix} \widetilde{0} & \widetilde{0} \\ \widetilde{\lambda} & \widetilde{0} \end{pmatrix} \cdot \exp(t\ \widetilde{A}) \cdot [\vec{S}_b(0)]\ \left(\begin{pmatrix} \widetilde{0} & \widetilde{0} \\ \widetilde{\lambda} & \widetilde{0} \end{pmatrix} \cdot \exp(t'\ \widetilde{A}) \cdot [\vec{S}_b(0)] \right)^t \rangle \\
&= \begin{pmatrix} \widetilde{0} & \widetilde{0} \\ \widetilde{\lambda} & \widetilde{0} \end{pmatrix} \cdot \exp(t\ \widetilde{A}) \cdot \langle [\vec{S}_b(0)]\ [\vec{S}_b(0)]^t \rangle \cdot \exp(t'\ \widetilde{A})^t \cdot \begin{pmatrix} \widetilde{0} & \widetilde{0} \\ \widetilde{\lambda} & \widetilde{0} \end{pmatrix}^t
\end{aligned} \tag{1.48}$$

The product $\vec{F}(t)\vec{F}(t')^t$ is not a Hermitian operator, consequently the noise correlation cannot be interpreted properly in a classical dynamics. If we use the symmetrized correlation obtained by interchanging t and t' in eq.1.45 and then take the transpose [36], the previous correlation becomes a Hermitian operator of the form

$$\langle \vec{F}(t)\vec{F}(t')^t\rangle_{sym} = \frac{1}{2}\begin{pmatrix} \widetilde{0} & \widetilde{0} \\ \widetilde{\lambda} & \widetilde{0} \end{pmatrix} \cdot \exp(t\ \widetilde{A}) \cdot \langle [\vec{S}_b(0)]\ [\vec{S}_b(0)]^t$$

$$+(\vec{S}_b(0)]\ [\vec{S}_b(0)]^t)^t\rangle \cdot \exp(t'\ \widetilde{A})^t \cdot \begin{pmatrix} \widetilde{0} & \widetilde{0} \\ \widetilde{\lambda} & \widetilde{0} \end{pmatrix}^t \tag{1.49}$$

The elements of $\langle [\vec{S}_b(0)]\ [\vec{S}_b(0)]^t + (\vec{S}_b(0)]\ [\vec{S}_b(0)]^t)^t\rangle$ are diagonal and real. As a matter of fact, each element is of the form $\langle S_{b_i}(0)\ S_{b_j}(0) + S_{b_j}(0)\ S_{b_i}(0)\rangle$, and according to eq.1.47 all the off diagonal terms are zero.

Similarly using the identity

$$\begin{aligned} &\langle [\vec{S}_b(0)]\ [\vec{S}_b(0)]^t + (\vec{S}_b(0)]\ [\vec{S}_b(0)]^t)^t\rangle \cdot [\exp(t\ \widetilde{A})]^t \\ &= \exp(-t\ \widetilde{A}) \cdot \langle [\vec{S}_b(0)]\ [\vec{S}_b(0)]^t + (\vec{S}_b(0)]\ [\vec{S}_b(0)]^t)^t\rangle \end{aligned} \tag{1.50}$$

eq.1.46 becomes

$$\langle \vec{F}(t)\vec{F}(t')^t\rangle_{sym} = \frac{1}{2}\begin{pmatrix} \widetilde{0} & \widetilde{0} \\ \widetilde{\lambda} & \widetilde{0} \end{pmatrix} \cdot \exp((t-t')\ \widetilde{A}) \cdot \langle [\vec{S}_b(0)]\ [\vec{S}_b(0)]^t$$

$$+(\vec{S}_b(0)]\ [\vec{S}_b(0)]^t)^t\rangle \cdot \begin{pmatrix} \widetilde{0} & \widetilde{0} \\ \widetilde{\lambda} & \widetilde{0} \end{pmatrix}^t \tag{1.51}$$

or

$$\langle \vec{F}(t)\vec{F}(t')^t \rangle_{sym} = \delta_{ij}\delta_{i,N+1}\frac{1}{2}\sum_s \lambda_s^2 \frac{\hbar}{\omega_s}\coth\left[\frac{\hbar\omega_s}{2kT_1}\right]\cos\omega_s(t-t')$$

$$+\delta_{ij}\delta_{i,2N}\frac{1}{2}\sum_s \lambda_s^2 \frac{\hbar}{\omega_s}\coth\left[\frac{\hbar\omega_s}{2kT_2}\right]\cos\omega_s(t-t') \tag{1.52}$$

If we let $\hbar \to 0$ then

$$\lim_{\hbar\to 0}\hbar\coth\left[\frac{\hbar\omega_j}{2kT}\right] = \frac{2kT}{\omega_j} \tag{1.53}$$

and

$$\langle \vec{F}(t)\vec{F}(t')^t \rangle_{sym} = \delta_{ij}\delta_{i,N+1}kT_L\sum_s \frac{\lambda_s^2}{\omega_{L_s}^2}\cos\omega_{L_s}(t-t')+$$

$$\delta_{ij}\delta_{i,2N}kT_R\sum_s \frac{\lambda_{R_s}^2}{\omega_{R_s}^2}\cos\omega_{R_s}(t-t') \tag{1.54}$$

which is identical to the relations we obtained using the classical approach eq.1.32 where here we assume that the oscillators have unit mass.

If we treat the frequency distribution as continuous, then we can replace the sum in eq.1.52 by an integral as in eq.1.34, and the correlation reduces to eq.1.55, where we assume that the oscillators have unit mass.

$$\langle \vec{F}(t)\vec{F}(t')^t \rangle_{sym} = \delta_{ij}\delta_{i,N+1}\frac{1}{2}\int_0^\infty d\omega_L g(\omega_L)\frac{\hbar\lambda_L^2(\omega_L)}{\omega_L}\coth\left[\frac{\hbar\omega_L}{2kT_L}\right]\cos\omega_L(t-t')+$$

$$\delta_{ij}\delta_{i,2N}\frac{1}{2}\int_0^\infty d\omega_R g(\omega_R)\frac{\hbar\lambda_R^2(\omega_R)}{\omega_R}\coth\left[\frac{\hbar\omega_R}{2kT_R}\right]\cos\omega_R(t-t') \tag{1.55}$$

1.3 Conclusion

In this chapter we derived the generalized Langevin equations (GLE) for a general classical system in contact with two heat baths. At first we interpreted the noise classically then quantum mechanically and we showed that the quantum noise correlations reduce to their classical counterpart in the high temperature limit. These equations will be used in later chapters to solve for the displacements and momenta of the different particles in a variety of macromolecules and calculate different system properties.

One may object that by only interpreting the noise quantum mechanically may not produce the low temperature behavior of the system properties. However, there is very little difference between a quantum and a linear classical system. The dynamics are such that it smoothly crosses over to the classical regime [16]. This would be the case at low temperatures, where nonlinearity can be neglected, and the system interactions can be linearized. The other advantage of this quasi-classical approximation is that it converges to its classical counterpart in the high temperature limit, where both the noise and the system can be analyzed classically.

It is worth mention that most carbon based materials such as graphene and carbon nanotubes have considerably high Debye temperature, even 300 K is considered low and the system stays linear even at these temperatures. Accordingly,

the proposed dynamics can still reproduce the quantum results.

Chapter 2

Using Normal Modes to Calculate and Optimize Thermal Conductivity in Functionalized Macromolecules

2.1 Introduction

In this chapter we introduce a new technique to calculating thermal conductivity of functionalized molecules in general and use graphene nano-sheets as a case study. We show by linearizing the interatomic interactions, and by numerically calculating the normal modes, that the total heat flux, throughout the functionalized macromolecule is a function of the temperature difference of the hot and cold baths. Even more interestingly, we show that we can control the heat transport throughout the system by varying the functionalized chains.

It may be objected that linearizing interactions dramatically changes the dynamics of the system. However, we are interested in determining the major bottlenecks to thermal conductivity at the interface and these are present even in the linear approximation. Non-linear corrections may alter the magnitude of our results, but not the essential principles for optimization. This will be demonstrated in chapter 4.

2.2 The Analytical Technique

2.2.1 Site Displacement

In this section, we shall develop the general Langevin formalism that we apply to a specific system in section 2.3. We shall present this general case first and then indicate briefly how the results will simplify for our special cases.

Consider a system made of N particles connected by springs. We will apply a driving random force to the first and last particles. Each particle obeys the

equation of motion:

$$m_i \ \ddot{X}_i = -\sum_j K_{ij} \ X_j + (\gamma_i \ \dot{X}_i + F_i(t))(\delta_{i,1} + \delta_{i,N}) \tag{2.1}$$

where m_i, X_i,respectively are the mass and displacement of particle i, K_{ij} is the spring constant between particles i and j, γ_i the damping force given by Stokes's law, $F_i(t)$ is the Langevin force on particle i, the overhead dot refers to time derivative, and δ_{ij} is the Kronecker delta function restricting the driving and damping to the first and last particles.

We can write the set of N coupled differential equations as

$$\widetilde{M} \ \ddot{\vec{X}} + \widetilde{\Gamma} \ \dot{\vec{X}} + \widetilde{K} \ \vec{X} = \vec{F}(t) \tag{2.2}$$

where $\widetilde{M}$, $\widetilde{\Gamma}$, $\widetilde{K}$ are respectively the mass, damping and spring constants matrices and $\vec{F}(t)$ is the random Langevin force vector.

The statistics of the Langevin sources are defined by:

$$< F_i(t) >= 0 \tag{2.3}$$

$$< F_i(t_1) \ F_j(t_2) >= 2 \ \gamma_i \ k_B \ T_i \ \delta_{ij}\delta(t_1 - t_2) \tag{2.4}$$

where T_i is the temperature of the source i, k_B is the Boltzman constant, and $<>$ stands for temporal average.

Consider the homogeneous form of equation eq.2.2

$$\widetilde{M} \ \ddot{\vec{X}} + \widetilde{\Gamma} \ \dot{\vec{X}} + \widetilde{K} \ \vec{X} = 0 \tag{2.5}$$

We search for a solution to eq.2.5 of the form $\vec{X} = \vec{a} \ e^{\lambda t}$, where $\vec{a}$ is independent

of the time t. Plugging this solution in eq.2.5 gives.

$$\widetilde{M}\ \lambda^2\ \vec{a} + \lambda\ \widetilde{\Gamma}\ \vec{a} + \widetilde{K}\ \vec{a} = 0 \tag{2.6}$$

This is a quadratic eigenvalue problem for λ. To solve this eigenvalue problem we introduce a second set of coefficients

$$\vec{b} = \lambda\ \vec{a} \tag{2.7}$$

and eq.2.6 becomes

$$\lambda\ \widetilde{M}\ \vec{b} + \widetilde{\Gamma}\ \vec{b} + \widetilde{K}\ \vec{a} = 0 \tag{2.8}$$

producing an eigenvalue equation of the form

$$\begin{pmatrix} \widetilde{0} & \widetilde{1} \\ \widetilde{K} & \widetilde{\Gamma} \end{pmatrix} \begin{pmatrix} \vec{a} \\ \vec{b} \end{pmatrix} = \lambda \begin{pmatrix} \widetilde{1} & \widetilde{0} \\ \widetilde{0} & -\widetilde{M} \end{pmatrix} \begin{pmatrix} \vec{a} \\ \vec{b} \end{pmatrix} \tag{2.9}$$

where $\widetilde{1}$ is the unity matrix. Thus we see that *even in the presence of dissipation,* we can find normal, uncoupled modes for the system.

In general we generate complex eigenvalues λ_k and complex eigenvectors $\vec{a}_k$. However, if λ_k and $\vec{a}_k$ are solutions to the eigenvalue problem then their complex conjugates λ_k^* and $\vec{a}_k^*$ are solutions as well. Let

$$\lambda_k = -\eta_k + i\omega_k \tag{2.10}$$

and

$$\vec{a}_k = \vec{u}_k + i\vec{v}_k \tag{2.11}$$

then

$$\vec{a}_k\ e^{\lambda_k t} = (\vec{u}_k + i\vec{v}_k)\ e^{-\eta_k t + i\omega_k t} \tag{2.12}$$

is a solution to the homogenous equation of motion eq.2.5 and so is

$$\vec{a}_k^* e^{\lambda_k^* t} = (\vec{u}_k - i\vec{v}_k)\ e^{-\eta_k t - i\omega_k t} \tag{2.13}$$

Thus we can define the real solutions $\chi_k^{(1)}(t)$ and $\chi_k^{(2)}(t)$ where

$$\chi_k^{(1)}(t) = e^{-\eta_k t}\ \ (\vec{u}_k \cos(\omega_k t) - \vec{v}_k \sin(\omega_k t)) \tag{2.14}$$

$$\chi_k^{(2)}(t) = e^{-\eta_k t}\ (\vec{u}_k \sin(\omega_k t) + \vec{v}_k\ \cos(\omega_k t)) \tag{2.15}$$

and from that the general solution to the homogenous problem is

$$\vec{\chi}(t)^{hom} = \sum_k B_k^{(1)} \chi_k^{(1)}(t) + B_k^{(2)} \chi_k^{(2)}(t) \tag{2.16}$$

where $B_k^{(1)}$ and $B_k^{(2)}$ are constants that depend on the boundary conditions.

The solution to the driven problem of eq.2.2 is

$$\vec{\chi}(t) = \vec{\chi}(t)^{hom} + \int_0^t \widetilde{G}(t,t')\ \vec{F}(t')dt' \tag{2.17}$$

where $G(t,t')$ is the Green function solution to the differential equation

$$\widetilde{M}\ \frac{\partial^2 \widetilde{G}}{\partial t^2} + \widetilde{\Gamma}\ \frac{\partial \widetilde{G}}{\partial t} + \widetilde{K}\widetilde{G} = \widetilde{1}\ \delta(t-t') \tag{2.18}$$

Normally we need to specify the boundary conditions at $t = 0$. However we are interested in the steady state solution to the problem so the initial conditions are irrelevant. We can choose any initial condition that is convenient. In particular we can choose $\vec{\chi}(0) = 0$ and $\dot{\vec{\chi}}(0) = 0$. With these conditions, the homogeneous

term is zero, and our steady state solution is:

$$\vec{\chi}(t) = \int_0^t \widetilde{G}(t,t')\ \vec{F}(t')dt' \tag{2.19}$$

We look for for a solution to the Green function of the form

$$\widetilde{G}(t,t') = \left(\widetilde{C}^{(1)}\ \widetilde{\chi}^{(1)}(t-t') + \widetilde{C}^{(2)}\ \widetilde{\chi}^{(2)}(t-t')\right)\ \eta(t-t') \tag{2.20}$$

where $\widetilde{C}^{(1)}$ and $\widetilde{C}^{(2)}$ are matrices to be determined, $\eta(t-t')$ is the Heaviside step function. and

$$\widetilde{\chi}^{(1)}_{ij} = (\chi^{(1)}_i)_j \ \ and \ \ \widetilde{\chi}^{(2)}_{ij} = (\chi^{(2)}_i)_j \tag{2.21}$$

particularly, $(\chi^{(\alpha)}_i)_j$ is the j^{th} component of the i^{th} solution $\chi^{(\alpha)}_i$ to the homogeneous equation of motion eq.2.5, and $\alpha\ \epsilon\ \{1,2\}$.

We introduce the operator $\widetilde{\Omega}$ such that

$$\widetilde{\Omega} = \widetilde{M}\ \frac{\partial^2}{\partial t^2} + \widetilde{\Gamma}\ \frac{\partial}{\partial t} + \widetilde{K} \tag{2.22}$$

Eq.2.18 reduces to

$$\widetilde{\Omega}\widetilde{G} = \widetilde{1}\ \delta(t-t') \tag{2.23}$$

inserting eq.2.20 in eq.2.23 produces:

$$
\begin{aligned}
&\widetilde{\Omega}\ G(t,t') = \\
&\eta(t-t')\ \widetilde{\Omega}\ \left[\widetilde{C}^{(1)}\ \widetilde{\chi}^{(1)}(t-t') + \widetilde{C}^{(2)}\ \widetilde{\chi}^{(2)}(t-t')\right] \\
&+2\widetilde{M}\ \frac{\partial}{\partial t}\left[\widetilde{C}^{(1)}\ \widetilde{\chi}^{(1)}(t-t') + \widetilde{C}^{(2)}\ \widetilde{\chi}^{(2)}(t-t')\right]\delta(t-t') \\
&+\widetilde{M}\left[\widetilde{C}^{(1)}\ \widetilde{\chi}^{(1)}(t-t') + \widetilde{C}^{(2)}\ \widetilde{\chi}^{(2)}(t-t')\right]\ \delta'(t-t') \\
&+\Gamma\ \left[\widetilde{C}^{(1)}\ \widetilde{\chi}^{(1)}(t-t') + \widetilde{C}^{(2)}\ \widetilde{\chi}^{(2)}(t-t')\right]\delta(t-t') \\
&= \widetilde{1}\ \delta(t-t')
\end{aligned}
\tag{2.24}
$$

At $(t-t'=0)$ We want this to equal the identity matrix $\widetilde{1}$. This will happen if

$$
\begin{aligned}
&\widetilde{C}^{(1)}\ \widetilde{\chi}^{(1)}(0) + \widetilde{C}^{(2)}\ \widetilde{\chi}^{(2)}(0) = 0 \\
&\left(\widetilde{C}^{(1)}\ \widetilde{\dot{\chi}}^{(1)}(0) + \widetilde{C}^{(2)}\ \widetilde{\dot{\chi}}^{(2)}(0)\right)_{ij} = \frac{1}{2}\delta_{ij}\widetilde{M}^{-1}_{ij}
\end{aligned}
\tag{2.25}
$$

This is a set of $2\ N^2$ variables $\widetilde{C}^{\alpha}_{ij}$ where $\alpha\ \epsilon\ \{1,2\}$ and $2\ N^2$ separate equations. This problem is solvable and the solution can be found numerically. Once these coefficients are found the displacement of particles as a function of time can be constructed out of the solution in eq.2.19.

2.2.2 Thermal Heat Flux

In this section we develop an expression of the thermal heat flux as a function of the hot and cold bath temperatures using the steady state solution to the

displacements found in section 2.2.1; eq.2.19. We will use the result derived in appendix A.1; eq. (A7) as an expression of the heat flux j_{ij} between particles i and j.

$$\begin{aligned} aj_{ij} = & \frac{\partial V_{ij}}{\partial x_i}\ \dot{x}_i + \frac{\partial V_{ij}}{\partial y_i}\ \dot{y}_i + \frac{\partial V_{ij}}{\partial z_i}\ \dot{z}_i \\ & -\frac{\partial V_{ij}}{\partial x_j}\ \dot{x}_j - \frac{\partial V_{ij}}{\partial y_j}\ \dot{y}_j - \frac{\partial V_{ij}}{\partial z_j}\ \dot{z}_j \end{aligned} \tag{2.26}$$

where

$$V_{ij} = (x_i, y_i, z_i) \begin{bmatrix} K_{3i-2,3j-2} & K_{3i-2,3j-1} & K_{3i-2,3j} \\ K_{3i-1,3j-2} & K_{3i-1,3j-1} & K_{3i-1,3j} \\ K_{3i,3j-2} & K_{3i,3j-1} & K_{3i,3j} \end{bmatrix} \begin{pmatrix} x_j \\ y_j \\ z_j \end{pmatrix} \tag{2.27}$$

and (x_i, y_i, z_i) and (x_j, y_j, z_j) are the components of the displacements of particles i and j respectively. The K's are the elements of the K matrix involving the displacements of particles i and j.

$$\begin{aligned} aj_{ij} = & K_{3i-2,3j-2}(x_j\dot{x}_i - x_i\dot{x}_j) + K_{3i-1,3j-1}(y_j\dot{y}_i - y_i\dot{y}_j) \\ & + K_{3i,3j}(z_j\dot{z}_i - z_i\dot{z}_j) + K_{3i-2,3j-1}(y_j\dot{x}_i - x_i\dot{y}_j) \\ & + K_{3i-1,3j-2}(x_j\dot{y}_i - y_i\dot{x}_j) + K_{3i-2,3j}(z_j\dot{x}_i - x_i\dot{z}_j) \\ & + K_{3i,3j-2}(x_j\dot{z}_i - z_i\dot{x}_j) + K_{3i-1,3j}(z_j\dot{y}_i - y_i\dot{z}_j) \\ & + K_{3i,3j-1}(y_j\dot{z}_i - z_i\dot{y}_j) \end{aligned} \tag{2.28}$$

Now that we have a working expression of the thermal heat flux j_{ij}, the next step is to replace the site displacement and velocities, by the steady state solution eq.2.19 and its time derivative. In fact all the terms in parentheses in eq.2.28 are

of the form $I_{ij} = (\dot{\vec{\chi}})_{3i-l}(\vec{\chi})_{3j-s} - (\dot{\vec{\chi}})_{3j-s}(\vec{\chi})_{3i-l}$, where (s, l) are integers between 1 and 3. Which is also expressed as.

$$I_{3i-l,3j-s} = \sum_{mn}$$

$$\int_0^t dt_1 \int_0^t dt_2 \; \dot{\widetilde{G}}_{3i-l,m}(t-t_1)\widetilde{G}_{3j-s,n}(t-t_2)F_m(t_1)F_n(t_2) \tag{2.29}$$

$$-\int_0^t dt_1 \int_0^t dt_2 \; \widetilde{G}_{3i-l,m}(t-t_1)\dot{\widetilde{G}}_{3j-s,n}(t-t_2)F_m(t_1)F_n(t_2)$$

using eq.2.4, and noting that we are only applying a driving force to the first and last particles. Eq.2.29 reduces to

$$I_{3i-l,3j-s} =$$

$$2\gamma_N kT_N \sum_{n=1}^{3} \int_0^t dt_1 \widetilde{G}_{3i-l,3N-n}(t-t_1)\dot{\widetilde{G}}_{3j-s,3N-n}(t-t_1) \tag{2.30}$$

$$-2\gamma_1 kT_1 \sum_{m=1}^{3} \int_0^t dt_1 \widetilde{G}_{3i-l,m}(t-t_1)\dot{\widetilde{G}}_{3j-s,m}(t-t_1)$$

and eq.2.28 becomes

$$j_{ij} = \sum_{l=1}^{3}\sum_{s=1}^{3} \frac{K_{3i-l,3j-s}}{a} \; I_{3i-l,3j-s} \tag{2.31}$$

Let S_{ij} and S'_{ij} be the coefficients of T_1 and T_N in eq.2.30

$$S'_{ij} = 2\gamma_N k \sum_{n=1}^{3} \int_0^t dt_1 \widetilde{G}_{i3N-n}(t-t_1)\dot{\widetilde{G}}_{j3N-n}(t-t_1)$$

$$S_{ij} = 2\gamma_1 k \sum_{m=1}^{3} \int_0^t dt_1 \widetilde{G}_{im}(t-t_1)\dot{\widetilde{G}}_{jm}(t-t_1) \tag{2.32}$$

Eq.2.31 reduces to

$$j_{ij} = T_N \sum_{l=1}^{3}\sum_{s=1}^{3} \frac{K_{3i-l,3j-s}}{a}\ S'_{3i-l,3j-s} - \\ T_1 \sum_{l=1}^{3}\sum_{s=1}^{3} \frac{K_{3i-l,3j-s}}{a}\ S_{3i-l,3j-s} \tag{2.33}$$

The coefficients of T_1 and T_N in eq.2.33 can be calculated numerically using the expression of the Green functions found in section 2.2.1; eq.2.20. In principle we can apply the Langevin driving force to any of the atoms in the system. In order to estimate the thermal conductivity we choose to couple to atoms at the furthest extremes of the chain. The rationale is that they are furthest from the stiffer incorporated molecule and thus best connected to the fluctuating heat bath.

The localized heat flux j_i is the sum of all the individual contributions from the sites j nearest to i:

$$j_i = \sum_j j_{ij} \tag{2.34}$$

The total heat flux is the sum of the localized contribution

$$j = \sum_i j_i = \sum_{ij} j_{ij} = D_h\ T_N - D_c\ T_1 \tag{2.35}$$

where

$$D_h = \sum_{ij}\sum_{sl=1}^{3} \frac{K_{3i-l,3j-s}}{a}\ S'_{3i-l,3j-s} \\ D_c = \sum_{ij}\sum_{sl=1}^{3} \frac{K_{3i-l,3j-s}}{a}\ S_{3i-l,3j-s} \tag{2.36}$$

We will numerically show in section 2.3 that the total heat flux j in eq.2.35

is proportional to the temperature difference of the hot and cold baths (i.e., $D_h = D_c$).

2.2.3 Participation Ratio

In order to better understand how to optimize structures we find it useful to calculate the participation ratio (P) [25]. This quantity is commonly used in electronic problems to describe the degree to which an electron is localized in space [1]. The participation ratio is defined as

$$P = \frac{\left(\sum_{n=1}^{n=N} {\psi_n}^2\right)^2}{L^d \sum_{n=1}^{n=N} {\psi_n}^4} \tag{2.37}$$

where N is the total number of modes, $\mid \psi >$ is the eigenvector describing the normal mode, L the system linear size and d is the Euclidean dimension of the system, giving the total number of atoms $L^d = N$.

The participation ratio is in the order of 1 for extended modes and $\approx 1/N$ for localized modes. The intuition is that systems with more low energy, high participation ratio modes will be better at conducting heat.

2.3 Application

In this section we shall present the application of the results of section 2.2 for two special cases, a one dimensional linear chain and a small two dimensional functionalized sheet of graphene.

2.3.1 One Dimensional Chain

Consider a linear chain of N coupled atoms, the first and the last of which interact with heat baths. The schematic diagram of this set up is drawn in Fig.2.1 for $N = 4$. For simplicity Only nearest neighbor interactions will be considered and

it is assumed that adjacent atoms are coupled with springs of spring constant K. Let x_l be the displacement of the l^{th} particle. The hamiltonian of this system is

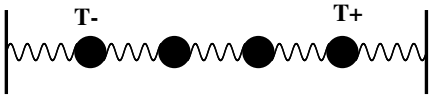


Figure 2.1: A pictorial representation of a linear chain of $N = 4$ mutually coupled oscillators in interaction with two thermal reservoirs working at different temperatures. Here $T_1 = T_+$ and $T_N = T_-$.

$$H = \sum_i \frac{{p_i}^2}{2m} + \frac{1}{2}K(x_{i+1} - x_i)^2 \tag{2.38}$$

where m is the mass of the particles. We set $m = a = 1$, where a is the lattice constant, and $K = 1$.

In this one dimensional case eq.2.26 and eq.2.30 reduce to:

$$j_{ij} = \left(\frac{K}{a}\right)(x_j\dot{x}_i - x_i\dot{x}_j) = \left(\frac{K}{a}\right) I_{ij} \tag{2.39}$$

where

$$\begin{aligned} I_{ij} = {} & 2\gamma_N k T_N \int_0^t dt_1 \widetilde{G}_{iN}(t - t_1)\dot{\widetilde{G}}_{jN}(t - t_1) \\ & -2\gamma_1 k T_1 \int_0^t dt_1 \widetilde{G}_{i1}(t - t_1)\dot{\widetilde{G}}_{j1}(t - t_1) \end{aligned} \tag{2.40}$$

The total heat flux is

$$j = \sum_{ij} j_{ij} = \left(\frac{K}{a}\right) \sum_{ij} I_{ij} = D_h T_N - D_c T_1 \tag{2.41}$$

where

$$D_h = 2\gamma_N k \left(\frac{K}{a}\right) \sum_{ij} \int_0^t dt_1 \widetilde{G}_{iN}(t-t_1)\dot{\widetilde{G}}_{jN}(t-t_1)$$
$$Dc = 2\gamma_1 k \left(\frac{K}{a}\right) \sum_{ij} \int_0^t dt_1 \widetilde{G}_{i1}(t-t_1)\dot{\widetilde{G}}_{j1}(t-t_1) \tag{2.42}$$

Fig.2.2 is a plot of the coefficients of T_N and T_1 in eq.2.41 as a function of time for a chain of 4 atoms. As illustrated these coefficients converge to the same value. This means that in the steady state regime the total heat flux j is proportional to the temperature difference of the hot and cold baths, the proportionality constant is the thermal conductance of the chain λ_c and .

$$j = \lambda_c (T_N - T_1) \tag{2.43}$$

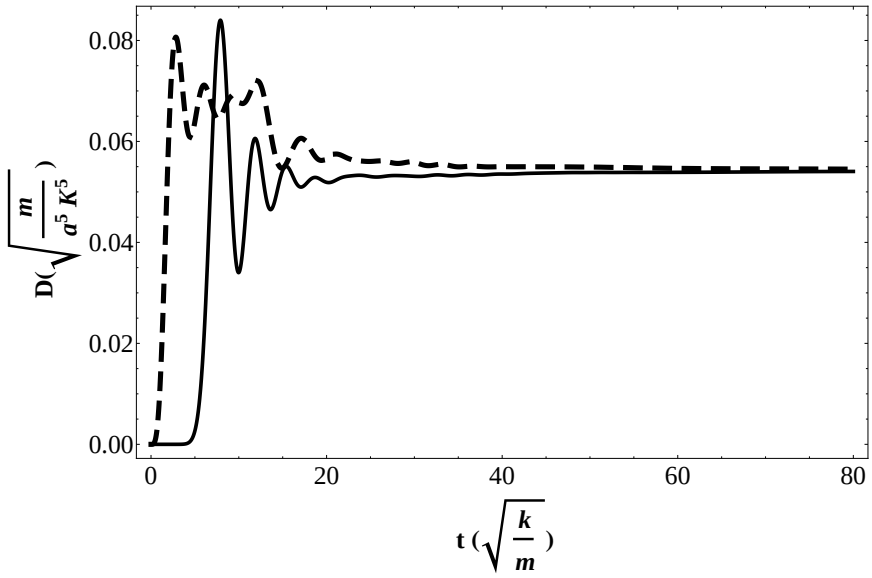


Figure 2.2: $\left(D_h = \frac{K}{a}\sum_{ij} S'_{ij}\right)$, and $\left(D_c = \frac{K}{a}\sum_{ij} S_{ij}\right)$ as a function of time (t) for a chain of 4 atoms. As expected these factors converge to the same value, This means that in the steady state regime the total heat flux j is proportional to the temperature difference of the hot and cold baths.

2.3.2 Two Dimensional Sheet of Graphene

In this application we consider a hexagonal sheet of graphene made of 36 carbon atoms bonded together in a honeycomb structure. We attach two alkane chains to opposite boundaries of the graphene sheet and to the heat baths as shown in fig.2.3. The alkane chains are n-pentane. The Tersoff-Berner (TB) force field [33, 34] is used to describe the interactions among the atoms in the graphene sheet. The Nath, Escobedo, and Pablo revised (NERD) [15**?**] potential is used to describe the interactions in the chains and the bond between the chains and the graphene.

We relax the system by minimizing the site potential in the functionalized graphene sheet, this is done by using a multiobjective optimization technique[32]. Additional information about the (TB) and (NERD) force fields are found in Appendix B.

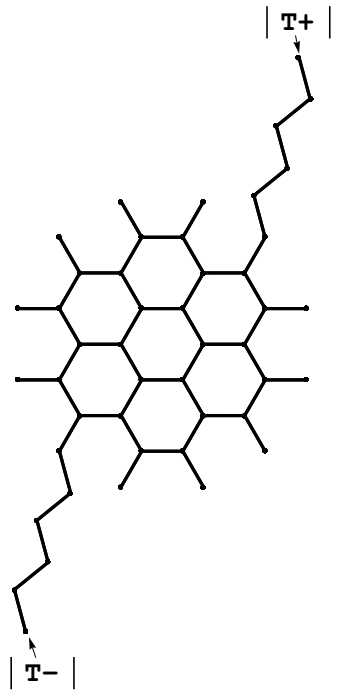


Figure 2.3: A pictorial representation of a functionalized sheet of graphene. The number of atoms in the graphene sheet is 36, The alkane chains are n-pentane. The end of the chains interact with two thermal reservoirs working at different temperatures.

The next step to solving the problem of heat conduction in the functionalized graphene is to find the normal modes of the structure. At this point we assume that the site displacements are very small and approximate the potential (E) by a second order Taylor expansion around the sites equilibrium positions.

$$E = \frac{1}{2} \sum_{ij} \frac{\partial^2 V}{\partial \zeta_i \, \partial \zeta_j} \, \zeta_i \, \zeta_j \tag{2.44}$$

the second derivatives of the potential energy are the elements of the $\widetilde{K}$ matrix that was introduced in section 2.2

$$\widetilde{K}_{ij} = \frac{\partial^2 V}{\partial \zeta_i \, \partial \zeta_j} \tag{2.45}$$

We then proceed as described in section 2.2 and solve for the Green function and the particles displacement in the stationary regime. We numerically calculate the heat flux from eqs.2.26, 2.30, 2.34, 2.35 as a function of the hot and cold bath temperatures.

2.3.2.1 Numerical results of thermal heat flux in functionalized graphene

The total heat flux in the functionalized graphene sheet was numerically calculated. Fig.2.4 represents the time evolution of the ratio of the hot and cold temperature coefficients (D_h) and (D_c) in eq.2.35 and the thermal conductance of the graphene (λ_g) calculated using the same technique by taking the chains off the graphene and attaching two opposite sites to hot and cold baths. As expected, in the steady state regime these factors converge to the same value. This confirms as in the previous case of linear chains that the heat flux is proportional to the temperature difference of the hot and cold baths. The proportionality constant is the thermal conductance of the functionalized grapehene.

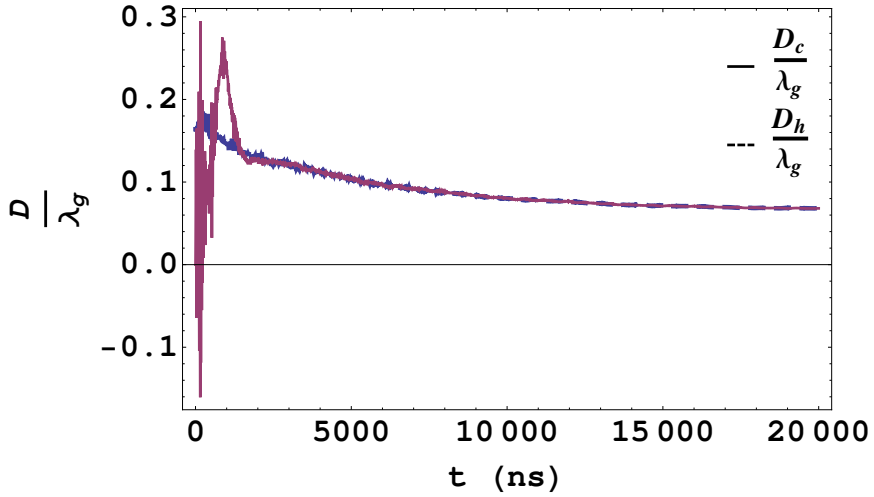


Figure 2.4: (a) Time evolution of (D_h/λ_g) and (D_c/λ_g) eq.2.42. As expected (D_h/λ_g) and (D_c/λ_g) converge to the same value, This means that in the steady state regime the total heat flux is proportional to the temperature difference of the hot and cold baths.

2.3.2.2 Effect of changing the length of the chains on the thermal conduction

In this section we shall use the technique just developed to investigate the effect of changing the length of the chains on the thermal conduction of heat throughout the functionalized graphene. Fig.2.5 summarizes the results of thermal conductance for chain lengths between $N = 3$ and $N = 11$. In each case we connect two identical chains on opposite sides of the boundaries to the graphene sheet. The opposite ends of each chain are connected to two heat baths at temperatures $T+$ and $T-$. Based on these results functionalized graphene with odd alkane chains performs better in terms of thermal conductance than with even alkane chains. For each type of chains, the thermal conductance increases with the chain length for smaller alkane chains but then decreases with longer chains.

To understand the underlying causes of this results, we calculated the participation ratio (P) for each normal mode in each configuration. The extended modes, the main contributor to the heat transport can be identified by their higher participation ratios. In contrary low participation ratio modes contribute

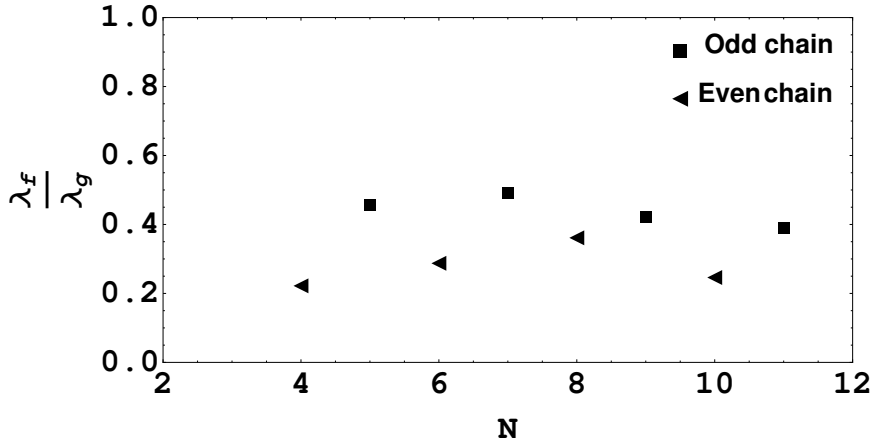
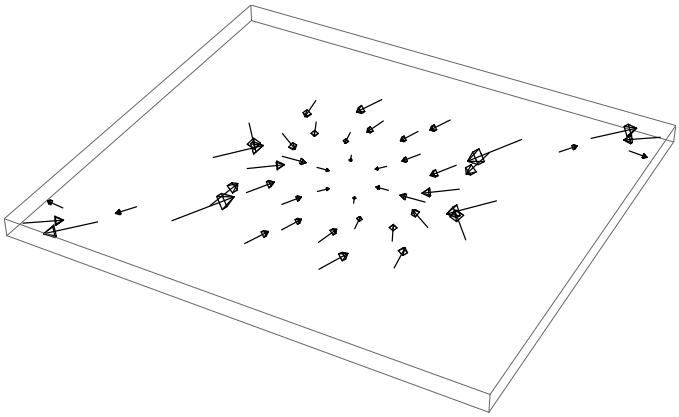


Figure 2.5: The ratio of the Thermal conductance of functionalized graphene λ_f to the thermal conductance of graphene λ_g as a function of chain length.

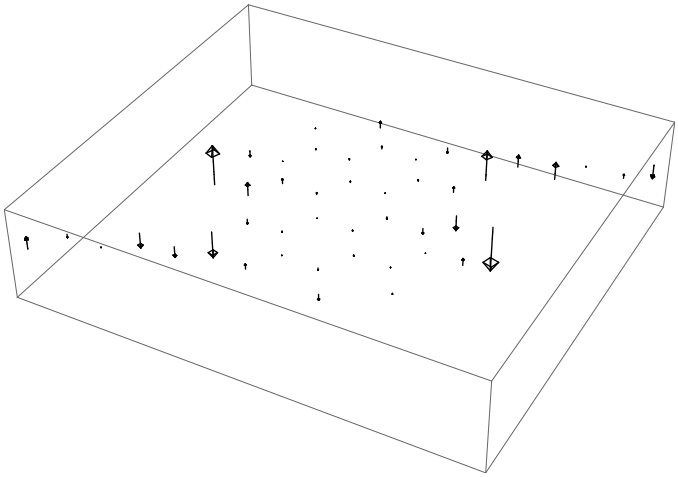
less to the heat transport. Fig.2.6 is a pictorial representation of the site displacements of a high and low participation ratio mode for the structure in fig.2.3, note the larger magnitude of the site displacement, and the extent of the mode with larger participation ratio. Fig.2.7 represents the total number of modes with increasing participation ratio for configurations similar to the structure in fig.2.3 with five, six, and eight chain sites ($N = 5, 6, 8$), note that the number of extended modes with high participation ratios decreases with the increase in the size of the chains. This is fairly noticeable for longer chains, and in fact explains the longer chains smaller thermal conductance. Particularly for even and odd chains as shown in fig.2.7(a) this pattern also include some of the low participation ratio modes. Odd chains perform better than even chains in conducting heat because of their larger number of moderate and high participation ratio modes contributing to the heat transport.

2.4 Conclusion

Improving heat transport in functionalized graphene is important to a large number of systems. In this chapter we have demonstrated an efficient and straightforward method for calculating the thermal heat flux. The results of this simulation



(a)

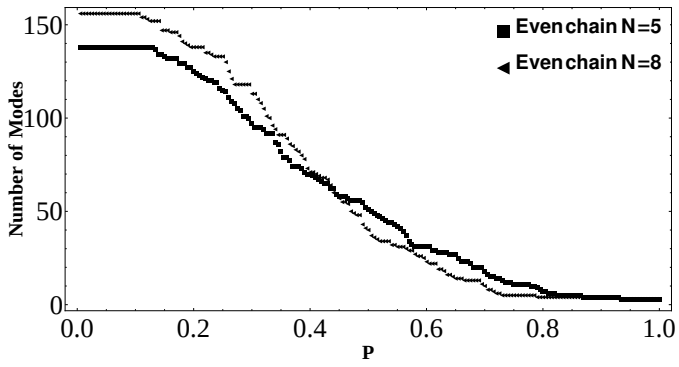


(b)

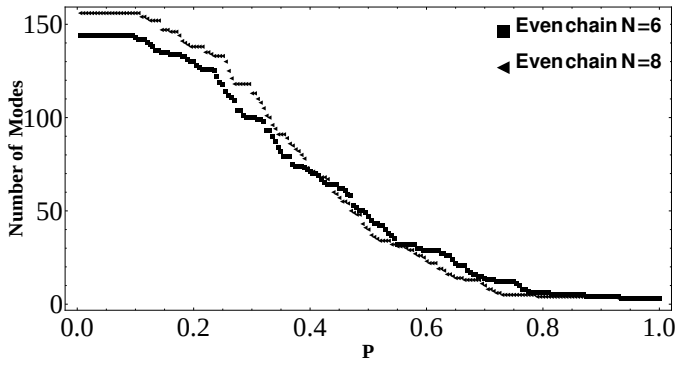
Figure 2.6: Pictorial representation of a high participation ratio mode ($P = 0.86$) (a), and a low participation ratio mode ($P = 0.13$).

can be used to design and test different configurations and to find the one that conveys the largest amount of heat. As an application of this method We investigated the effect of changing the length of the chains on the overall thermal conduction. The numerical results showed that odd alkane chains perform better than even alkane chains. In addition, very long alkane chains deteriorate the overall heat transport. This can be seen as the limit of simply embedding the stiff material in a very soft, infinite matrix.

There are many ways this approach can be expanded. For ease of application we chose to only drive the outermost ends of the functionalized chains. This can



(a)



(b)

Figure 2.7: Number of modes with increasing participation ratios for functionalized graphene configurations with five, six and eight chain sites.

easily be expanded to include driving many or all of the atoms in the system. However, the Langevin approach assumes complete incoherence between all the driving forces. This will not be true on an atomic level since the local phonon environment will have some non-zero coherence length. The physical details of the local environment and its coherence are interesting in their own right, but should not profoundly change results found in this approach: systems in which the external chains are well-coupled to the main structure will still have superior thermal conductivity to those that do not.

A more critical problem in this approach is that is entirely classical. This in part by design, since we produce systems of equations that are rapidly, and easily soluble. However, the Langevin equation is well known to produce equipartition.[14] This means that all modes, even those with extremely high frequency, will have

a non-zero occupation. This probably results in an overestimate of the thermal conductivity since some high participation modes may have too high an energy to have any occupation at room temperature. Mathematically, this arises from the assumption of a delta-function correlation in time for the driving forces, since all frequencies must be included to have zero correlation time. Possible solutions include using a more complicated set of driving forces that are explicitly quantum mechanical,[31] and inserting a fictitious correlation time into the driving force (Ornstein-Uhlenbeck noise) that is itself chosen to be temperature dependent to mimic the effect of a Bose-Einstein suppression of high energy modes.

Chapter 3

Normal Mode Analysis with Thermal Colored Noise

3.1 Introduction

In nature, white noise does not occur. It is an idealization used in our imperfect description of real phenomena. A more adequate description would be based on correlated noise[22, 8]. In this chapter we study the heat transport in carbon based macromolecules using the generalized Langevin equations with memory kernel and Gaussian colored noise. Traditionally the term 'colored noise' is used for noise source with a frequency-dependent power spectrum in analogy to the spectrum of light. The interactions within the system are linearized and the memory kernel is assumed exponentially decaying over time. This is in fact an extension of the previous analysis developed in chapter.2, where now we include means to suppress high frequency modes through the noise correlation time. In addition, we can incorporate quantum driving forces that are temperature dependent to mimic the effect of Bose-Einstein suppression of high energy modes. We show that by branching the functional groups, and by optimizing the participation ratios of the different modes, one can in fact identify the configuration of the functional groups that best drive the heat to the macromolecule.

3.2 Analytical Technique

In this section, we shall develop the general Langevin formalism that we apply to a specific system in section 3.3. We shall present this general case first and then indicate briefly how the results will simplify for our special cases.

Consider a system made of N particles connected by springs. We will apply a driving random Gaussian force to the first and last particles (thermal colored

noise). Each particle obeys the equation of motion:

$$m_i\ \ddot{x_i}(t) = -\sum_j K_{ij}\ x_j(t) + \left(-\int_0^t dt' K(t-t')\ \dot{x}_i(t') + F_i(t)\right)(\delta_{i,1}+\delta_{i,N}) \quad (3.1)$$

where m_i, x_i,respectively are the mass and displacement of particle i, K_{ij} is the spring constant between particles i and j, $F_i(t)$ is the Langevin force on particle i, the overhead dot refers to time derivative, and δ_{ij} is the Kronecker delta function restricting the driving and damping to the first and last particles.

In solving the equations of motion eq.3.1 we consider two special cases. The classical approximation, where the noise is determined classically from the unknown initial positions and momenta of the particles in the bath according to Botzmann statistics. The quantum mechanical approximation, where the noise is interpreted quantum mechanically from the unknown initial positions and momenta of the different quantum oscillators in the bath according to Bose-Einstein statistics.

3.2.1 Classical noise

In this section, we shall solve the generalized equations of motion in the classical approximation. From the results developed in chapter 1, the noise term ($F(t)$) is related to the memory kernel by the fluctuation-dissipation theorem eq.3.2

$$\langle F_i(t)F_j(t')\rangle = \delta_{ij}k_BTK(t-t') \quad (3.2)$$

Particularly, for exponentially correlated noise, also known as Ornstein Uhlenbeck (O-U) noise, the random Gaussian force F(t) has a finite correlation time τ.

$$\begin{aligned} \langle F_i(t) \rangle &= 0 \\ \langle F_i(t)\ F_j(t') \rangle &= 2\frac{\gamma_i}{\tau}\delta_{ij} k_B T e^{-|t-t'|/\tau} \end{aligned} \tag{3.3}$$

Notice from fig.3.1 that as $\tau \rightarrow 0$ $e^{-|t-t'|/\tau}$ approximates a delta function and the correlation function in eq.3.3 reduces to $2\gamma_i\ \delta_{ij} k_B T \delta(t-t')$ and thus we recover the white-noise of eq.2.4. In practice approximate values of (γ) and (τ) appropriate for each medium can be determined from molecular dynamics simulations on a single particle Appendix.C.

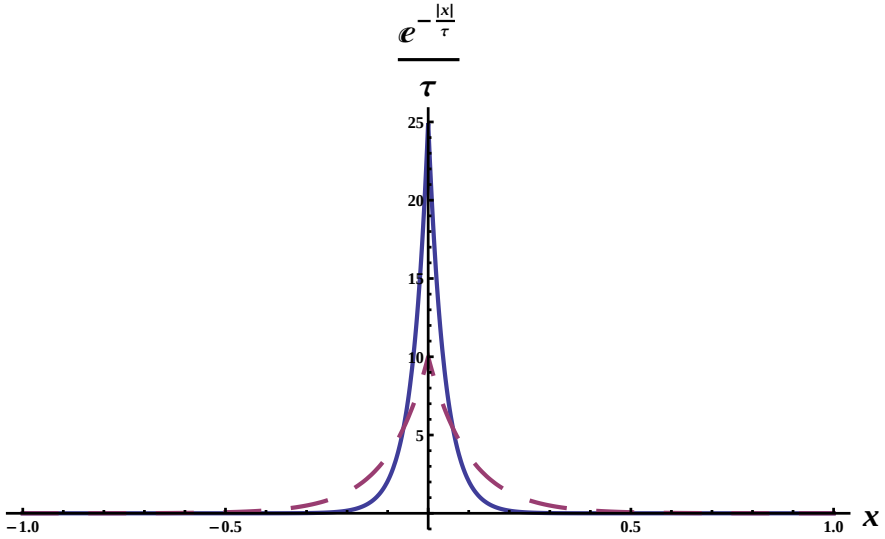


Figure 3.1: $e^{-|t|/\tau}$ as a function of t for different values of the parameter τ. The solid line ($\tau = 0.04$), the dashed line ($\tau = 0.1$)

Starting with the equation of motion and including the exponentially decaying kernel

$$m_i\ \ddot{x}_i(t) = -\sum_j K_{ij}\ x_j(t) + \left(-\int_0^t dt' \frac{\gamma_i}{\tau} e^{-|t-t'|/\tau}\ \dot{x}_i(t') + F_i(t) \right) (\delta_{i,1} + \delta_{i,N}) \tag{3.4}$$

We can easily extend the space of variables to a four dimensional space. The fourth variable $y_i(t)$ is the damping force such that

$$y_i(t) = \frac{\gamma_i}{\tau} \int_0^t dt' e^{-|t-t'|/\tau}\ \dot{x}_i(t') \tag{3.5}$$

our equations of motion eq.3.4 become:

$$\begin{aligned}
\dot{x}_i &= \frac{p_i(t)}{m_i} \\
\dot{p}_i(t) &= -\sum_j K_{ij}\ x_j(t) + [-y_i(t) + F_i(t)]\,(\delta_{i,1} + \delta_{i,N}) \\
\dot{y}_i(t) &= -\frac{1}{\tau} y_i(t) + \frac{\gamma_i}{m_i \tau} p_i(t) \\
\dot{F}_i(t) &= -\frac{1}{\tau} F_i(t) + \frac{\sqrt{2\gamma_i k_B T_i}}{\tau}\ \Gamma_i(t)
\end{aligned} \tag{3.6}$$

where the last equation describes O-U noise with the correlation function eq.3.3, and $\Gamma_i(t)$ is a Gaussian white noise, with

$$\langle \Gamma_i(t) \Gamma_j(t') \rangle = \delta_{ij} \delta(t - t') \tag{3.7}$$

This four equations can be reduced to a set of three equations if we introduce the variable $Y_i(t) = F_i(t) - y_i(t)$

$$\begin{aligned}
\dot{x}_i &= \frac{p_i(t)}{m_i} \\
\dot{p}_i(t) &= -\sum_j K_{ij}\ x_j(t) + Y_i(t)(\delta_{i,1} + \delta_{i,N}) \\
\dot{Y}_i(t) &= -\frac{1}{\tau} Y_i(t) - \frac{\gamma_i}{m_i \tau} p_i(t) + \frac{\sqrt{2\gamma_i k_B T_i}}{\tau}\ \Gamma_i(t)
\end{aligned} \tag{3.8}$$

This problem however, can be simplified even further if we introduce a new vector $\vec{S}$ such as

$$\vec{S} = (x_1, ...x_N, p_1, ...p_N, Y_1, 0....., 0, Y_N) \tag{3.9}$$

The previous equations (eq.3.8) can be written in the form

$$\dot{\vec{S}} = \widetilde{A} \cdot \vec{S} + \vec{\Gamma} \tag{3.10}$$

where $\vec{\Gamma} = (0, ..., 0, 0, ..., 0, \frac{\sqrt{2\gamma_1 k_B\ T}}{\tau}\Gamma_1, 0, ..., \frac{\sqrt{2\gamma_N k_B T}}{\tau}\ \Gamma_N)$, $\widetilde{A}$, $\widetilde{\Lambda}$ and $\widetilde{R}$ are defined as:

$$\widetilde{A} = \begin{pmatrix} \widetilde{0} & \widetilde{M^{-1}} & \widetilde{0} \\ -\widetilde{K} & \widetilde{0} & \widetilde{R} \\ \widetilde{0} & -\widetilde{\Lambda} \cdot \widetilde{M^{-1}}/\tau & -\widetilde{R}/\tau \end{pmatrix} \tag{3.11}$$

where

$$\widetilde{\Lambda} = \begin{pmatrix} \gamma_1 & 0 & ... & 0 \\ 0 & 0 & ... & 0 \\ 0 & 0 & ... & \gamma_N \end{pmatrix} \qquad \widetilde{R} = \begin{pmatrix} 1 & 0 & ... & 0 \\ 0 & 0 & ... & 0 \\ 0 & 0 & ... & 1 \end{pmatrix} \tag{3.12}$$

The differential equation eq.3.10 can be transformed into a simple eigenvalue problem where the general solution can be formulated using an adequate Green function. The following are the steps to getting this solution.

If $\widetilde{\theta}$ is the matrix of right (column) eigenvectors of the matrix $\widetilde{A}$, we first transform $\vec{S}$ with the rotation matrix $\widetilde{\theta}$ such that $\vec{S} = \widetilde{\theta}\vec{X}$. Replacing $\vec{S}$ with its new expression in eq.3.10 gives

$$\widetilde{\theta}\dot{\vec{X}} = \widetilde{A}\ \widetilde{\theta}\ \vec{X} + \vec{\Gamma} \tag{3.13}$$

which can be transformed to

$$\dot{\vec{X}} = (\widetilde{\theta}^{-1}\widetilde{A}\widetilde{\theta}) \cdot \vec{X} + \widetilde{\theta}^{-1}\vec{\Gamma} \tag{3.14}$$

If $(\widetilde{\theta}^{-1}\ \widetilde{A}\ \widetilde{\theta})$ is diagonal the previous problem reduces to a first order differential equation for the components of $\vec{X}$ of the form

$$\dot{X}_i = a_i X_i + (\widetilde{\theta}^{-1}\vec{\Gamma})_i \tag{3.15}$$

where a_i is the i^{th} eigenvalue of the matrix $\widetilde{A}$. The solution to this equation is known and is of the form:

$$X_i(t) = e^{a_i t}\ \left(\int_0^t d\tau_1 ! e^{-a_i\tau_1}\ (\widetilde{\theta}^{-1}\vec{\Gamma})_i\ +\ X_{io}\right) \tag{3.16}$$

If we take $\vec{S}(t=0) = 0$ then $X_{io} = 0$ and eq.3.16 reduces to

$$X_i(t) = e^{a_i t}\ \left(\int_0^t d\tau_1\ e^{-a_i\tau_1}\ (\widetilde{\theta}^{-1}\vec{\Gamma})_i(\tau_1)\right) \tag{3.17}$$

We can return to the original variables $\vec{S}$ from $\vec{S} = \widetilde{\theta}\vec{X}$. This results in

$$S_i(t) = \sum_k \widetilde{\theta}_{ik} X_k(t) = \sum_k \widetilde{\theta}_{ik} e^{a_k t}\ \left(\int_0^t d\tau_1\ e^{-a_k\tau_1}\ (\widetilde{\theta}^{-1}\vec{\Gamma})_k(\tau_1)\right) \tag{3.18}$$

where

$$(\widetilde{\theta}^{-1}\vec{\Gamma})_k = \widetilde{\theta}^{-1}_{k,2N+1}\Gamma_{2N+1} + \widetilde{\theta}^{-1}_{k,3N}\Gamma_{3N} \tag{3.19}$$

and

$$S_i(t) = \sum_k \widetilde{\theta}_{ik}\widetilde{\theta}^{-1}_{k,2N+1}\ e^{a_k t}\ \int_0^t d\tau_1\ e^{-a_k\tau_1}\ \Gamma_{2N+1}(\tau_1) + \sum_k \widetilde{\theta}_{ik}\widetilde{\theta}^{-1}_{k,3N}\ e^{a_k t}\ \int_0^t d\tau_1\ e^{-a_k\tau_1}\Gamma_{3N}(\tau_1) \tag{3.20}$$

The actual motion however is the real part of this complex solution $S^r{}_i(t) = (S_i(t) + S^*{}_i(t))/2$. The momentum and displacement are of the form

$$\langle S_i(t_1)S_j(t_2)\rangle = \sum_{k,n=1}^{3N} \widetilde{\theta}_{ik}\ \widetilde{\theta}_{jn}\ \widetilde{\theta}^{-1}_{k,2N+1}\ \widetilde{\theta}^{-1}_{n,2N+1}\ e^{(a_k t_1 + a_n t_2)} \left(\int_0^{t_1} d\tau_1\ \int_0^{t_2} d\tau_2\ e^{-(a_k\tau_1 + a_n\tau_2)}\ \delta(\tau_1-\tau_2)\right) \left(\frac{2\gamma_{2N+1}k_B}{\tau^2}T_L\right)$$
$$+ \sum_{k,n=1}^{3N} \widetilde{\theta}_{ik}\ \widetilde{\theta}_{jn}\ \widetilde{\theta}^{-1}_{k,3N}\ \widetilde{\theta}^{-1}_{n,3N}\ e^{(a_k t_1 + a_n t_2)} \left(\int_0^{t_1} d\tau_1\ \int_0^{t_2} d\tau_2\ e^{-(a_k\tau_1 + a_n\tau_2)}\ \delta(\tau_1-\tau_2)\right) \left(\frac{2\gamma_{3N}k_B}{\tau^2}T_R\right) \tag{3.21}$$

or

$$\langle S_i(t_1)S_j(t_2)\rangle = \sum_{k,n=1}^{3N} \widetilde{\theta}_{ik}\ \widetilde{\theta}_{jn}\ \widetilde{\theta}^{-1}_{k,2N+1}\ \widetilde{\theta}^{-1}_{n,2N+1}\ e^{(a_k t_1 + a_n t_2)} \left(\int_0^{\min(t_1,t_2)} d\tau_1\ e^{-(a_k+a_n)\tau_1}\right) \left(\frac{2\gamma_{2N+1}k_B}{\tau^2}T_L\right)$$
$$+ \sum_{k,n=1}^{3N} \widetilde{\theta}_{ik}\ \widetilde{\theta}_{jn}\ \widetilde{\theta}^{-1}_{k,3N}\ \widetilde{\theta}^{-1}_{n,3N}\ e^{(a_k t_1 + a_n t_2)} \left(\int_0^{\min(t_1,t_2)} d\tau_1\ e^{-(a_k+a_n)\tau_1}\right) \left(\frac{2\gamma_{3N}k_B}{\tau^2}T_R\right) \tag{3.22}$$

The above result can be extended to include additional driven sites as

$$\langle S_i(t_1)S_j(t_2)\rangle =$$

$$\sum_{k,n=1}^{3N}\left(\sum_{\alpha}\widetilde{\theta}_{ik}\ \widetilde{\theta}_{jn}\ \widetilde{\theta}^{-1}_{k,\alpha}\ \widetilde{\theta}^{-1}_{n,\alpha}\right)\ e^{(a_k t_1+a_n t_2)}\left(\int_0^{\min(t_1,t_2)} d\tau_1\ e^{-(a_k+a_n)\tau_1}\right)\left(\frac{2\gamma_\alpha k_B}{\tau^2}T_L\right)$$

$$+\sum_{k,n=1}^{3N}\left(\sum_{\beta}\widetilde{\theta}_{ik}\ \widetilde{\theta}_{jn}\ \widetilde{\theta}^{-1}_{k,\beta}\ \widetilde{\theta}^{-1}_{n,\beta}\right)\ e^{(a_k t_1+a_n t_2)}\left(\int_0^{\min(t_1,t_2)} d\tau_1\ e^{-(a_k+a_n)\tau_1}\right)\left(\frac{2\gamma_\beta k_B}{\tau^2}T_R\right) \tag{3.23}$$

where α runs over the sites in contact with the hot bath and β runs over the sites in contact with the cold bath.

3.2.2 Quantum noise

In this section we shall solve the modified Langevin equations in the quasi-classical approximation. Starting with the equations of motion eq.3.1 with the quantum noise correlation derived in chapter 1 eq.3.24

$$\langle\vec{F}_i(t)\vec{F}_j(t')^t\rangle_{sym} = \delta_{ij}\frac{\gamma_i}{\pi}\int_0^\infty d\omega\frac{\omega}{1+\tau^2\omega^2}\hbar\coth\left[\frac{\hbar\omega}{2kT}\right]\cos\omega(t-t') \tag{3.24}$$

We introduce a new vector $\vec{S}'$ such as

$$\vec{S}' = (x_1,.....x_N,p_1,.....p_N,y_1,0.....,0,y_N) \tag{3.25}$$

The equations of motion can be transformed into

$$\dot{x}_i = \frac{p_i(t)}{m_i}$$

$$\dot{p}_i(t) = -\sum_j K_{ij}\ x_j(t) + \left[-y_i(t) + F_i(t)\right](\delta_{i,1} + \delta_{i,N}) \tag{3.26}$$

$$\dot{y}_i(t) = -\frac{1}{\tau} y_i(t) + \frac{\gamma_i}{m_i \tau} p_i(t)$$

or

$$\dot{\vec{S}}' = \widetilde{A}' \cdot \vec{S}' + \vec{\Pi} \tag{3.27}$$

where

$$\widetilde{A}' = \begin{pmatrix} \widetilde{0} & \widetilde{M^{-1}} & \widetilde{0} \\ -\widetilde{K} & \widetilde{0} & -\widetilde{R} \\ \widetilde{0} & \widetilde{\Lambda} \cdot \widetilde{M^{-1}}/\tau & -\widetilde{R}/\tau \end{pmatrix} \tag{3.28}$$

and

$$\vec{\Pi} = (0, ..., 0, F_1, 0, ...0, F_N, 0, ..., 0,) \tag{3.29}$$

The solution to the equations of motion eq.3.27 follow the same steps of sec.3.2.1 and are of the form

$$S_i(t) = \sum_k \widetilde{\theta'}_{ik} e^{a_k t} \ \left(\int_0^t d\tau_1\ e^{-a_k \tau_1}\ (\widetilde{\theta'}^{-1} \vec{\Pi})_k(\tau_1) \right) \tag{3.30}$$

where

$$(\widetilde{\theta'}^{-1} \vec{\Pi})_k = \widetilde{\theta'}^{-1}_{k,N+1} \Pi_{N+1} + \widetilde{\theta'}^{-1}_{k,2N} \Pi_{2N} \tag{3.31}$$

and $\widetilde{\theta'}$ is is the matrix of right (column) eigenvectors of the matrix $\widetilde{A}'$, and a_i its i^{th} eigenvalue.

$$S_i(t) = \sum_k \widetilde{\theta}_{ik}\widetilde{\theta}^{-1}_{k,N+1}\ e^{a_k t}\ \int_0^t d\tau_1\ e^{-a_k\tau_1}\ \Pi_{N+1}(\tau_1) + \sum_k \widetilde{\theta}_{ik}\widetilde{\theta}^{-1}_{k,2N}\ e^{a_k t}\ \int_0^t d\tau_1\ e^{-a_k\tau_1}\Pi_{2N}(\tau_1) \tag{3.32}$$

The momentum and position correlations can be obtained as

$$\begin{aligned}\langle S_i(t_1)S_j(t_2)\rangle = &\sum_{k,n=1}^{3N} \widetilde{\theta}_{ik}\ \widetilde{\theta}_{jn}\ \widetilde{\theta}^{-1}_{k,N+1}\ \widetilde{\theta}^{-1}_{n,N+1}\ e^{(a_k t_1 + a_n t_2)} \\ &\left(\int_0^{t_1} d\tau_1\ \int_0^{t_2} d\tau_2\ e^{-(a_k\tau_1 + a_n\tau_2)} < \Pi_{N+1}(\tau_1)\Pi_{N+1}(\tau_2) >\right) \\ &+ \sum_{k,n=1}^{3N} \widetilde{\theta}_{ik}\ \widetilde{\theta}_{jn}\ \widetilde{\theta}^{-1}_{k,2N}\ \widetilde{\theta}^{-1}_{n,2N}\ e^{(a_k t_1 + a_n t_2)} \\ &\left(\int_0^{t_1} d\tau_1\ \int_0^{t_2} d\tau_2\ e^{-(a_k\tau_1 + a_n\tau_2)} < \Pi_{2N}(\tau_1)\Pi_{2N}(\tau_2) >\right)\end{aligned} \tag{3.33}$$

or

$$\langle S_i(t_1)S_j(t_2)\rangle =$$
$$\sum_{k,n=1}^{3N} \widetilde{\theta}_{ik}\ \widetilde{\theta}_{jn}\ \widetilde{\theta}^{-1}_{k,N+1}\ \widetilde{\theta}^{-1}_{n,N+1}\ e^{(a_k t_1 + a_n t_2)} \frac{\gamma_{N+1}}{\pi} \int_0^\infty d\omega \frac{\omega}{1+\tau^2\omega^2} \hbar \coth\left[\frac{\hbar\omega}{2kT_L}\right]$$

$$\left(\int_0^{t_1} d\tau_1 \int_0^{t_2} d\tau_2\ e^{-(a_k\tau_1 + a_n\tau_2)} \cos\omega(\tau_1-\tau_2)\right)$$

$$+ \sum_{k,n=1}^{3N} \widetilde{\theta}_{ik}\ \widetilde{\theta}_{jn}\ \widetilde{\theta}^{-1}_{k,2N}\ \widetilde{\theta}^{-1}_{n,2N}\ e^{(a_k t_1 + a_n t_2)} \frac{\gamma_{2N}}{\pi} \int_0^\infty d\omega \frac{\omega}{1+\tau^2\omega^2} \hbar \coth\left[\frac{\hbar\omega}{2kT_R}\right]$$

$$\left(\int_0^{t_1} d\tau_1 \int_0^{t_2} d\tau_2\ e^{-(a_k\tau_1 + a_n\tau_2)} \cos\omega(\tau_1-\tau_2)\right)$$

(3.34)

The above result can be extended to include additional driven sites as

$$\langle S_i(t_1)S_j(t_2)\rangle =$$
$$\sum_{k,n=1}^{3N} \left(\sum_\alpha \frac{\gamma_\alpha}{\pi}\ \widetilde{\theta}_{ik}\ \widetilde{\theta}_{jn}\ \widetilde{\theta}^{-1}_{k,\alpha}\ \widetilde{\theta}^{-1}_{n,\alpha}\right)\ e^{(a_k t_1 + a_n t_2)} \int_0^\infty d\omega \frac{\omega}{1+\tau^2\omega^2} \hbar \coth\left[\frac{\hbar\omega}{2kT_L}\right]$$

$$\left(\int_0^{t_1} d\tau_1 \int_0^{t_2} d\tau_2\ e^{-(a_k\tau_1 + a_n\tau_2)} \cos\omega(\tau_1-\tau_2)\right)$$

$$+ \sum_{k,n=1}^{3N} \left(\sum_\beta \frac{\gamma_\beta}{\pi}\ \widetilde{\theta}_{ik}\ \widetilde{\theta}_{jn}\ \widetilde{\theta}^{-1}_{k,\beta}\ \widetilde{\theta}^{-1}_{n,\beta}\right)\ e^{(a_k t_1 + a_n t_2)} \int_0^\infty d\omega \frac{\omega}{1+\tau^2\omega^2} \hbar \coth\left[\frac{\hbar\omega}{2kT_R}\right]$$

$$\left(\int_0^{t_1} d\tau_1 \int_0^{t_2} d\tau_2\ e^{-(a_k\tau_1 + a_n\tau_2)} \cos\omega(\tau_1-\tau_2)\right)$$

(3.35)

where α runs over the sites in contact with the hot bath and β runs over the sites

in contact with the cold bath.

3.3 Application

In this section we shall present the application of the results of section 3.2 for a one dimensional linear chain and a small sheet of functionalized graphene.

3.3.1 One dimensional linear chain

Consider a linear chain of N coupled atoms, the first and the last of which interact with thermal heat baths. A schematic diagram of this set up is drawn in fig.3.2 for $N = 6$. For simplicity only nearest neighbor interactions will be considered and it is assumed that adjacent atoms are coupled with springs of spring constant K. Let x_l be the displacement of the l^{th} particle. The Hamiltonian of this system is eq.3.36.

$$H = \sum_i \frac{{p_i}^2}{2m_i} + \frac{1}{2}K(x_{i+1} - x_i)^2 \tag{3.36}$$

where m_i is the mass of particle i. We set $m_i = a = 1$, where a is the lattice constant, and $K = 1$.

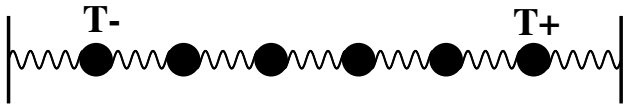


Figure 3.2: A pictorial representation of a linear chain of $N = 6$ mutually coupled oscillators in interaction with two thermal reservoirs working at different temperatures. Here $T_H = T_+$ and $T_C = T_-$.

3.3.1.1 Heat flux: Classical noise

Using the result of eq.3.23 and the definition in appendix A.2 we numerically calculate the coefficients of the hot and cold heat bath temperatures, namely D_h

and D_c respectively according to eq.3.37. Fig.3.3 is a plot of these coefficients as a function of time for a chain of 6 atoms. As illustrated these coefficients converge to identical but opposite values. This means that in the steady state regime the total heat flux j is proportional to the temperature difference of the hot (T_H) and cold (T_C) baths, the proportionality constant is the thermal conductance of the chain λ_c

$$j = D_h\ T_R + D_c\ T_L = \lambda_c(T_H - T_C) \tag{3.37}$$

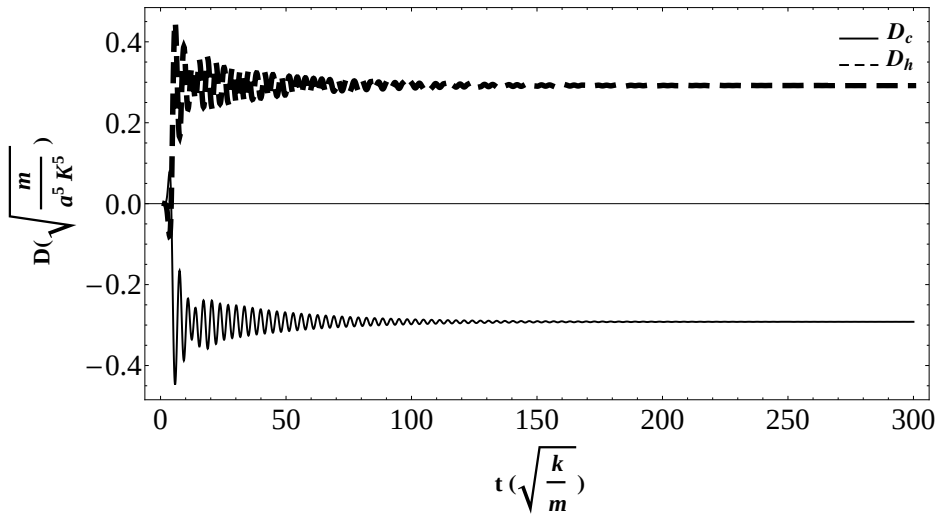


Figure 3.3: (D_h), and (D_c) as a function of time (t) for a chain of 6 atoms with the correlation time $\tau = 0.5$ ($\sqrt{k/m}$). As expected these factors converge to the same but opposite values.

3.3.1.2 Heat flux: Quantum noise

Using the result of eqs.3.35 and the definition in appendix A.2, we numerically calculate the thermal conductance according to eq.3.38. Fig.3.4 is a plot of this property as a function of the temperature for the chain in fig.3.2. As expected, the thermal conductance increases with temperature to ultimately meet its classical value at $T > \theta_D \approx 2\sqrt{\hbar/(k\tau)}$, where k and $\hbar$ are respectively the Boltzmann and

Plank constants

$$D = \lim_{T_H \to T_C} \frac{j}{T_H - T_C} = \frac{\partial j}{\partial T} \tag{3.38}$$

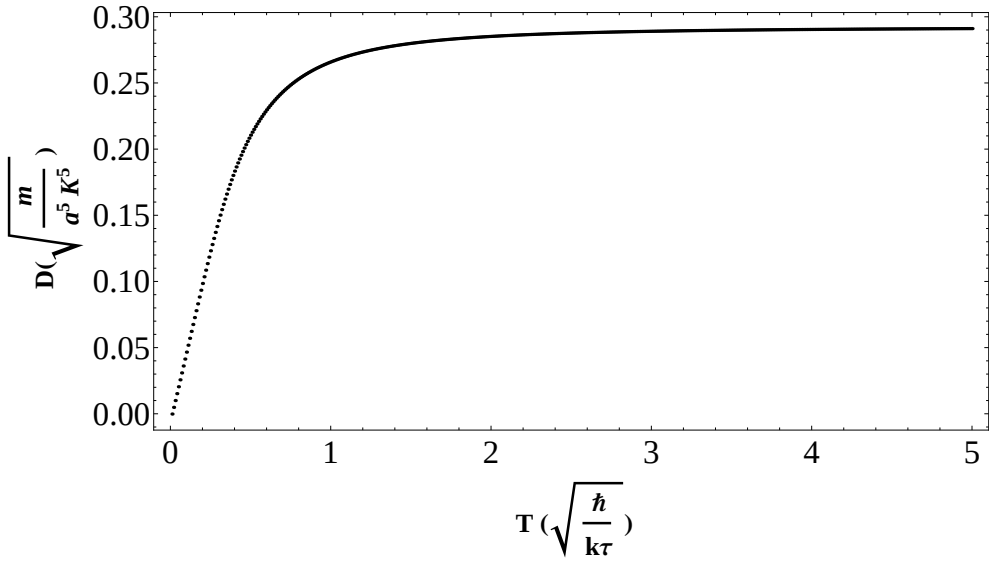


Figure 3.4: Thermal conductance versus temperature for a chain of 6 atoms with the correlation time $\tau = 0.5$ ($\sqrt{k/m}$). As expected increases with temperature to final reach its classical limit.

3.3.1.3 Heat capacity of the chain

To check the reliability of this analysis we calculated the heat capacity as a function of temperature according to the definition in appendix .A.4. As shown in fig.3.5 the heat capacity of the linear chain in fig.3.2 increases with temperature to finally meet its expected classical counterpart for $T > \theta_D \approx 2\sqrt{\hbar/(k\tau)}$.

3.3.2 Two dimensional Sheet of Graphene

In this application we consider a hexagonal sheet of graphene made of 54 carbon atoms bonded together in a honeycomb structure. We attach six alkane chains to opposite boundaries of the graphene sheet and to the heat baths as shown in

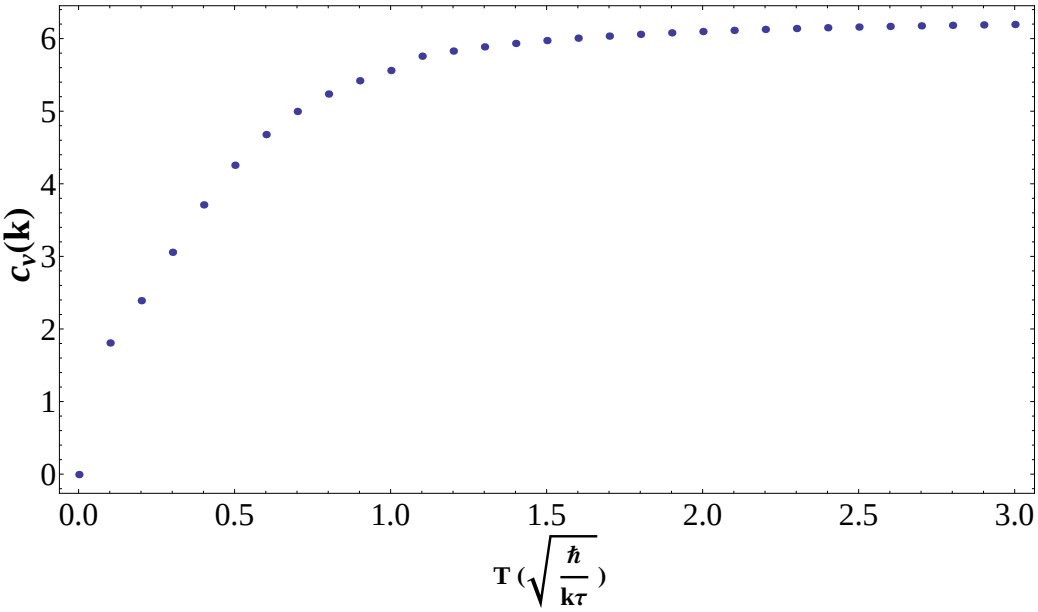


Figure 3.5: Heat capacity (C_v) as a function of temperature of the linear 1D chain of coupled harmonic oscillators of size N=6, where k is the Boltzmann constant, and $\hbar$ is Planck constant.

fig.3.6. The alkane chains are n-pentane. The Tersoff-Berner (TB) force field is used to describe the interactions among the atoms in the graphene sheet. The Nath, Escobedo, and Pablo revised (NERD) potential is used to describe the interactions in the chains and the bond between the chains and the graphene.

3.3.2.1 Heat flux

Following the steps of sec.3.3.1.2 we numerically calculated the ratio of thermal conductance of the functionalized graphene configuration shown in fig.3.6 and that of graphene without side chains, as a function of temperature. Fig.3.12 is a representation of this characteristic. As indicated the thermal conductance increases with temperature, and converges to its maximum classical values for $T > \theta_D \approx 2\sqrt{\hbar/(k\tau)}$.

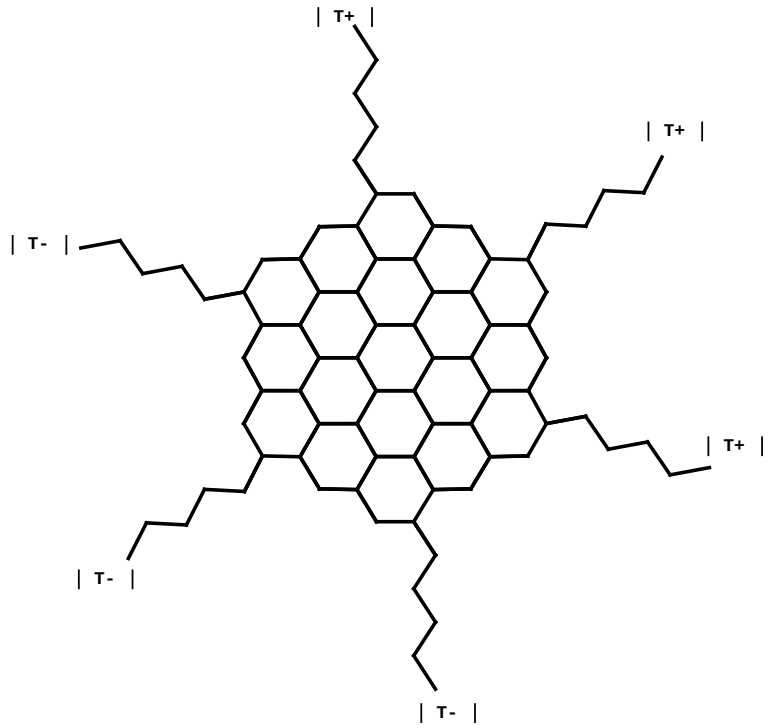


Figure 3.6: A pictorial representation of a functionalized sheet of graphene. The number of atoms in the graphene sheet is 54, The alkane chains are n-pentane. The end of the chains interact with two thermal reservoirs working at temperatures T_+ and T_-.

3.3.3 Improving the thermal conductivity of functionalized graphene

In the quest to improving the thermal conductivity to the graphene, we suggest the following:

- Modifying the length of the chains, since this can improve the stiffness of the functional groups, possibly increasing the number of sites in contact with the source of heat which may lead to larger thermal conductivities.
- Branching the chains which may increase the number of sites in contact with the heat baths, eventually the stiffness of the functional groups, and possibly the heat flux.
- Modifying the chains, by identifying a chain configuration that better couple to the graphene.

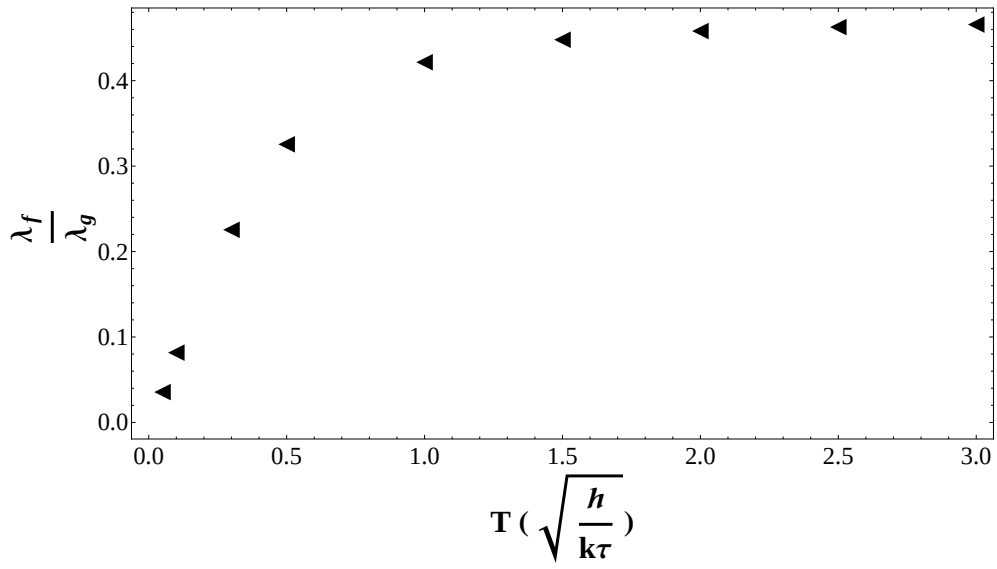


Figure 3.7: Ratio of the thermal conductance of the functionalized graphene configuration and that of pristine graphene as a function of temperature, where k is the Boltzmann constant, and $\hbar$ is Planck constant.

Our main goal in this section is to identify the best configuration of the functional groups that will ultimately convey the largest amount of heat to the graphene. We proceed this quest in the classical approximation since improving the thermal conductivity in this regime will also be reflected at low temperatures.

3.3.3.1 Effect of changing the length of the chains on the thermal conduction

In this section we shall use the technique developed in this chapter to investigate the effect of changing the length of the chains on the thermal conduction of heat throughout the functionalized graphene. Fig.3.8 summarizes the classical results of thermal conductance for configurations similar to the one in fig.3.6 with five, six, seven and eight sites (N = 5, 6, 7, 8). Based on these results, an increase in the number of sites in contact with the source of heat for any chain length will improve the thermal conductance throughout the macromolecule. This can be seen as the limit of simply linking several current of heat to a single junction. In addition, odd chains overall perform better than even chains when the same

conditions are applied. To understand the underlying causes of these results we calculated the average temperature profile ($T =< 3/2m\ v^2 >$) between the hot and cold baths. Fig.3.9 represents the steady state temperature of each site of the graphene configuration shown in fig.3.8, the vertical lines represent the normalized values of the site temperatures. Notice the large temperature gap from the hot chains (left) to the colder graphene (middle). The interfacial thermal resistance (Kapitza resistance) between the soft chains and the stiff graphene is responsible for this finite temperature discontinuity. The vibrational modes of the chains can only weakly couple to the one of the graphene which makes it harder for the heat to flow through and eventually explain the smaller conductance compared to the graphene. In addition, The average temperature gap was calculated for configurations similar to the one in fig.3.6 with five, six, seven and eight sites (N = 5, 6, 7, 8), the results are reported in table.3.1, the temperature gap confirms the patten seen in fig.3.8 the larger the temperature gap the smaller the thermal conductance. We also calculated the participation ratios of the different modes for chain lengths N=5, and N=6. Fig.3.10 displays the total number of normal modes with increasing participation ratio. The graphene configuration with N=5 has more moderate to high participation ratio modes (extended modes) than the one with N=6, which reinforces the close connection between participation ratio and coupling of phonon modes between graphene and chains.

3.3.3.2 Effect of branching the chains on the thermal conduction

In this section we investigate the effect of branching the chains on the thermal conduction of heat to the graphene. We consider the functionalized graphene configurations shown in fig.3.4, we then change the length and the branching sites, and calculate the thermal conductance of each configuration in the classical regime. Tables.3.2 and 3.3 represent the ratio of the thermal conductance of the double and triple branched chains configurations 3.11(b) and 3.11(c) with

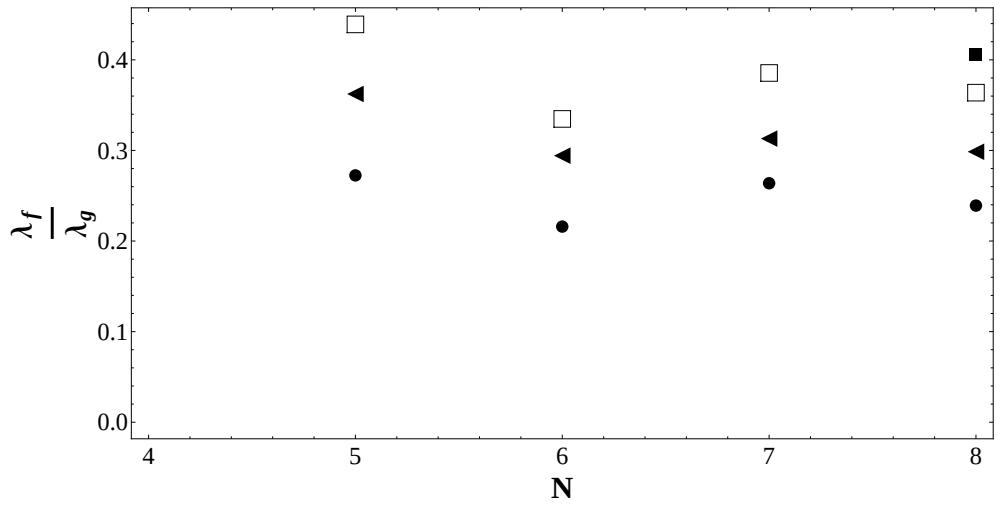


Figure 3.8: The ratio of the Thermal conductances of functionalized graphene λ_f and graphene λ_g as a function of chain length N. (solid disk): heating one site, (solid triagle): heating two sites, (empty square): heating three sites, (solid square): heating four sites.

respect to the non-branched configuration 3.11(a) for a graphene sheets of 54 and 96 atoms respectively. According to these results, increasing the number of sites in contact with the source of heat by branching the functional groups, does improve the overall thermal conduction throughout the macromolecule. Branching the functional groups however, does not improve the coupling to the graphene, as illustrated in figs.3.12 and 3.13, the number of extended modes (modes with moderate to larger participation ratios) decreases with the branching of the functional groups. The larger thermal conductance is attributed to the additional heated sites which can be seen as the limit of simply linking several current of heat to a single junction.

3.3.3.3 Effect of changing the chains site masses and strength of their interactions

In several occasions throughout this thesis, we confirmed the close connection between the extended modes (modes with moderate to high participation ratios) and the conduction of heat, we arrived at the persisting conclusion that improving

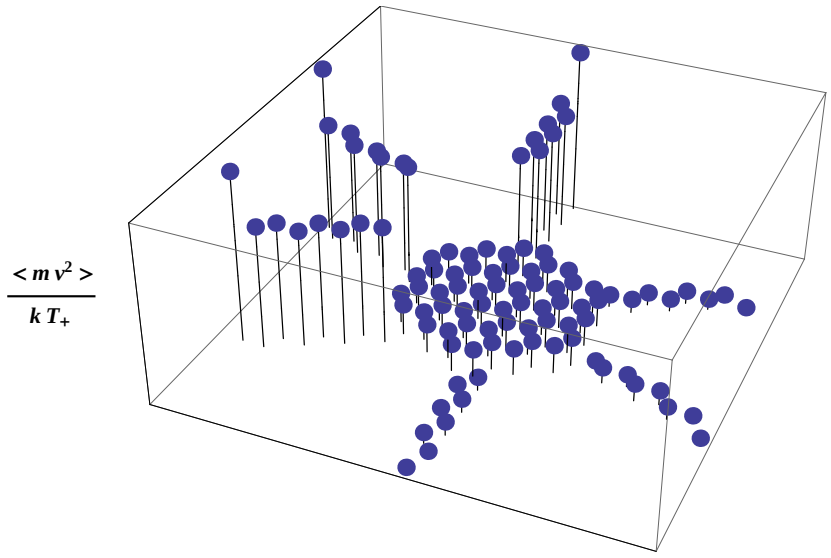


Figure 3.9: Ratio of the average temperature profile ($T =< m\ v^2 >$) between the hot and cold baths and kT_+ for the graphene configuration in fig.3.8, k is the Boltzmann constant, T_+ is the temperature of the heat bath.

the participation ratios of the different modes will in fact enhance the thermal properties of the macromolecule. In the rest of this section, we allow the site masses and strength of the interactions in the chains to vary and we seek the chain configuration that maximizes the participation ratios of the different normal modes. Since all the different modes and their participation ratios depend on the same variables, namely the site masses and strength of the interactions, maximizing the participation ratio of one mode often does not simultaneously maximize the participation ratios of the other modes, and there is usually no unique optimal solution. Our goal however is to extract a trend or trends that lead to maximizing the heat flux to the graphene. We proceed in our quest with a goal programming strategy where we seek to minimize the weighted sum of the deviation of the participation ratios from the goal value of 1 for the graphene configuration shown in fig.3.14. Specifically, the constrained minimization problem in eq.3.39 is to be solved. We assume the chains are identical. To simplify the analysis, we start with the parameters of the alkanes and we seek to adjust the site masses and strength of their interactions. The weights are taken to be

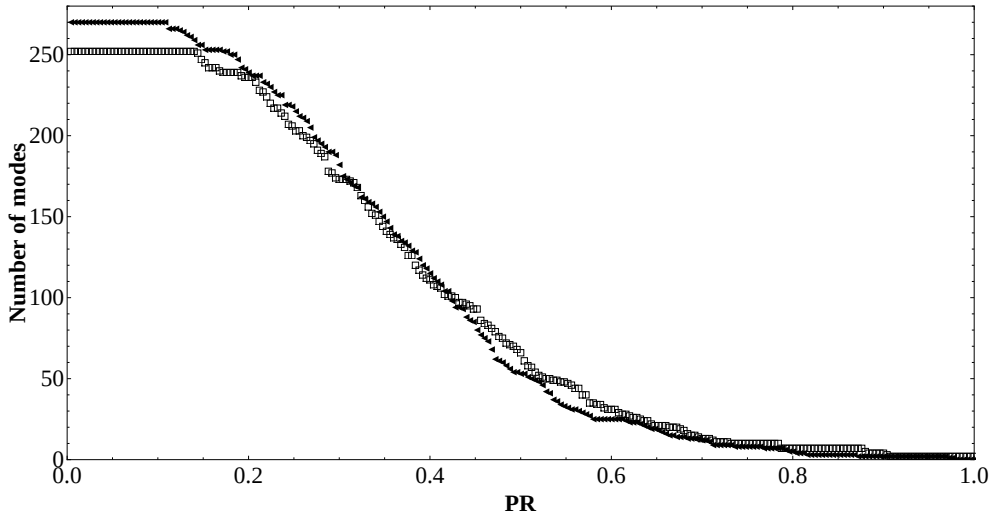


Figure 3.10: Number of normal modes versus participation ratio (PR). (solid triangle): functionalized graphene with chains of length (N=6), (empty square): functionalized graphene with chains of length (N=5).

the participation ratios of the different modes in the alkane configuration.

$$Min \sum w_i (1 - PR_i)^+ \tag{3.39}$$

the (+) stands for the positive part of the real number. The weights reflect the relative importance, and normalize the deviation to take into account the relative scales and units.

The optimization was done over wide range of intervals, and for chain lengths N=5 and N=7. In each interval we record the characteristics of the different variations and compare it to the same characteristics from other intervals. Overall the pattern seemed to hold among all the different intervals. According to these results, one can improve the coupling to the graphene and therefore the overall conduction of heat by using stiffer but not heavy chains. Heavier chains do not couple as well as lighter chains. As an application to these results, we consider perfluorinated alkanes[29]. While the molecular groups are heavier than the alkanes, these chains are known for their larger stiffness, particularly their torsional strength fig.3.15. This example is taken to show that, even though, the

N	$\frac{\Delta T}{k_B(T_+ - T_-)}$
5	0.608
6	0.714
7	0.627
8	0.701

Table 3.1: Ratio of the temperature drop across the chain graphene interface $k_B(T_+ - T_-)$ as a function of chain length (N). k_B is the Boltzmann constant, T_+ and T_- are respectively the temperatures of the hot and cold heat bath.

chains are stiff, which makes them a good candidate for improving the thermal conduction throughout the functionalized graphene, they are heavy which makes it harder for these functional groups to thermally couple to the graphene. To confirm this conclusion, we calculated the thermal conductance of functionalized graphene configurations similar to the one in fig.3.14 with side chains of lengths $N = 5$ and $N = 6$, then compare it to identical configurations with alkanes. These results confirm the results of optimization.

3.4 Conclusion

In this chapter we investigated heat transport in macromolecules and graphene in particular using Langevin dynamics with colored and quantum mechanical noise. The results of this analysis where used to identify the configuration of the functional groups that best conduct heat to the graphene. It was shown that stiffer but lighter chains couple better to the graphene and produce higher thermal conductivities. In addition, branching the functional groups overall improves the thermal conduction, this however is attributed to the additional heating sites due to branching and not to the better coupling of phonon modes between the chains

Chain size	Br@	Brsize	#SPC	$\frac{\lambda_{b_{54}}}{\lambda_{nb_{54}}}$	$\frac{\lambda_{b_{96}}}{\lambda_{nb_{96}}}$
5	2	3	1	1.11	1.11
-	-	-	2	1.04	1.10
-	-	-	3	1.03	1.06
6	2	4	1	1.14	1.03
-	-	-	2	1.07	0.96
-	-	-	3	1.07	0.96
6	3	3	1	1.25	1.44
-	-	-	2	1.27	1.26
-	-	-	3	1.24	1.24
7	2	5	1	1.04	1.13
-	-	-	2	1.03	0.92
-	-	-	3	0.94	0.87
7	3	5	1	1.02	1.17
-	-	-	2	1.10	1.08
-	-	-	3	1.01	0.99

Table 3.2: **Configuration (b)**: Ratio of thermal conductance of branched λ_b and unbranched functional groups, λ_{nb}. Br@(branched at), Brsize (branched size), #SPC (number of sites per chain). The subscripts 54 and 96 refer to the size of the graphene sheet

.

Chain size	Br@	Brsize	#SPC	$\frac{\lambda_{b_{54}}}{\lambda_{nb_{54}}}$	$\frac{\lambda_{b_{96}}}{\lambda_{nb_{96}}}$
5	2	3	1	1.41	1.17
-	-	-	2	1.34	1.23
-	-	-	3	1.29	1.06
6	2	4	1	1.71	1.38
-	-	-	2	1.59	1.16
-	-	-	3	1.58	1.15
6	3	3	1	1.94	1.31
-	-	-	2	1.92	1.26
-	-	-	3	1.74	1.19
7	2	5	1	1.33	1.09
-	-	-	2	1.40	0.97
-	-	-	3	1.31	0.92
7	3	5	1	1.49	1.37
	-	-	2	1.54	1.15
	-	-	3	1.46	1.07

Table 3.3: **Configuration (c)**: Ratio of thermal conductance of branched and λ_b and unbranched functional groups λ_{nb}. Br@(branched at), Brsize (branched size), #SPC (number of sites per chain). The subscripts 54 and 96 refer to the size of the graphene sheet

.

N	λ_f/λ_s
5	0.294
6	0.290

Table 3.4: Ratio of the thermal conductances of functionalized graphene with fluorinated alkanes (λ_f) and that of functionalized graphene with alkanes with the same chain length (λ_s).

and graphene.

In this approach however, we considered linear interactions only, we assumed, since the Debye temperature of most carbon based materials including graphene is high that the effect of the non linear corrections is low and will not have major impact on the general results of optimization. Possible ways to extend this approach is to include the non linear corrections and check the consistency of these results. This requires solving the generalized Langevin equation numerically and will be discussed in chapter 4.

We used time correlated noises with no spatial dependence in the entire analysis. This is not quite realistic since the local phonon environment may have some non-zero coherence length of the same order as the mean phonon wavelemgth, a more realistic description should be based on random noises that are correlated in space and time. This will be discussed in chapter 5.

Finally, it was recently reported [9] that by functionalizing graphene, it is possible to prevent the agglomeration of these flakes in polymer solutions, and guarantee stable dispersion of graphene fillers. These oils are frequently used in the industry and analyzing the thermal properties of the functionalized graphene-oil system may lead to the design of enhanced lubricants for extreme applications such as heat conductive lubricants. The Langevin equations can be modified to account for the effect of the surrounding medium. This is can be accom-

plished by modeling the particle medium interactions by an average dissipative field that manifest through additional damping coefficients which in average can be extracted from Stokes law for the medium.

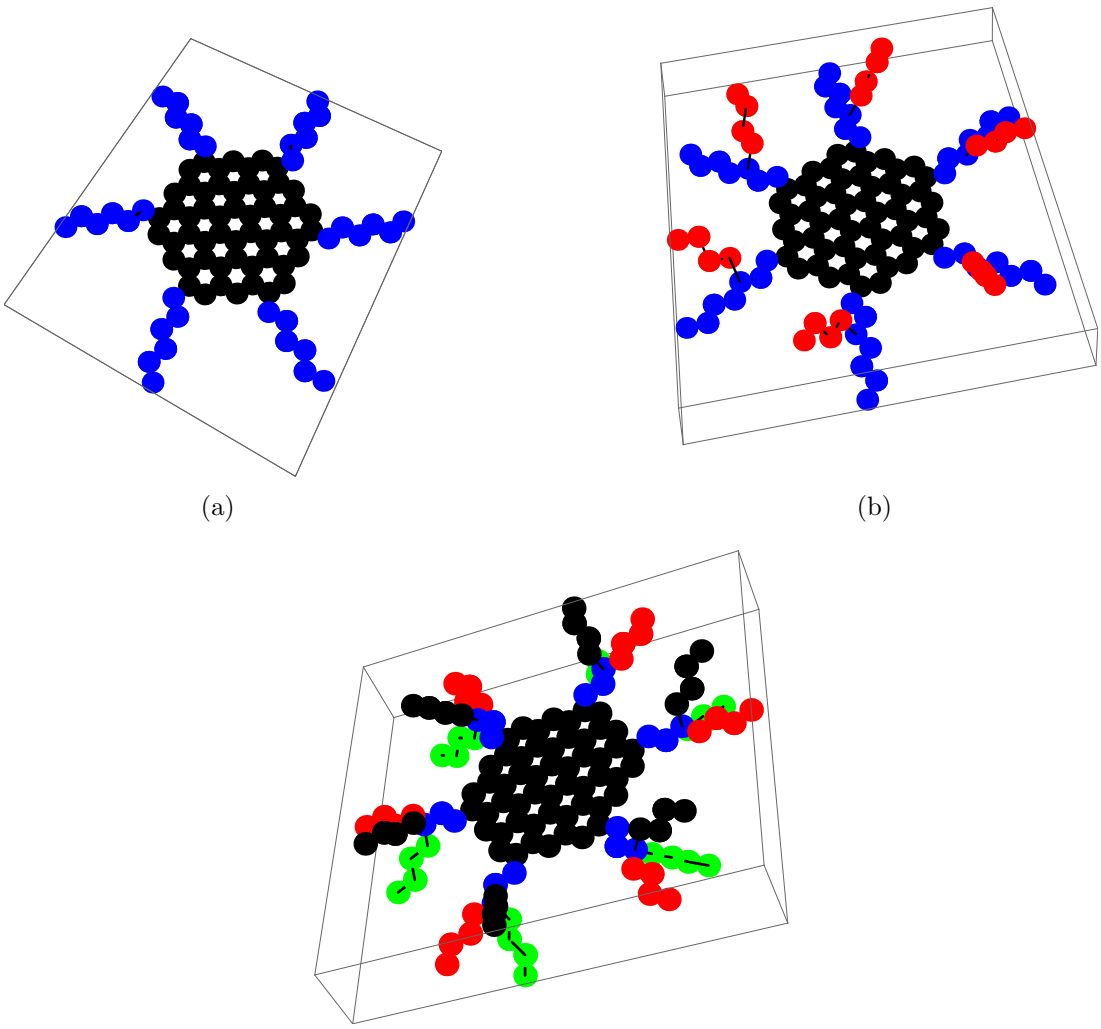


Figure 3.11: Pictorial representation of a branched and unbranched sheets of graphene. The number of atoms in the graphene sheet is 54. The end of the chains interact with two thermal reservoirs working at different temperatures.

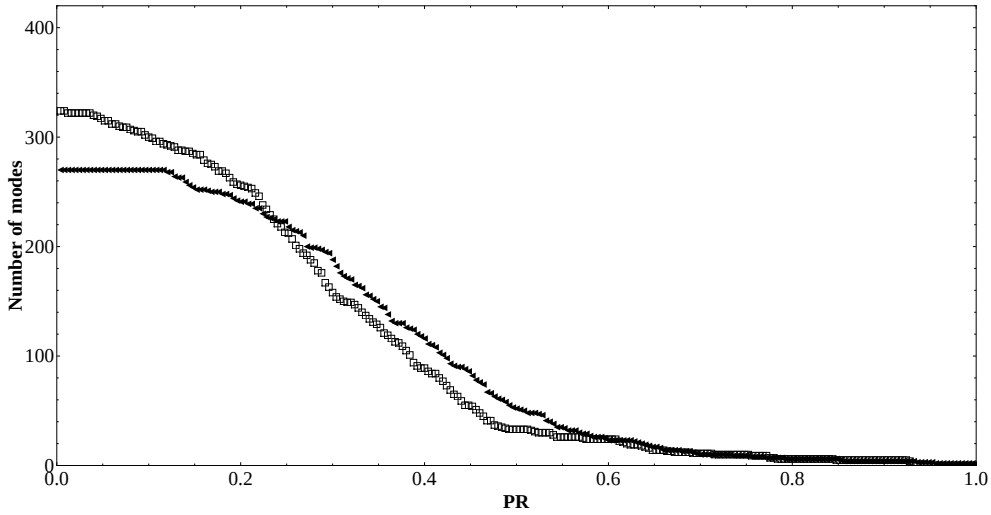


Figure 3.12: Number of normal modes versus participation ratio (PR). (solid triangle): non branched N=5 (fig.3.11(a)), (empty square): double branched N=5 (fig.3.11(b)).

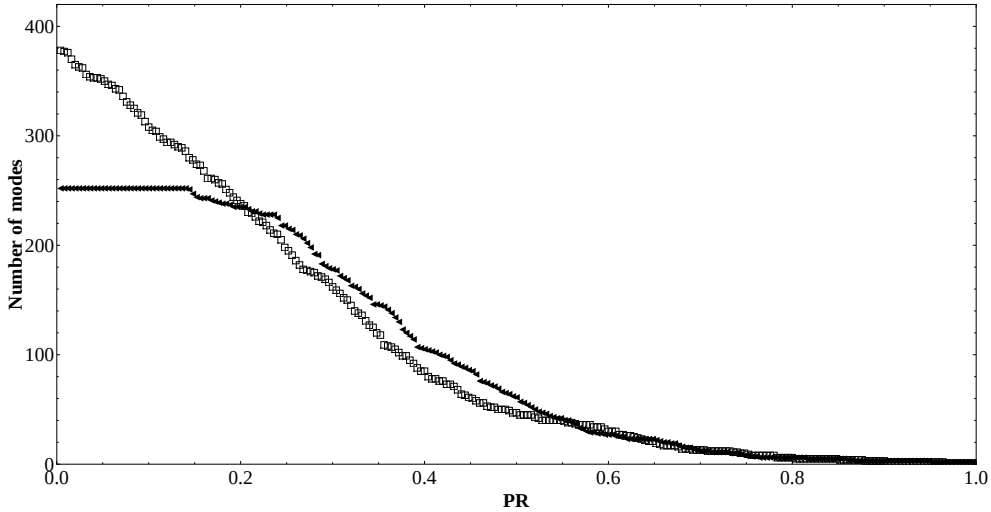


Figure 3.13: Number of normal modes versus participation ratio (PR). (solid triangle): not branched N=5 (fig.3.11(a)), (empty square): triple branched N=5 (fig.3.11(c)).

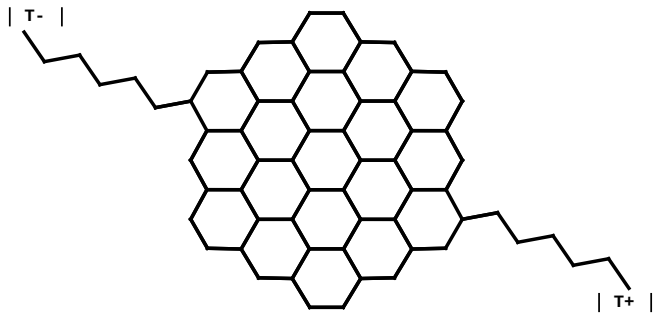


Figure 3.14: Pictorial representation of a graphene sheet of 54 carbon atoms functionalized with two organic chains of size $N = 6$.

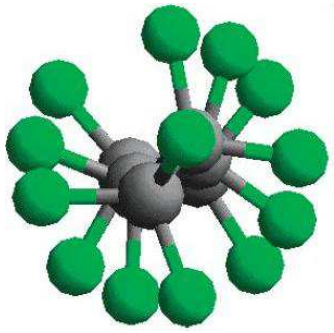


Figure 3.15: Quantum optimized structure of perfluorohexane. The dark spheres represent the carbon atoms, the green sphere are the fluorine atoms. The helical C-C-C-C twist angle of 16.8^o corresponds to a dihedral angle of 163.2^o and to a projected 1-5 27^o [30].

Chapter 4

Classical Langevin Equations with Thermal Colored Noise, Numerical Solution

4.1 Introduction

The process of thermal energy transfer is a random process. The energy does not simply enter one end of the specimen and proceed ballistically to the other end, but diffuses through the specimen, suffering frequent collisions, geometrical scattering and scattering by other phonons. In this chapter we shall develop the background to numerically solving the generalized classical Langevin equations for a system of interacting particles in contact with heat baths using a fourth order Runge-Kutta Method[12, 27]. The results of this numerical technique will be used to calculate some of the thermal properties of the system and to foresee the extent to which the normal mode approach used in the previous analysis is capable of predicting the best configurations to optimizing heat throughout the system.

4.2 Development

In this section we shall develop the steps to numerically solving eq.4.1 with the correlation eq.4.2 using a fourth order power expansion in time of the displacement. We first present the steps to this numerical solution and then apply it in sec.4.4 to a linear chain, small pristine graphene sheet and a small functionalized graphene sheet.

$$m_i\ \ddot{x}_i(t) = -\frac{\partial U}{\partial x_i} + \left(-\int_0^t dt' K(t-t')\ \dot{x}_i(t') + F_i(t) \right) (\delta_{i,1} + \delta_{i,N}) \qquad (4.1)$$

$$\begin{aligned} \langle F_i(t) \rangle &= 0 \\ \langle F_i(t)\ F_j(t') \rangle &= \frac{\gamma_i}{\tau} \delta_{ij} k_B T e^{-|t-t'|/\tau} \end{aligned} \tag{4.2}$$

where U is the interaction potential among all the different sites in the system, m_i, x_i,respectively are the mass and displacement of particle i, γ_i is a damping coefficient, $F_i(t)$ is the Langevin force on particle i, the overhead dot refers to time derivative, and δ_{ij} is the Kronecker delta function restricting the driving and damping to the first and last particles.

We follow the steps outlined in chapter.4 and introduce the variable in eq.3.5, then eq.4.1 becomes of the form

$$\begin{aligned} \dot{x}_i &= \frac{p_i(t)}{m_i} \\ \dot{p}_i(t) &= -\frac{\partial U}{\partial x_i} + \left[-y_i(t) + F_i(t)\right] \left(\delta_{i,1} + \delta_{i,N}\right) \\ \dot{y}_i(t) &= -\frac{1}{\tau} y_i(t) + \frac{\gamma_i}{m_i \tau} p_i(t) \\ \dot{F}_i(t) &= -\frac{1}{\tau} F_i(t) + \frac{\sqrt{2\gamma_i k_B T_i}}{\tau}\ \Gamma_i(t) \end{aligned} \tag{4.3}$$

where the last equation describes O-U noise, and $\Gamma_i(t)$ is a Gaussian white noise, with correlation

$$\begin{aligned} \langle \Gamma_i(t) \rangle &= 0 \\ \langle \Gamma_i(t) \Gamma_j(t') \rangle &= \delta_{ij} \delta(t - t') \end{aligned} \tag{4.4}$$

These four equations can be reduced to a set of three equations eq.4.5 if we introduce the variable $Y_i(t) = F_i(t) - y_i(t)$

$$\dot{x}_i = \frac{p_i(t)}{m_i}$$

$$\dot{p}_i(t) = -\frac{\partial U}{\partial x_i} + Y_i(t)(\delta_{i,1} + \delta_{i,N}) \tag{4.5}$$

$$\dot{Y}_i(t) = -\frac{1}{\tau}Y_i(t) - \frac{\gamma_i}{m_i\tau}p_i(t) + \frac{\sqrt{2\gamma_i k_B T_i}}{\tau}\ \Gamma_i(t)$$

Eq.4.5 can be put in a vector form eq.4.6, where $f(\vec{S})$ is a function of the component of $\vec{S}$ eqs.4.7, 4.8, and 4.9.

$$\dot{\vec{S}} = f(\vec{S}) + \Gamma(t) \tag{4.6}$$

$$\vec{S} = \begin{pmatrix} x_i \\ p_i \\ Y_i\ (\delta_{i,1} + \delta_{i,N}) \\ . \end{pmatrix} \tag{4.7}$$

$$f(\vec{S}) = \begin{pmatrix} \frac{S_{i+N}}{m_i} \\ -\frac{\partial U}{\partial S_{i-N}} + S_{i+N}\ (\delta_{i,N+1} + \delta_{i,2N}) \\ [-\frac{1}{\tau}S_i(t) - \frac{\gamma_{i-2N}}{\tau m_{i-2N}}S_{i-N}(t)]\ (\delta_{i,2N+1} + \delta_{i,3N}) \\ . \end{pmatrix} \tag{4.8}$$

$$\vec{\Gamma} = \begin{pmatrix} 0 \\ 0 \\ \frac{\sqrt{2\gamma_i k_B\ T_i}}{\tau}\Gamma_i\ (\delta_{i,2N+1} + \delta_{i,3N}) \\ . \end{pmatrix} \tag{4.9}$$

The problem reduces to knowing how to solve a set of equations of the form eq.4.6 which can be done through a basic expansion in time of $f_i(\vec{S})$. We proceed as follow:

We break eq.4.6 into its respective components then integrate between t and $t + \Delta t$ to solve $\vec{S}(t + \Delta t)$, where Δt is a short time step

$$\dot{S}_i(t) = f_i(\vec{S}(t)) + \Gamma_i(t) \qquad i = 1, ..., 3N \tag{4.10}$$

$$\int_0^{\Delta t} \dot{S}_i(t + x)dx = S_i(t + \Delta t) - S_i(t) = \int_0^{\Delta t} f_i(\vec{S}(t + x))dx + (\delta_{i,2N+1} + \delta_{i,3N})\ \frac{\sqrt{2\gamma_1 k_B\ T_i}}{\tau} \int_0^{\Delta t} \Gamma_i\ (t + x)dx \qquad i = 1, ..., 3N \tag{4.11}$$

The value of $S_i(t+\Delta t)$ depends on $S_i(t)$, and the behavior of f_i and Γ_i in the neighborhood of $\vec{S}(t + \Delta t)$. That is, the behavior f_i and Γ_i in the neighborhood of $\vec{S}(t+\Delta t)$ can shed some light on the nature of the solution at $\vec{S}(t+\Delta t)$. This is the fundamental basis for one of the successful and widely used one-step methods known as the Runge-Kutta method. The Runge-Kutta method is also one of the few methods in numerical analysis that does not rely directly on polynomial

approximation. The basic method assumes that the solution $\vec{S}(t+\Delta t)$ can be represented by a power series with reference to Δt. This can be achieved by expanding each component of $\vec{f}(\vec{S})$ in a Taylor series around $\vec{S}(t+\Delta t)$.

$$
\begin{aligned}
&f_i(\vec{S}(t+\Delta t)) = f_i(\vec{S}(t)) + \frac{\partial}{\partial S_k} f_i(\vec{S}(t))\ [S_k(t+\Delta t) - S_k(t)] + \\
&\frac{1}{2}\left(\frac{\partial^2}{\partial S_j\ \partial S_k} f_i(\vec{S}(t))\right)\ [S_k(t+\Delta t) - S_k(t)][S_j(t+\Delta t) - S_j(t)] + ...
\end{aligned}
\tag{4.12}
$$

To keep track of the order of each derivative, we introduce the following notation

$$
\begin{aligned}
&f_i(S(t)) = f_i \\
&\frac{\partial}{\partial S_j} f_i(\vec{S}(t)) = f_{i,j} \\
&\frac{\partial^2}{\partial S_j\ \partial S_k} f_i(\vec{S}(t)) = f_{i,jk} \\
&\frac{\partial^3}{\partial S_j\ \partial S_k\ \partial S_m} f_i(\vec{S}(t)) = f_{i,jkm} \\
&\frac{\partial^4}{\partial S_j\ \partial S_k\ \partial S_m\ \partial S_l} f_i(\vec{S}(t)) = f_{i,jkml} \\
&\delta S_i(x) = S_i(t+x) - S_i(t)
\end{aligned}
\tag{4.13}
$$

If a sum over repeated indices is assumed

$$S_i(t+\Delta t) - S_i(t) = \int_0^{\Delta t} [f_i + f_{i,k}\ \delta S_k + \frac{1}{2}\ f_{i,jk}\ \delta S_k\ \delta S_j + \frac{1}{6}\ f_{i,jkm}\ \delta S_k\ \delta S_j\ \delta S_m +$$

$$\frac{1}{24}\ f_{i,jkml}\ \delta S_k\ \delta S_j\ \delta S_m\ \delta S_l + ...]\ dx + (\delta_{i,2N+1} + \delta_{i,3N})\ \frac{\sqrt{2\gamma_1 k_B\ T_i}}{\tau} \int_0^{\Delta t} \Gamma_i\ (t+x)dx$$

$$i = 1, ..., 3N \tag{4.14}$$

To expand consistently and produce a Taylor approximation of fourth order in Δt of $\vec{S}(t+\Delta t)$ one must keep in mind that $\int_o^{\Delta t} \Gamma(s)ds$ is $O(\Delta t^{1/2})$, that is the lowest order in the expansion. As a matter of fact if we introduce the stochastic Gaussian variable $\mid Z_{1,i} \mid$ as in eq.4.15, with average and standard deviation as calculated in eq.4.16, it is clear from that point that $(Z_{1,i})$ is of order $O(\Delta t^{1/2})$.

$$Z_{i,1}(\Delta t) = \frac{\sqrt{2\gamma_i k_B T_i}}{\tau} \int_0^{\Delta t} \Gamma_i(t+x)dx \tag{4.15}$$

$$\langle Z_{i,1}(\Delta t) \langle = \frac{\sqrt{2\gamma_i k_B T_i}}{\tau} \int_0^{\Delta t} \langle \Gamma_i(t+x) \rangle dx = 0$$

$$\langle Z^2{}_{i,1}(\Delta t) \rangle = \frac{2\gamma_i k_B T_i}{\tau^2} \int_0^{\Delta t} \int_0^{\Delta t} \langle \Gamma_i(t+x)\Gamma_i(t+s) \rangle dx\ ds$$

$$= \frac{2\gamma_i k_B T_i}{\tau^2} \int_0^{\Delta t} \int_0^{\Delta t} \delta(x-s)dx\ ds = \frac{\sqrt{2\gamma_i k_B T_i}}{\tau} \int_0^{\Delta t} ds = \frac{2\gamma_i k_B T_i}{\tau^2} \Delta t$$

(4.16)

The lowest order in the expansion eq.4.19 is then of order $O(\Delta t^{1/2})$ and defined as

$$\delta S_i^{1/2}(\Delta t) = \int_0^{\Delta t} \Gamma_i(t+x)\ dx = (\delta_{i,2N+1} + \delta_{i,3N})\ Z_{i,1}(\Delta t) + O(\Delta t) \qquad (4.17)$$

Next we insert this result in the previous expansion eq.4.10 to get the next order eq.4.18

$$\delta S_i^1(\Delta t) = \int_0^{\Delta t} f_i\ dx = f_i\ \Delta t + O(\Delta t^{3/2}) \qquad (4.18)$$

The next order in the expansion is eq.4.19

$$\begin{aligned}
\delta S_i^{3/2}(\Delta t) &= \int_0^{\Delta t} f_{i,k}\ \delta S_k^{1/2}(x)\ dx + O(\Delta t^2) \\
&= f_{i,k}\ (\delta_{k,2N+1} + \delta_{k,3N})\ \textstyle\int_0^{\Delta t}\ Z_{k,1}(x)\ dx + O(\Delta t^2) \\
&= (\delta_{k,2N+1} + \delta_{k,3N})\ f_{i,k}\ Z_{k,2}(\Delta t) + O(\Delta t^2) \\
&= (\delta_{i,N+1} - \frac{1}{\tau}\ \delta_{i,2N+1})\ Z_{2N+1,2}(\Delta t) + (\delta_{i,2N} - \frac{1}{\tau}\ \delta_{i,3N})\ Z_{3N,2}(\Delta t) + O(\Delta t^2)
\end{aligned} \qquad (4.19)$$

where

$$\int_0^{\Delta t}\ Z_{k,1}(x)\ dx = Z_{k,2}(\Delta t) \qquad (4.20)$$

Similarly

$$\delta S_i^2(\Delta t) = \frac{1}{2}\ f_{i,k}\ f_k\ \Delta t^2 + O(\Delta t^{5/2}) \qquad (4.21)$$

$$\delta S_i^{5/2}(\Delta t) = (\delta_{j,2N+1} + \delta_{j,3N})\ f_{i,k}\ f_{k,j}\ Z_{j,3}(\Delta t) + O(\Delta t^3)$$

$$= f_{i,k}\ f_{k,2N+1}\ Z_{2N+1,3}(\Delta t) + f_{i,k}\ f_{k,3N}\ Z_{3N,3}(\Delta t) + O(\Delta t^3)$$

$$= (f_{i,N+1} - \frac{1}{\tau}\ f_{i,2N+1})\ Z_{2N+1,3}(\Delta t) +$$

$$(f_{i,2N} - \frac{1}{\tau}\ f_{i,3N})\ Z_{3N,3}(\Delta t) + O(\Delta t^3)$$

$$= (\delta_{i,1} - \frac{\gamma}{m\ \tau}\ \delta_{i,2N+1} - \frac{1}{\tau}\ (\delta_{i,N+1} - \frac{1}{\tau}\ \delta_{i,2N+1}))\ Z_{2N+1,3}(\Delta t) +$$

$$(\delta_{i,N} - \frac{\gamma}{m\ \tau}\ \delta_{i,3N} - \frac{1}{\tau}\ (\delta_{i,2N} - \frac{\gamma}{m\ \tau}\ \delta_{i,3N}))\ Z_{3N,3}(\Delta t) + O(\Delta t^3) \tag{4.22}$$

where

$$\int_0^{\Delta t}\ Z_{j,2}(x)\ dx = Z_{j,3}(\Delta t) \tag{4.23}$$

and

$$\delta S_i^3(\Delta t) = \frac{1}{6}\ [f_{i,k}\ f_{k,j}\ f_j + f_{i,jk}\ f_j\ f_k]\ \Delta t^3 + O(\Delta t^{7/2}) \tag{4.24}$$

$$\delta S_i^{7/2}(\Delta t) = (\delta_{m,2N+1} + \delta_{m,3N})\ f_{i,k}\ f_{k,j}\ f_{j,m}\ Z_{m,4} + O(\Delta t^4)$$

$$= f_{i,k}\ f_{k,j}\ f_{j,2N+1}\ Z_{2N+1,4} + f_{i,k}\ f_{k,j}\ f_{j,3N}\ Z_{3N,4} + O(\Delta t^4)$$

$$= f_{i,k}\ f_{k,j}\ (\delta_{j,N+1} - \frac{1}{\tau}\delta_{j,2N+1})\ Z_{2N+1,4} +$$

$$f_{i,k}\ f_{k,j}\ (\delta_{j,2N} - \frac{1}{\tau}\delta_{j,3N})\ Z_{3N,4} + O(\Delta t^4)$$

$$= [f_{i,1} - \frac{\gamma}{m\ \tau}\ (\delta_{i,N+1} - \frac{1}{\tau}\ \delta_{i,2N+1}) - \frac{1}{\tau}(\delta_{i,1} - \frac{\gamma}{m\ \tau}\ \delta_{i,2N+1} - \frac{1}{\tau}\ (\delta_{i,N+1} -$$

$$\frac{1}{\tau}\ \delta_{i,2N+1}))]Z_{2N+1,4}(\Delta t) +$$

$$[f_{i,N} - \frac{\gamma}{m\ \tau}\ (\delta_{i,2N} - \frac{1}{\tau}\ \delta_{i,3N}) - \frac{1}{\tau}(\delta_{i,N} - \frac{\gamma}{m\ \tau}\ \delta_{i,3N} -$$

$$\frac{1}{\tau}\ (\delta_{i,2N} - \frac{1}{\tau}\ \delta_{i,3N}))]Z_{3N,4}(\Delta t)$$

(4.25)

where

$$\int_0^{\Delta t}\ Z_{m,3}(x)\ dx = Z_{m,4}(\Delta t) \tag{4.26}$$

Finally

$$\delta S_i^4(\Delta t) = \frac{1}{24}\ [f_{i,k}\ f_{k,j}\ f_{j,m} f_m + f_{i,jkm}\ f_j\ f_k\ f_m + f_{i,k}\ f_{k,jm}\ f_j\ f_m + 6\ f_{i,kj}\ f_{k,m}\ f_j\ f_m]\ \Delta t^4 \tag{4.27}$$

From this fourth order expansion one can write the solution to eq.4.5 as the

sum of a deterministic term $S_{i_{det}}(t+\Delta t)$ and a random term $S_{i_{ran}}(t+\Delta t)$, such that

$$S_i(t+\Delta t) = S_i(t) + S_{i_{det}}(t+\Delta t) + S_{i_{ran}}(t+\Delta t) \tag{4.28}$$

and

$$S_{i_{det}}(t+\Delta t) = \delta S_i^1(\Delta t) + \delta S_i^2(\Delta t) + \delta S_i^3(\Delta t) + \delta S_i^4(\Delta t) \tag{4.29}$$

$$S_{i_{ran}}(t+\Delta t) = \delta S_i^{1/2}(\Delta t) + \delta S_i^{3/2}(\Delta t) + \delta S_i^{5/2}(\Delta t) + \delta S_i^{7/2}(\Delta t) \tag{4.30}$$

All the $Z_{i,k}$ up to the fourth order ($k = 4$) are Gaussian random variables, with the covariant matrix eq.4.31

$$\frac{\tau^2}{2\gamma_i k_B T_i} < Z_{i,n}(\Delta t)\ Z_{i,m}(\Delta t) >= \begin{pmatrix} \Delta t & \frac{1}{2}\Delta t^2 & \frac{1}{3!}\Delta t^3 & \frac{1}{4!}\Delta t^4 \\ \frac{1}{2}\Delta t^2 & \frac{1}{3}\Delta t^3 & \frac{3}{4!}\Delta t^4 & \frac{4}{5!}\Delta t^5 \\ \frac{1}{3!}\Delta t^3 & \frac{3}{4!}\Delta t^4 & \frac{6}{5!}\Delta t^5 & \frac{10}{6!}\Delta t^6 \\ \frac{1}{4!}\Delta t^4 & \frac{4}{5!}\Delta t^5 & \frac{10}{6!}\Delta t^6 & \frac{20}{7!}\Delta t^7 \end{pmatrix} \tag{4.31}$$

for example

$$< Z_{i,1}(h)\ Z_{i,2}(h) >= \int_0^h dy \int_0^y d\gamma \int_0^h dx \ < \Gamma_i(t+\gamma)\ \Gamma(t+x) >=$$

$$\frac{2\gamma_i k_B T_i}{\tau^2} \int_0^h dy \int_0^y d\gamma \int_0^h dx\ \delta(\gamma - x) = \int_0^h dy \int_0^y d\gamma = \int_0^h y\ dy = \frac{1}{2}h^2$$

(4.32)

The rest of the elements of matrix eq.4.31 are calculated in a similar way.

Using the covariance matrix eq.4.31 one constructs the random variables $Z_{i,k}$ as linear combinations of four independent Gaussian variables: x_i , y_i , u_i, w_i, where each of these variable has zero average and variance $\sqrt{\Delta t}$. Using the Gram Schmidt process

$$x_i = Z_{i,1}$$

$$\frac{\Delta t}{2\sqrt{3}}\ y_i = Z_{i,2} - \frac{< Z_{i,2}\ x_i >}{< x_i\ x_i >}\ x_i = Z_{i,2} - \frac{1}{2}\Delta t\ x_i$$

$$\frac{\Delta t^2}{\sqrt{3}}\ u_i = Z_{i,3} - \frac{< Z_{i,3}\ x_i >}{< x_i\ x_i >}\ x_i - \frac{< Z_{i,3}\ y_i >}{< y_i\ y_i >}\ y_i = Z_{i,3} - \frac{1}{3!}\Delta t^2\ x_i - \frac{2\sqrt{3}}{4!}\Delta t^2\ y_i$$

$$\frac{\Delta t^3}{120\sqrt{7}}\ w_i = Z_{i,4} - \frac{< Z_{i,4}\ x_i >}{< x_i\ x_i >}\ x_i - \frac{< Z_{i,4}\ y_i >}{< y_i\ y_i >}\ y_i - \frac{< Z_{i,4}\ u_i >}{< u_i\ u_i >}\ u_i$$

$$= Z_{i,4} - \frac{1}{4!}\Delta t^3\ x_i - \frac{\sqrt{3}}{40}\Delta t^3\ y_i - \frac{1}{24\sqrt{5}}\Delta t^3\ u_i$$

(4.33)

Which can also be expressed in the form of

$$
\begin{aligned}
Z_{i,1} &= \frac{\sqrt{2\gamma_i k_B T_i}}{\tau} x_i \\
Z_{i,2} &= \frac{\sqrt{2\gamma_i k_B T_i}}{\tau} \Delta t \; [\frac{1}{2}\; x_i + \frac{1}{2\sqrt{3}}\; y_i] \\
Z_{i,3} &= \frac{\sqrt{2\gamma_i k_B T_i}}{\tau} \Delta t^2 [\frac{1}{3!} x_i + \frac{2\sqrt{3}}{4!} y_i + \frac{1}{\sqrt{6}} u_i] \\
Z_{i,4} &= \frac{\sqrt{2\gamma_i k_B T_i}}{\tau} \Delta t^3 [\frac{1}{4!} x_i + \frac{\sqrt{3}}{40} y_i + \frac{1}{24\sqrt{5}} u_i + \frac{1}{120\sqrt{7}} w_i]
\end{aligned}
\tag{4.34}
$$

It is important to note that one does not have to use the Taylor expansion for the deterministic part of the solution. Any fourth-order procedure will give the needed accuracy. By using the fourth-order Runge-Kutta algorithm [26] for the deterministic propagation and adding the random forces as given in eq.4.30, one has a fourth-order algorithm which will depend only on the first derivatives of the function ($f(\vec{S})$).

4.3 Program structure diagram

In this section we shall outline the program structure diagram used to implement the technique developed in sec.4.2.

- Generating the random variables (x_i , y_i , u_i, w_i). For each coordinate (i), in each run (r), for each random variable, populate as many random numbers as the number of steps of the ongoing simulation (the numbers must be extracted from a random distribution of average zero and standard deviation ($\sigma = \sqrt{\Delta t}$)),

- Calculating the deterministic solution ($S_{i_{det}}(t + \Delta t)$). For each coordinate

(i), in each step $(t+\Delta t)$, calculate the deterministic solution $(S_{i_{det}}(t+\Delta t))$ using a forth order RungeKutta algorithm.

- Calculating the random solution $(S_{i_{ran}}(t+\Delta t))$. For each coordinate (i), in each step $(t+\Delta t)$, calculate the random solution $(S_{i_{ran}}(t+\Delta t))$ according to eq.4.30
- Add the deterministic and random solution to find the solution to eq.4.10 at $(t+\Delta t)$
- Calculate heat flux and average kinetic energy
- Loop over the number of steps (Δt)
- Average over the total number of runs

4.4 Application

In this section we shall apply the technique developed in sec.4.2 to numerically solve for the displacements and momenta as a function of time for a one dimensional linear chain, a small pristine graphene sheet and different configurations of functionalized sheets of graphene. The results of these simulations will be used to calculate some of the thermal properties of the system.

4.4.1 One dimensional linear chain; Classical approximation

Consider a linear chain of N coupled atoms, the first and the last of which interact with thermal heat baths, a schematic diagram of this set up is drawn in Fig.4.1 for $N = 6$. For simplicity only nearest neighbor interactions will be considered and it is assumed that adjacent atoms are coupled with springs of spring constant k. Let x_l be the displacement of the l^{th} particle. The Hamiltonian of this system is

$$H = \sum_i \frac{{p_i}^2}{2m} + \frac{1}{2}k(x_{i+1} - x_i)^2 \tag{4.35}$$

where m is the mass of the particles. We set $m = a = 1$, where a is the lattice constant, and $k = 1$.

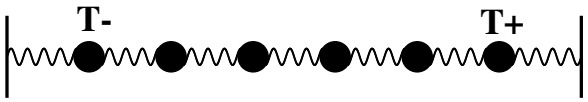


Figure 4.1: A pictorial representation of a linear chain of $N = 6$ mutually coupled oscillators in interaction with two thermal reservoirs working at different temperatures. Here $T_1 = T_+$ and $T_N = T_-$.

The simulation was conducted over 200 runs at a time step of $\Delta t = 0.01$ in units of $\sqrt{k/m}$, the curves in fig.4.2 represent the average heat flux across the different sections of the chain $< J_i >= (1/2)\ k < (x_{i+1} - x_i)(\dot{x}_{i+1} + \dot{x}_{ii}) >$. This result is compared to the analytical solution developed in a previous chapter illustrated in fig.4.3. Both the numerical simulation and the analytical solution produce identical results.

4.4.2 Two Dimensional Sheet of Pristine Graphene

In this application we consider a hexagonal sheet of pristine graphene made of 54 carbon atoms bonded together in a honeycomb structure, three sites on each side of the graphene sheet are in contact with heat baths at respective temperatures of $k_B T_+ = 0.07\ (eV)$ and $k_B T_- = 0.06\ (eV)$, a schematic diagram of this set up is drawn in Fig4.4. We conducted our simulation over 800 runs at a time step of $(\Delta t = 5\ 10^{-3}\ ns)$ for a total number of steps equal to 20000. We calculated the heat flux at every step according to the result in appendix.A.2 and then averaged over the total number of runs. Fig.4.5 is a representation of the result of this simulation. In the steady state regime, the heat flux throughout the graphene

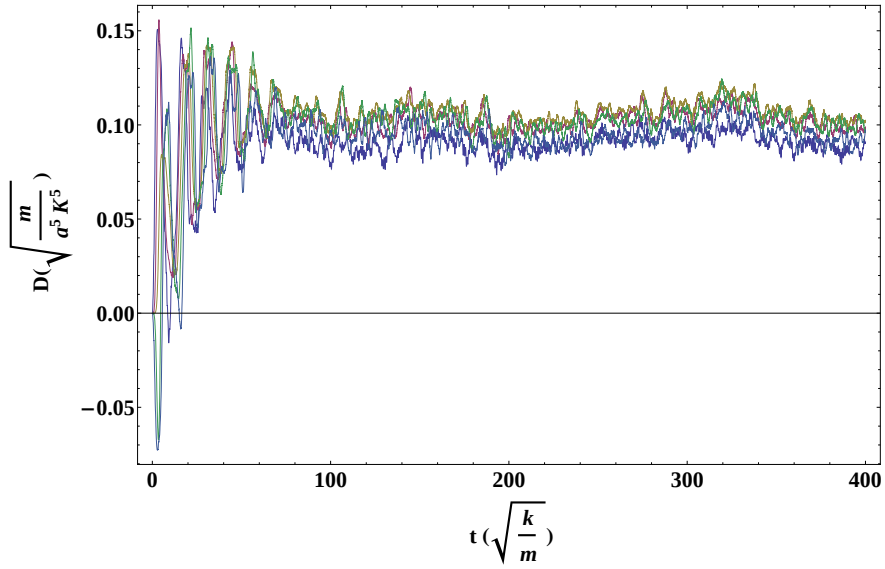


Figure 4.2: Numerical results of heat Flux $J_i = (1/2)k(x_{i+1} - x_i)(\dot{x}_{i+1} + \dot{x}_{ii})$ for a linear chain of $N = 6$ mutually coupled oscillators in interaction with two thermal reservoirs working at different temperatures ($k_B T_- = 1$ (Ka^2) and $T_+ = 2$ (Ka^2)), ($\tau = 0.1$ $\sqrt{K/m}$). The curves represent the heat flux across the different sections of the chain

converges to a value that is roughly 30% smaller than the one calculated using the normal mode analysis outlined in chapter 3. The normal mode analysis which assumes that heat flows ballistically from one site to another and by ignoring all phonon scattering overestimates the amount of heat flowing through the system Non-linear interaction are responsible for 30% reduction in heat flux.

4.4.3 Two Dimensional Sheet of functionalized graphene

In this application we consider a hexagonal sheet of pristine graphene made of 54 carbon atoms bonded together in a honeycomb structure. We attach six alkane chains to opposite boundaries of the graphene sheet and to two different heat baths as shown in fig.4.6 for n-pentene ($N = 5$). We change the length of the chains from $N = 5$ to $N = 7$, and then simulate the thermal heat flux and the velocity autocorrelations throughout the macromolecule. Fig.4.6 represents the time variation of the ratio of the average net heat flux throughout the functionalized graphene configuration shown in fig.4.6 and that of the same configuration

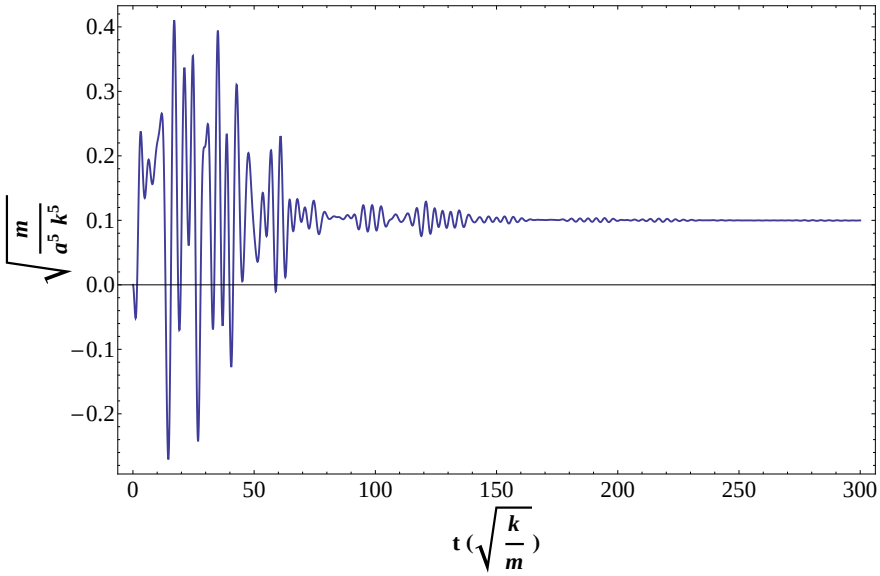


Figure 4.3: Analytical results of heat Flux $J_i = (1/2)k(x_{i+1} - x_i)(\dot{x}_{i+1} + \dot{x}_{ii})$ for a linear chain of $N = 6$ mutually coupled oscillators in interaction with two thermal reservoirs working at different temperatures (($k_B T_- = 1$ (Ka^2) and $T_+ = 2$ (Ka^2)), $(\tau = 0.1\ \sqrt{K/m})$.

calculated using normal mode analysis. The steady state flux is about 30% to 40% lower, this can be interpreted as the result of the difference in elasticity between chains and graphene, and the extent to which phonons are scattered by other phonons. As a matter of fact, the time variation of the average temperatures $T = \langle m\ v^2 \rangle$ on both side of the graphene/alkane interface is reported in fig.4.7, notice the large temperature jump from the alkanes to the graphene. The vibrational modes of the soft alkanes can hardly couple to the phonons of the stiff graphene. A profile of the average temperature across the graphene is also reported in fig to illustrate the temperature gradient across the macromolecule.

The steady state average temperature difference across the interface $\Delta T = \Delta\langle m\ v^2 \rangle$ on the side in contact with the hot bath was calculated for configurations identical to the one in fig.4.6, with side chains of length ranging from $N = 5$ to $N = 7$, the results are reported in Tab.4.1. The temperature difference increases with the chain length and is even larger for even chains compared to odd chains. Odd chains by far couple better to the graphene, a result that conforms to the

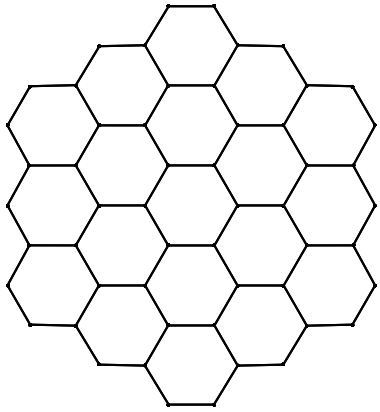


Figure 4.4: A pictorial representation pristine graphene. The number of atoms in the graphene sheet is 54.

normal mode analysis.

N	$\frac{\Delta\langle m\ v^2\rangle}{k_B T_+}$
5	0.453
6	0.602
7	0.492

Table 4.1: Ratio of the average kinetic energy $\langle m\ v^2\rangle$ and $k_B T_+$ as a function of chain length (N), k_B is the Boltzmann constant, T_+ is the temperatures of the hot bath.

4.5 Conclusion

In this chapter we developed the steps to solving the generalized classical Langevin equations for a system of interacting particles in contact with heat baths using a forth order Runge Kutta Method. The results of this technique were used to simulate the heat flux through the system and the temperature drop across the interface between two regions of the system of different degrees of elasticity. We tested this method on a linear chains of particles connected by springs and

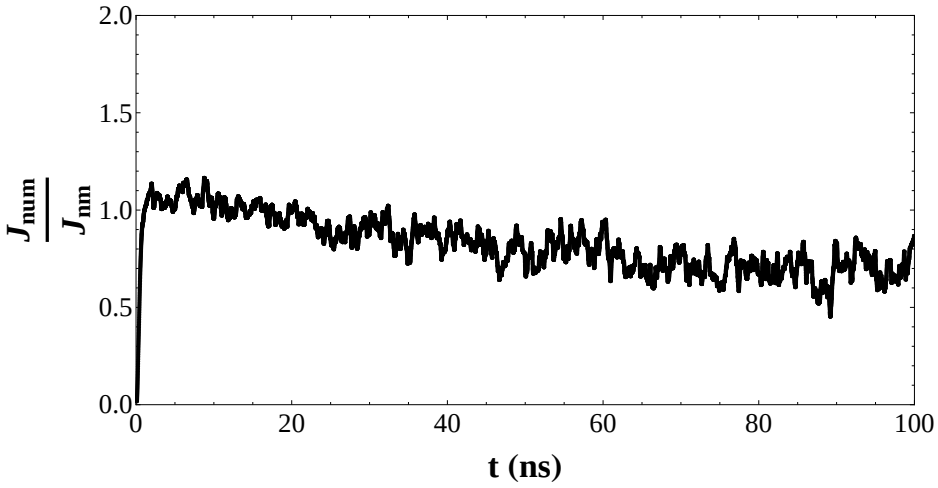


Figure 4.5: Time variation of the ratio of the numerical average heat flux (J_{num}) throughout the graphene configuration shown in fig.4.4 and the heat flux of pristine graphene from the normal mode analysis (J_{nm}). ($k_BT_+ = 0.008$ (eV) and $k_BT_- = 0.007$ (eV)), ($\tau = 0.50$) and ($\gamma = 1$).

the results were identical to the analytical solution. We then applied this technique to a small sheet of functionalized graphene, and compared its results to the normal mode analysis described in chapter 3 for an identical system. It was shown that the temperature difference and thus the interface resistance at the alkane/graphene interface varied with the length of the side chains are qualitatively identical for the simulation and normal mode analysis, the numerical values are however off by at least 30%. Non-linear corrections altered the magnitude of our results, but not the general behavior of the system.

There are several ways this technique can be expanded, for ease of application we chose classical noise with no space dependence. This can be expanded to those systems where the random driving forces are quantum mechanical and have characteristic correlation length comparable to the distance between system particles.

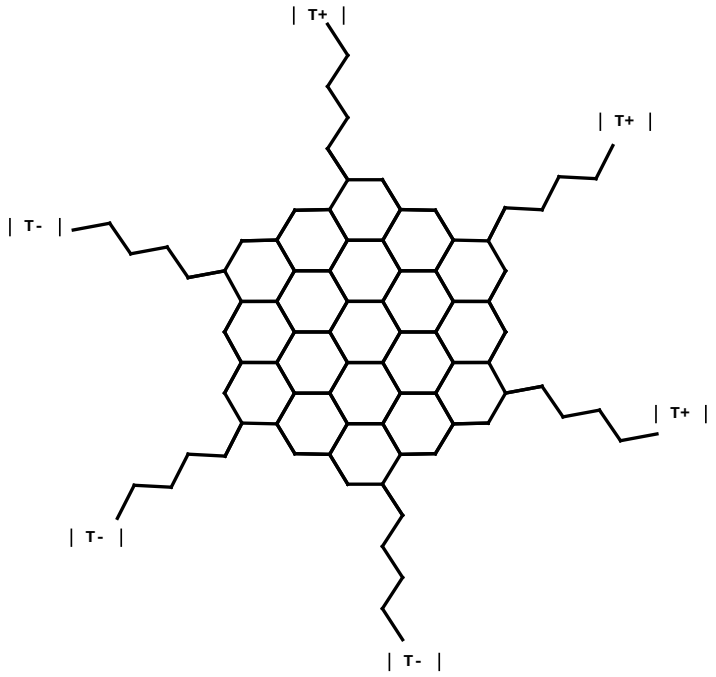


Figure 4.6: A pictorial representation of a functionalized sheet of graphene. The number of atoms in the graphene sheet is 54, The alkane chains are n-pentane. The end of the chains interact with two thermal reservoirs working at different temperatures T_+ and T_-.

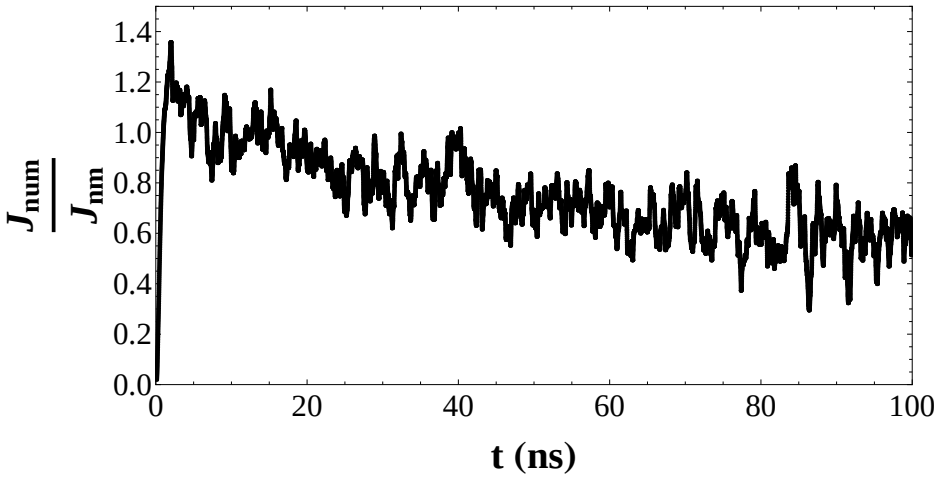


Figure 4.7: Time variation of the ratio of the numerical average heat flux (J_{num}) throughout the graphene configuration shown in fig.4.6 and the heat flux of the same configuration calculated from the normal mode analysis (J_{nm}). ($k_BT_h = 0.008$ (eV) and $k_BT_c = 0.007$ (eV)), ($\tau = 0.50$) and ($\gamma = 1$).

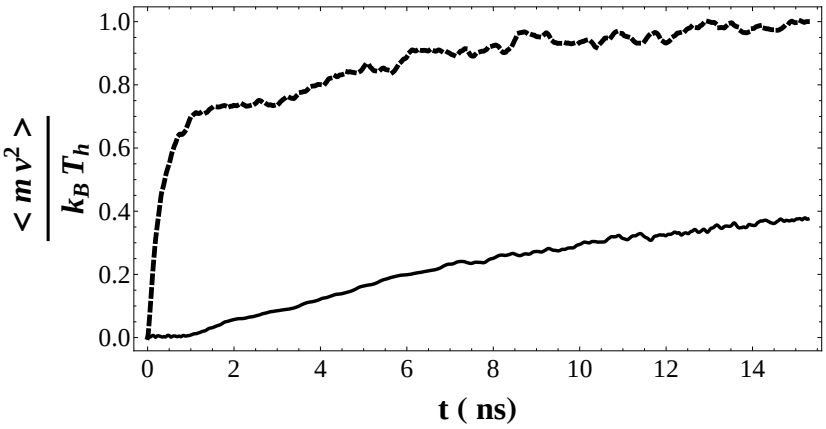


Figure 4.8: Ratio of the time variation of the average temperature $T = \langle m\ v^2 \rangle$ across the alkanes/graphene interface and $k_B\ T_h$.

Chapter 5

Classical Langevin Equations with Time and Space Correlated Noise

5.1 Introduction

Colored noise, even though more realistic and adequate at mimicking the effect of a heat bath on a single particle, may not be suitable for systems of two or more interacting particles. This is because the origin of the drag and random stochastic forces is the same for all particles involved. The fluctuation-dissipation theorem relating these forces should also account for their spatial dependence, and the extent to which the noise on one site may affected the noise on other sites. In this chapter we consider the dynamics of interacting particles which are driven by correlated (not-independent) noise sources. We investigate the effect of spatial correlations in the noise on the dynamical correlations in the relative motion of the particles. As an application we compare results of heat flux with space correlated noises versus colored noises.

5.2 Development

Consider a system made of N particles, $2p$ of which interact with two identical heat baths of respective temperatures T_R and T_L as shown in fig.5.1 The interactions among the particles in the system are described by the potential $U(q_{s_1}, ..., q_{s_N})$ where q_{s_i} refer to the position of the i^{th} particle in the system. If p_{s_i} is the momentum the i^{th} particle in the system, the corresponding system Hamiltonian is of the form

$$H_s = \sum_{1}^{N} \frac{p_{s_i}^2}{2m_{s_i}} + U(q_{s_1}, ..., q_{s_N}) \tag{5.1}$$

In this analysis we model each bath as a collection of an infinite number of non interacting particles each attached to the system by a spring. The Hamiltonians of the left (H_L) and right (H_R) oscillator baths are

$$H_R = \sum_{i=1}^{N_R} \frac{p_{R_i}^2}{2m_{R_i}} + \sum_{i=1}^{N_R} \sum_{j=1}^{p} \frac{1}{2} m_{R_i} \omega_{R_{ij}}^2 \left(q_{R_i} - \frac{\lambda_{R_{ij}}}{m_{R_i} \omega_{R_{ij}}^2} q_{s_j} \right)^2 \tag{5.2}$$

$$H_L = \sum_{1}^{N_L} \frac{p_{L_i}^2}{2m_{L_i}} + \sum_{i=1}^{N_R} \sum_{j=1}^{p} \frac{1}{2} m_{L_i} \omega_{L_{ij}}^2 \left(q_{L_i} - \frac{\lambda_{L_{ij}}}{m_{L_i} \omega_{L_{ij}}^2} q_{s_j} \right)^2 \tag{5.3}$$

where the p_{R_i}, p_{L_j}, q_{R_i}, q_{L_j} are respectively the momenta and displacements of the oscillators in the right and left heat baths. $\omega_{R_{ij}}, \omega_{L_{ij}}$, m_{R_i}, m_{L_j} are respectively the oscillator frequencies and masses. $\lambda_{R_{ij}}, \lambda_{L_{ij}}$ are the coupling constants

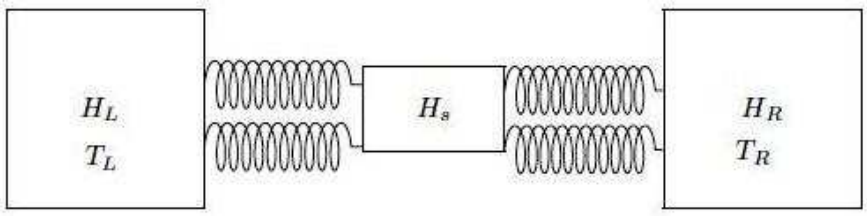


Figure 5.1: Pictorial representation of the system described by the Hamiltonian H_s where p sites on each side interact with two heat bath described by the Hamiltonian H_L and H_R.

The Hamiltonian of the entire system and baths is

$$H = H_s + H_R + H_L \tag{5.4}$$

The equations of motion of the heat bath particles are

$$
\begin{aligned}
\dot{q}_{R_i} &= \frac{p_{R_i}}{m_{R_i}} \\
\dot{p}_{R_i} &= -\sum_{j=1}^{p} m_{R_i}\omega_{R_{ij}}^2 (q_{R_i} - \frac{\lambda_{R_{ij}}}{m_{R_i}\omega_{R_{ij}}^2} q_{s_j}) \\
\dot{q}_{L_i} &= \frac{p_{L_i}}{m_{L_i}} \\
\dot{p}_{L_i} &= -\sum_{j=1}^{p} m_{L_i}\omega_{L_{ij}}^2 (q_{L_i} - \frac{\lambda_{L_{ij}}}{m_{L_i}\omega_{L_{ji}}^2} q_{s_j})
\end{aligned}
\tag{5.5}
$$

Eqs.5.5 can be transformed into a simplified vector equations eq.5.7 by introducing the following vectors

$$
\begin{aligned}
\vec{S}_{b_R}(t) &= \left(q_{R_1}, ..., q_{R_{N_R}}, p_{R_1}, ..., p_{R_{N_R}}\right) \\
\vec{S}_{b_L}(t) &= \left(q_{L_1}, ..., q_{L_{N_L}}, p_{L_1}, ..., p_{L_{N_L}}\right) \\
\vec{S}_s(t) &= \left(q_{s_1}, ..., q_{s_N}, p_{s_1}, ..., p_{s_N}\right)
\end{aligned}
\tag{5.6}
$$

$$
\begin{aligned}
\dot{\vec{S}}_{b_R}(t) &= \begin{pmatrix} \widetilde{0} & \widetilde{M_R^{-1}} \\ -\widetilde{K_R} & \widetilde{0} \end{pmatrix} \vec{S}_{b_R}(t) + \begin{pmatrix} \widetilde{0} & \widetilde{0} \\ \widetilde{\lambda_R}^t & \widetilde{0} \end{pmatrix} \cdot \vec{S}_s(t) \\
\dot{\vec{S}}_{b_L}(t) &= \begin{pmatrix} \widetilde{0} & \widetilde{M_L^{-1}} \\ -\widetilde{K_L} & \widetilde{0} \end{pmatrix} \vec{S}_{b_L}(t) + \begin{pmatrix} \widetilde{0} & \widetilde{0} \\ \widetilde{\lambda_L}^t & \widetilde{0} \end{pmatrix} \cdot \vec{S}_s(t)
\end{aligned}
\tag{5.7}
$$

where and $\widetilde{M}^{-1}$ is a diagonal matrix with elements $\widetilde{M_{ij}^{-1}} - \delta_{ij}/m_i$, $\widetilde{K}$ is also diagonal with elements $K_{ij} = \delta_{ij} m_i \sum_{k}^{p} {\omega_{ik}}^2$, and δ_{ij} is the Kronecker delta function

Take

$$\widetilde{A} = \begin{pmatrix} \widetilde{0} & \widetilde{M^{-1}} \\ -\widetilde{K} & \widetilde{0} \end{pmatrix} \tag{5.8}$$

The solution to eq.5.7 for each bath is of the form

$$\vec{S}_b(t) = \exp(t\ \widetilde{A}) \cdot \vec{S}_b(0) + \int_0^t dt'\ \exp((t-t')\ \widetilde{A}) \cdot \begin{pmatrix} \widetilde{0} & \widetilde{0} \\ \widetilde{\lambda}^t & \widetilde{0} \end{pmatrix} \cdot \vec{S}_s(t') \tag{5.9}$$

An integration by parts leads to the form:

$$\vec{S}_b(t) = -\widetilde{A}^{-1} \cdot \begin{pmatrix} \widetilde{0} & \widetilde{0} \\ \widetilde{\lambda}^t & \widetilde{0} \end{pmatrix} \cdot \vec{S}_s(t) + \exp(t\ \widetilde{A}) \cdot [\vec{S}_b(0) + \widetilde{A}^{-1} \cdot \begin{pmatrix} \widetilde{0} & \widetilde{0} \\ \widetilde{\lambda}^t & \widetilde{0} \end{pmatrix} \cdot \vec{S}_s(0)] +$$

$$\int_0^t dt'\ \exp((t-t')\ \widetilde{A}) \cdot \widetilde{A}^{-1} \cdot \begin{pmatrix} \widetilde{0} & \widetilde{0} \\ \widetilde{\lambda}^t & \widetilde{0} \end{pmatrix} \cdot \frac{d}{dt}\left(\vec{S}_s(t')\right) \tag{5.10}$$

Assuming $\vec{S}_s(0) = 0$, eq.5.10 becomes

$$\vec{S}_b(t) = -\widetilde{A}^{-1} \cdot \begin{pmatrix} \widetilde{0} & \widetilde{0} \\ \widetilde{\lambda}^t & \widetilde{0} \end{pmatrix} \cdot \vec{S}_s(t) + \exp(t\ \widetilde{A}) \cdot \vec{S}_b(0) +$$

$$\int_0^t dt'\ \exp((t-t')\ \widetilde{A}) \cdot \widetilde{A}^{-1} \cdot \begin{pmatrix} \widetilde{0} & \widetilde{0} \\ \widetilde{\lambda}^t & \widetilde{0} \end{pmatrix} \cdot \frac{d}{dt}\left(\vec{S}_s(t')\right) \tag{5.11}$$

Now we turn our attention to the system. The equations of motion of the system particles are of the form

$$\dot{q}_{s_i} = \frac{p_{s_i}}{m_{s_i}}$$

$$\dot{p}_{s_i} = -\frac{\partial U}{\partial q_{s_i}} + \sum_{j=1}^{N_R} \lambda_{R_{ji}} \left(q_{R_j} - \frac{\lambda_{R_{ji}}}{m_{R_j}\omega_{R_{ji}}^2} q_{s_i} \right) + \sum_{j=1}^{N_L} \lambda_{L_{ji}} \left(q_{L_j} - \frac{\lambda_{L_{ji}}}{m_{L_j}\omega_{L_{ji}}^2} q_{s_i} \right) \tag{5.12}$$

Eq.5.12 can be transformed into a more compact form as

$$\dot{\vec{S}}_s(t) = \vec{f}(\vec{S}_s(t)) + \begin{pmatrix} \widetilde{0} & \widetilde{0} \\ \widetilde{\lambda_R} & \widetilde{0} \end{pmatrix} \cdot \vec{S}_{b_R}(t) - \widetilde{\eta}_R \cdot \vec{S}_s(t) + \begin{pmatrix} \widetilde{0} & \widetilde{0} \\ \widetilde{\lambda_L} & \widetilde{0} \end{pmatrix} \cdot \vec{S}_{b_L}(t) - \widetilde{\eta}_L \cdot \vec{S}_s(t) \tag{5.13}$$

where

$$\vec{f}(\vec{S}_s(t)) = \left(0, ..., 0, -\frac{\partial U}{\partial q_{s_1}}, ..., -\frac{\partial U}{\partial q_{s_N}} \right) \tag{5.14}$$

and

$$\widetilde{\eta} = \begin{pmatrix} \widetilde{0} & -\widetilde{M}^{-1} \\ \delta_{ij} \sum_{k=1}^{N} \frac{\lambda_{ki}^2}{m_k\ \omega_{ki}^2} & \widetilde{0} \end{pmatrix} \tag{5.15}$$

Substituting $\vec{S}_b$ by its expression from eq.5.11 gives

$$\dot{\vec{S}}_s(t) = \vec{f}(\vec{S}_s(t)) - \left[\begin{pmatrix} \widetilde{0} & \widetilde{0} \\ \widetilde{\lambda_R} & \widetilde{0} \end{pmatrix} \cdot \widetilde{A}_R^{-1} \cdot \begin{pmatrix} \widetilde{0} & \widetilde{0} \\ \widetilde{\lambda_R}^t & \widetilde{0} \end{pmatrix} + \widetilde{\eta}_R \right] \cdot \vec{S}_s(t)$$

$$+ \begin{pmatrix} \widetilde{0} & \widetilde{0} \\ \widetilde{\lambda_R} & \widetilde{0} \end{pmatrix} \cdot \exp(t\ \widetilde{A}_R) \cdot \vec{S}_{b_R}(0) +$$

$$\int_0^t dt' \begin{pmatrix} \widetilde{0} & \widetilde{0} \\ \widetilde{\lambda_R} & \widetilde{0} \end{pmatrix} \cdot \exp((t-t')\ \widetilde{A}_R) \cdot \widetilde{A}_R^{-1} \cdot \begin{pmatrix} \widetilde{0} & \widetilde{0} \\ \widetilde{0} & \widetilde{\lambda_R}^t \end{pmatrix} \cdot \vec{S}_s(t') \tag{5.16}$$

$$- \left[\begin{pmatrix} \widetilde{0} & \widetilde{0} \\ \widetilde{\lambda_L} & \widetilde{0} \end{pmatrix} \cdot \widetilde{A}_L^{-1} \cdot \begin{pmatrix} \widetilde{0} & \widetilde{0} \\ \widetilde{\lambda_L}^t & \widetilde{0} \end{pmatrix} + \widetilde{\eta}_L \right] \cdot \vec{S}_s(t)$$

$$+ \begin{pmatrix} \widetilde{0} & \widetilde{0} \\ \widetilde{\lambda_L} & \widetilde{0} \end{pmatrix} \cdot \exp(t\ \widetilde{A}_L) \cdot \vec{S}_{b_L}(0) +$$

$$\int_0^t dt' \begin{pmatrix} \widetilde{0} & \widetilde{0} \\ \widetilde{\lambda_L} & \widetilde{0} \end{pmatrix} \cdot \exp((t-t')\ \widetilde{A}_L) \cdot \widetilde{A}_L^{-1} \cdot \begin{pmatrix} \widetilde{0} & \widetilde{0} \\ \widetilde{0} & \widetilde{\lambda_L}^t \end{pmatrix} \cdot \vec{S}_s(t')$$

This is the equation of motion for $\vec{S}_s(t)$, expressed in terms of its own history from 0 to t and the bath variables enter only through their initial values.

We introduce the stochastic Gaussian force as

$$\vec{F}(t) = \begin{pmatrix} \widetilde{0} & \widetilde{0} \\ \widetilde{\lambda_R} & \widetilde{0} \end{pmatrix} \cdot \exp(t\ \widetilde{A}_R) \cdot \vec{S}_b(0) \tag{5.17}$$

We assume that at $t = 0$, the bath particles initial positions and momenta

are distributed according to the canonical distribution eq.5.19[10], where $\beta = (k_B T)^{-0.5}$, H_b is the bath particles energy at $t = 0$, and (**det**) stands for determinant.

$$H_b = \sum_{i=1}^{N} \frac{p_i^2}{2m_i} + \sum_{i=1}^{N} \sum_{j=1}^{N} q_i(0) \left(\sum_{s=1}^{p} \frac{1}{2} m_i \omega_{is}^2 \delta_{ij} \right) q_j(0) \tag{5.18}$$

$$P(\vec{S}_b(0)) = \left(\frac{2\pi}{\beta} \right)^N det(\widetilde{K})^{-1/2} \, e^{-\beta H_b} \tag{5.19}$$

The expectation value of any function F is

$$\langle F \rangle = \int d\vec{q}(0) \, d\vec{p}(0) \, F \, P(\vec{S}_b(0)) \tag{5.20}$$

Accordingly we have the following relations

$$\begin{aligned} &\langle \vec{S}_b(0) \rangle = 0 \\ &\langle p_i(0) \, p_j(0) \rangle = k_B T \, M_{ij} \, \delta_{ij} \\ &\langle p_i(0) \, q_j(0) \rangle = 0 \\ &\langle q_i(0) \, q_j(0) \rangle = k_B T \, \widetilde{K}_{ij}^{-1} \end{aligned} \tag{5.21}$$

which can be transformed into a simpler form as

$$\langle \vec{S}_b(0) \cdot \vec{S}_b(0)^t \rangle = k_B T \begin{pmatrix} \widetilde{K}^{-1} & 0 \\ 0 & \widetilde{M} \end{pmatrix} \tag{5.22}$$

From these relations we derive the statistics of the noise eq.5.17

$$\langle \vec{F}(t) \rangle = 0$$

$$\langle \vec{F}(t)\vec{F}(t')^t \rangle = \langle \begin{pmatrix} \widetilde{0} & \widetilde{0} \\ \widetilde{\lambda_R} & \widetilde{0} \end{pmatrix} \cdot \exp(t\ \widetilde{A}) \cdot \left(\vec{S}_b(0) \cdot \vec{S}_b(0)^t \right) \cdot \exp(t'\ \widetilde{A})^t \cdot \begin{pmatrix} \widetilde{0} & \widetilde{0} \\ \widetilde{\lambda_R} & \widetilde{0} \end{pmatrix}^t \rangle \tag{5.23}$$

one can easily prove that

$$\widetilde{A} = \begin{pmatrix} \widetilde{0} & \widetilde{I} \\ -\widetilde{I} & 0 \end{pmatrix} \cdot \left(\vec{S}_b(0) \cdot \vec{S}_b(0)^t \right)^{-1} \tag{5.24}$$

and that

$$\left(\vec{S}_b(0)\vec{S}_b(0)^t \right) \cdot \left[\exp \left(t \begin{pmatrix} \widetilde{0} & \widetilde{I} \\ -\widetilde{I} & 0 \end{pmatrix} \cdot \left(\vec{S}_b(0) \cdot \vec{S}_b(0)^t \right)^{-1} \right) \right]^t = \exp \left(-t \begin{pmatrix} \widetilde{0} & \widetilde{I} \\ -\widetilde{I} & 0 \end{pmatrix} \cdot \left(\vec{S}_b(0) \cdot \vec{S}_b(0)^t \right)^{-1} \right) \cdot \left(\vec{S}_b(0) \cdot \vec{S}_b(0)^t \right) \tag{5.25}$$

Consequently

$$\langle \vec{F}(t)\vec{F}(t')^t \rangle = k_B T_{R/L} \begin{pmatrix} \widetilde{0} & \widetilde{0} \\ \widetilde{\lambda_R} & \widetilde{0} \end{pmatrix} \cdot \exp((t-t')\ \widetilde{A}) \cdot \langle \left(\vec{S}_b(0) \cdot \vec{S}_b(0)^t \right) \rangle \cdot \begin{pmatrix} \widetilde{0} & \widetilde{0} \\ \widetilde{\lambda_R} & \widetilde{0} \end{pmatrix}^t$$

$$= k_B T_{R/L} \widetilde{L}(t-t') \tag{5.26}$$

where

$$\widetilde{L}(t-t') = \begin{pmatrix} \widetilde{0} & \widetilde{0} \\ \widetilde{\lambda_R} & \widetilde{0} \end{pmatrix} \cdot \exp((t-t')\ \widetilde{A}) \cdot \langle \left(\vec{S}_b(0) \cdot \vec{S}_b(0)^t \right) \rangle \cdot \begin{pmatrix} \widetilde{0} & \widetilde{0} \\ \widetilde{\lambda_R} & \widetilde{0} \end{pmatrix}^t \tag{5.27}$$

Knowing that one can write

$$\langle \left(\vec{S}_b(0) \cdot \vec{S}_b(0)^t \right) \rangle = \widetilde{A}^{-1} \cdot \begin{pmatrix} \widetilde{0} & \widetilde{I} \\ -\widetilde{I} & 0 \end{pmatrix} \tag{5.28}$$

Eq.5.27 becomes

$$\widetilde{L}(t-t') = - \begin{pmatrix} \widetilde{0} & \widetilde{0} \\ \widetilde{\lambda_L} & \widetilde{0} \end{pmatrix} \cdot \exp((t-t')\ \widetilde{A}_L) \cdot \widetilde{A}_L^{-1} \cdot \begin{pmatrix} \widetilde{0} & \widetilde{0} \\ \widetilde{0} & \widetilde{\lambda_L}^t \end{pmatrix} \tag{5.29}$$

By writing

$$\exp((t)\ \widetilde{A}) = \sum_n \frac{t^n \widetilde{A}^n}{n!} = \sum_n \frac{t^{2n} \widetilde{A}^{2n}}{(2n)!} + \sum_n \frac{t^{2n+1} \widetilde{A}^{2n+1}}{(2n+1)!} \tag{5.30}$$

on can check that the elements of $\widetilde{A}^{2n+1}$ are all off diagonal, accordingly they do not contribute to $\widetilde{L}(t-t')$, and eq.5.29 simplifies to .

$$\widetilde{L}(t-t') = -\begin{pmatrix} \widetilde{0} & \widetilde{0} \\ \widetilde{\lambda_L} & \widetilde{0} \end{pmatrix} \cdot \exp((t-t')\ \widetilde{A}_L) \cdot \begin{pmatrix} \widetilde{0} & -\widetilde{K}^{-1} \cdot \widetilde{\lambda}^t \\ \widetilde{0} & \widetilde{0} \end{pmatrix} \tag{5.31}$$

the elements of which are of the form

$$\widetilde{L}_{ij}(t-t') = \sum_{k=1}^{N} \lambda_{ik}\ \lambda_{jk}\ \frac{\cos\left[\left(\sqrt{\sum_{l=1}^{p} \omega_{kl}^2}\right)\ (t-t')\right]}{m_k \sum_{l=1}^{p} \omega_{kl}^2} \tag{5.32}$$

Assuming all the m_k to be the identical among the bath particles, and ω_{kl} to be the same for all $l's$ and equal to ω_k, eq.5.32 becomes

$$\widetilde{L}_{ij}(t-t') = \sum_{k=1}^{N} \lambda_{ik}\ \lambda_{jk}\ \frac{\cos(\sqrt{p}\ \omega_k\ (t-t'))}{m_k(\sqrt{p}\ \omega_k)^2} \tag{5.33}$$

If we treat the frequency distribution as continuous, then we can replace the sum in the previous equation by an integral eq.5.34 and eq.5.33 becomes

$$\sum \to N \int_0^{+\infty} g(\omega)\ d\omega \tag{5.34}$$

$$\widetilde{L}_{ij}(t) = \int_0^{+\infty} \frac{N\ \lambda_i(\omega)\ \lambda_j(\omega)}{p\ m(\omega)\ \omega^2}\ g(\omega)\cos(\sqrt{p}\ \omega t)\ d\omega \tag{5.35}$$

If now $N\ \lambda_i(\omega)\ \lambda_j(\omega)\ g(\omega)/m(\omega) \propto \omega^2$ for all frequencies then eq.5.35 becomes

the Dirac delta function eq.5.36 and the noise is white.

$$\widetilde{L}_{ij}(t) \propto \int_0^{+\infty} \cos(\sqrt{p}\ \omega t)\ d\omega \propto \delta(t) \tag{5.36}$$

If $N\ \lambda_i(\omega)\ \lambda_j(\omega)\ g(\omega)/m(\omega) \propto \omega^2/(1+p\ \tau^2\ \omega^2)$ for all frequencies then eq.5.35 becomes an exponentially decaying function of time eq.5.37 and the noise is colored.

$$\widetilde{L}_{ij}(t) \propto \int_0^{+\infty} \frac{1}{1+p\ \tau^2\ \omega^2} \frac{\cos(\sqrt{p}\ \omega t)}{p}\ d\omega \propto \frac{1}{\tau p^{3/2}}\ e^{-t/\tau} \tag{5.37}$$

The second and fifth terms in eq.5.16 which can be taught of as additional coupling between the system parameters due to the presence of the noise can be simplified according to

$$\widetilde{C} = \left[\begin{pmatrix} \widetilde{0} & \widetilde{0} \\ \widetilde{\lambda_R} & \widetilde{0} \end{pmatrix} \cdot \widetilde{A}_R^{-1} \cdot \begin{pmatrix} \widetilde{0} & \widetilde{0} \\ \widetilde{\lambda_R}^t & \widetilde{0} \end{pmatrix} + \widetilde{\eta}_R \right]$$

$$= \begin{pmatrix} \widetilde{0} & -\widetilde{M}^{-1} \\ \delta_{ij} \sum_{k=1}^{N} \frac{\lambda_{ki}^2}{m_k \ \omega_{ki}^2} & \widetilde{0} \end{pmatrix} - \begin{pmatrix} \widetilde{0} & \widetilde{0} \\ \widetilde{\lambda} \cdot \widetilde{K}^{-1} \cdot \widetilde{\lambda}^t & \widetilde{0} \end{pmatrix}$$

$$= \begin{pmatrix} \widetilde{0} & -\widetilde{M}^{-1} \\ \delta_{ij} \sum_{k=1}^{N} \frac{\lambda_{ki}^2}{m_k \ \omega_{ki}^2} - \sum_{k=1}^{N} \left(\frac{\widetilde{\lambda}_{ik} \ \widetilde{\lambda}_{kj}^t}{m_k \ \sum_{s=1}^{p} \omega_{ks}^2} \right) & \widetilde{0} \end{pmatrix} \tag{5.38}$$

$$= \begin{pmatrix} \widetilde{0} & -\widetilde{M}^{-1} \\ \delta_{ij} \sum_{k=1}^{N} \frac{\lambda_{ki}^2}{m_k \ \omega_{ki}^2} - \sum_{k=1}^{N} \left(\frac{\widetilde{\lambda}_{ik} \ \widetilde{\lambda}_{jk}}{m_k \ p \ \omega_{ki}^2} \right) & \widetilde{0} \end{pmatrix}$$

If the number of oscillators in the bath is infinite then the previous equations becomes

$$\widetilde{C} = \begin{pmatrix} \widetilde{0} & -\widetilde{M}^{-1} \\ \delta_{ij} \int_0^\infty \frac{N \ \lambda^2}{m \ \omega^2} \ g(\omega) \ d\omega - S_{ij} \int_0^\infty \frac{N \ \lambda^2}{m \ p \ \omega^2} \ g(\omega) \ d\omega & \widetilde{0} \end{pmatrix} \tag{5.39}$$

where $S_{ij} = 1$ if i and j are in contact with the heat bath, otherwise $S_{ij} = 0$.

If $N \ \lambda^2(\omega) \ g(\omega)/m(\omega) \propto \omega^2/(1 + p \ \tau^2 \ \omega^2)$ for all frequencies then eq.5.39 becomes

$$\widetilde{C} = \begin{pmatrix} & \widetilde{0} & -\widetilde{M^{-1}} \\ \delta_{ij}\int_0^\infty \frac{1}{(1+p\ \tau^2\ \omega^2)}\ d\omega - \frac{S_{ij}}{p}\ \int_0^\infty \frac{1}{(1+p\ \tau^2\ \omega^2)}\ d\omega & & \widetilde{0} \end{pmatrix} \tag{5.40}$$

or

$$\widetilde{C} = \begin{pmatrix} \widetilde{0} & -\widetilde{M^{-1}} \\ \widetilde{E} & \widetilde{0} \end{pmatrix} \tag{5.41}$$

where

$$\widetilde{E} = \begin{pmatrix} \frac{\pi\ \delta_{ij}}{2\ \tau\sqrt{p}} - \frac{\pi\ S_{ij}}{2\ \tau p^{3/2}} \end{pmatrix} \tag{5.42}$$

5.2.1 Solving Langevin equations with spatial correlated noise

In this section, we shall solve the generalized Langevin equations with space and time correlated noise

$$m_{s_i}\ \ddot{q}_{s_i}(t) = -\sum_j K_{ij}\ q_{s_j}(t) - \sum_j \widetilde{E}_{ij}\ q_{s_j} - \sum_j \widetilde{S}_{ij} \int_0^t dt' \widetilde{L}_{ij}(t-t')\ \dot{q}_{sj}(t') + F_i(t) \tag{5.43}$$

where $\widetilde{S_{ij}} = 1$ if i and j are in contact with the same heat bath and zero if not.

The noise term $(F_i(t))$ is related to the memory kernel by the fluctuation-dissipation theorem

$$\langle F_i(t)F_j(t')\rangle = \widetilde{S}_{ij}k_BT\widetilde{L}_{ij}(t-t') \tag{5.44}$$

Particularly, for exponentially correlated noise, also known as Ornstein Uhlenbeck noise

$$\begin{aligned}\langle F_i(t)\rangle &= 0\\ \langle F_i(t)\ F_j(t')\rangle &= \frac{\gamma_{ij}}{\tau\ p^{3/2}}\widetilde{S}_{ij}k_BTe^{-|t-t'|/\tau}\end{aligned} \tag{5.45}$$

and the equations of motion eq.5.43 become

$$m_{s_i}\ \ddot{q_{s_i}}(t) = -\sum_j K_{ij}\ q_{s_j}(t) - \sum_j \widetilde{E}_{ij}\ q_{s_j} - \sum_j \frac{\widetilde{S}_{ij}}{p^{3/2}}\int_0^t dt' \frac{\gamma_{ij}}{\tau}\ e^{-|t-t'|/\tau}\ \dot{q}_{sj}(t') + F_i(t) \tag{5.46}$$

We introduce a new variable $y_j(t)$ such that

$$y_j(t) = \frac{1}{\tau}\int_0^t dt' e^{-|t-t'|/\tau}\ \dot{q}_{sj}(t') \tag{5.47}$$

our equations of motion eq.5.46 become:

$$\begin{aligned}\dot{q}_{s_i} &= \frac{p_{s_i}(t)}{m_i}\\ \dot{p}_{s_i}(t) &= -\sum_j K_{ij}\ q_{s_j}(t) - \sum_j \widetilde{E}_{ij}\ q_{s_j} - \sum_j \gamma_{ij}\ \frac{\widetilde{S}_{ij}}{p^{3/2}}\ y_j(t) + F_i(t)\\ \dot{y}_i(t) &= -\frac{1}{\tau}y_i(t) + \frac{1}{\tau\ m_{s_i}}p_{s_i}(t)\end{aligned} \tag{5.48}$$

This set of equations can be put in a more compact form if one introduces a new vector $\vec{S}$ such that

$$\vec{S} = (q_{s_1}, ...q_{s_N}, p_{s_1}, ...p_{s_N}, y_1, ..., y_N) \tag{5.49}$$

$$\dot{\vec{S}} = \widetilde{D}.\vec{S} + \vec{\Pi} \tag{5.50}$$

where

$$\widetilde{D} = \begin{pmatrix} \widetilde{0} & \widetilde{M}^{-1} & \widetilde{0} \\ -\widetilde{K} - \widetilde{E} & \widetilde{0} & -\widetilde{\Lambda} \\ \widetilde{0} & \widetilde{M}^{-1} \cdot \widetilde{R}/\tau & -\widetilde{R}/\tau \end{pmatrix} \tag{5.51}$$

$$\vec{\Pi} = (0, ..., 0, 0, F_1(t), ..., F_N(t), 0, ..., 0) \tag{5.52}$$

and $\widetilde{R}$ is a diagonal matrix with $R_{ii} = 1$ only if site i is in contact with the heat bath, and $\widetilde{\Lambda}_{ij} = \frac{\gamma_{ij}}{p^{3/2}}\ \widetilde{S}_{ij}$

If $\widetilde{\theta}$ is the matrix of right (column) eigenvectors of the matrix $\widetilde{D}$, we first transform $\vec{S}$ with the rotation matrix $\widetilde{\theta}$ such that $\vec{S} = \widetilde{\theta}\vec{X}$. Replacing $\vec{S}$ with its new expression in eq.5.50 gives

$$\widetilde{\theta}\dot{\vec{X}} = \widetilde{A}\widetilde{\theta}\vec{X} + \vec{\Pi} \tag{5.53}$$

which can be transformed to

$$\dot{\vec{X}} = (\widetilde{\theta}^{-1}\widetilde{A}\widetilde{\theta}) \cdot \vec{X} + \widetilde{\theta}^{-1}\vec{\Pi} \tag{5.54}$$

If $(\widetilde{\theta}^{-1}\widetilde{A}\widetilde{\theta})$ is diagonal, the previous problem reduces to a first order differential equation for the components of $\vec{X}$ of the form

$$\dot{X}_i = a_i\ X_i + (\widetilde{\theta}^{-1}\vec{\Pi})_i \tag{5.55}$$

where a_i is the i^{th} eigenvalue of matrix $(\widetilde{D})$. The solution to this equation is of the form

$$X_i(t) = e^{a_i\ t}\ \left(\int_0^t d\tau_1\ e^{-a_i\ \tau_1}\ (\widetilde{\theta}^{-1}\vec{\Pi})_i\ +\ X_{io} \right) \tag{5.56}$$

if we take $\vec{S}(t = 0) = 0$ then $X_{io} = 0$ and eq.5.56 reduces to

$$X_i(t) = e^{a_i\ t}\ \left(\int_0^t d\tau_1\ e^{-a_i\ \tau_1}\ (\widetilde{\theta}^{-1}\vec{\Pi})_i(\tau_1)\right) \tag{5.57}$$

We can return to the original variables $\vec{S}$ from $\vec{S} = \widetilde{\theta}\vec{X}$. This results in

$$S_i(t) = \sum_k \widetilde{\theta}_{ik} X_k(t) = \sum_k \widetilde{\theta}_{ik} e^{a_k\ t}\ \left(\int_0^t d\tau_1\ e^{-a_k\ \tau_1}\ (\widetilde{\theta}^{-1}\vec{\Pi})_k(\tau_1)\right) \tag{5.58}$$

The position and momentum correlations can be deduced accordingly

$$\begin{aligned}\langle S_i(t_1)S_j(t_2)\rangle &= \sum_{ks} \widetilde{\theta}_{ik}\ \widetilde{\theta}_{js} e^{a_k\ t_1 + a_s\ t_2}\ \int_0^{t_1}\int_0^{t_2} d\tau_1\ d\tau_2\ e^{-a_k\ \tau_1 - a_s\ \tau_2} \\ &\quad \langle(\widetilde{\theta}^{-1}\vec{\Pi})_k(\tau_1)\ (\widetilde{\theta}^{-1}\vec{\Pi})_s(\tau_2)\rangle \\ &= \sum_{ks} \widetilde{\theta}_{ik}\ \widetilde{\theta}_{js} e^{a_k\ t_1 + a_s\ t_2}\ \int_0^{t_1}\int_0^{t_2} d\tau_1\ d\tau_2\ e^{-a_k\ \tau_1 - a_s\ \tau_2} \sum_{lm} \\ &\quad \widetilde{\theta}^{-1}_{kl}\ \widetilde{\theta}^{-1}_{sm}\ \langle\vec{\Pi}_l(\tau_1)\ (\vec{\Pi})_m(\tau_2)\rangle\end{aligned} \tag{5.59}$$

or

$$\begin{aligned}\langle S_i(t_1)S_j(t_2)\rangle &= \frac{k_B T_c}{\tau} \sum_{ks}\sum_{lm} \widetilde{\theta}_{ik}\ \widetilde{\theta}_{js}\widetilde{\theta}^{-1}_{kl}\ \widetilde{\theta}^{-1}_{sm}\ \widetilde{\Lambda}_{lm} e^{a_k\ t_1 + a_s\ t_2} \\ &\quad \int_0^{t_1}\int_0^{t_2} dx_1\ dx_2\ e^{-a_k\ x_1 - a_s\ x_2}\ e^{-|x_1 - x_2|/\tau} + \\ &\quad \frac{k_B T_h}{\tau} \sum_{ks}\sum_{lm} \widetilde{\theta}_{ik}\ \widetilde{\theta}_{js}\widetilde{\theta}^{-1}_{kl}\ \ \widetilde{\theta}^{-1}_{sm}\ \widetilde{\Lambda}_{lm} e^{a_k\ t_1 + a_s\ t_2} \\ &\quad \int_0^{t_1}\int_0^{t_2} dx_1\ dx_2\ e^{-a_k\ x_1 - a_s\ x_2}\ e^{-|x_1 - x_2|/\tau}\end{aligned} \tag{5.60}$$

In the steady state regime the above correlations converge to

$$\begin{aligned}\langle S_i\ S_j\rangle = \frac{k_B T_c}{\tau}\sum_{ks}\sum_{lm}\widetilde{\theta}_{ik}\ \widetilde{\theta}_{js}\widetilde{\theta}^{-1}_{kl}\ \widetilde{\theta}^{-1}_{sm}\ \widetilde{\Lambda}_{lm} \\ \left(\frac{a_k+a_s-2/\tau}{(a_k+a_s)(a_k-1/\tau)(a_s-1/\tau)}\right)+ \\ \frac{k_B T_h}{\tau}\sum_{ks}\sum_{lm}\widetilde{\theta}_{ik}\ \widetilde{\theta}_{js}\widetilde{\theta}^{-1}_{kl}\ \widetilde{\theta}^{-1}_{sm}\ \widetilde{\Lambda}_{lm} \\ \left(\frac{a_k+a_s-2/\tau}{(a_k+a_s)(a_k-1/\tau)(a_s-1/\tau)}\right)\end{aligned} \tag{5.61}$$

where T_h and T_c are respectively the temperatures of the hot and cold baths.

5.3 Application

In this section we shall present the application of the results of section 5.2 for a one dimensional linear chain and a small sheet of functionalized graphene.

5.3.1 One dimensional linear chain

Consider a linear chain of N coupled atoms, We allow some of the sites on both ends to interact with two different heat baths. A schematic diagram of this set up is drawn in Fig.5.2 for $N = 6$. For simplicity only nearest neighbor interactions will be considered and it is assumed that adjacent atoms are coupled with springs of spring constant K. The hamiltonian of this system is

$$H = \sum_i \frac{{p_i}^2}{2m} + \frac{1}{2}K(x_{i+1}-x_i)^2 \tag{5.62}$$

where m is the mass of the particles. We set $m = a = 1$, where a is the lattice constant, and $K = 1$.

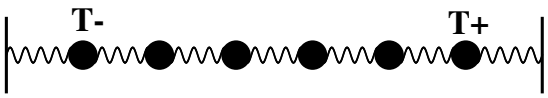


Figure 5.2: A pictorial representation of a linear chain of six ($N = 6$) mutually coupled oscillators interacting with two thermal reservoirs working at different temperatures. Here $T_R = T_+$ and $T_L = T_-$.

Using the results developed in the previous section and the definition of heat flux in Appendix.A.3, we calculated the ratio of the thermal conductance of the chain with spatial noise (λ_s) when the spatial correlation with the nearest neighbor and that of the same chain with colored noise (λ_t), the number of sites in contact with each heat bath was changed from $p = 1$ to $p = 3$ and was chosen to be identical for each bath. As illustrated in fig.5.3, the overall thermal conduction throughout the chain increased. The noise correlation manifest as additional coupling ($\widetilde{E}_i j$) between the system particles independent from the system's internal interactions. This additional coupling is responsible for the improved thermal conductance.

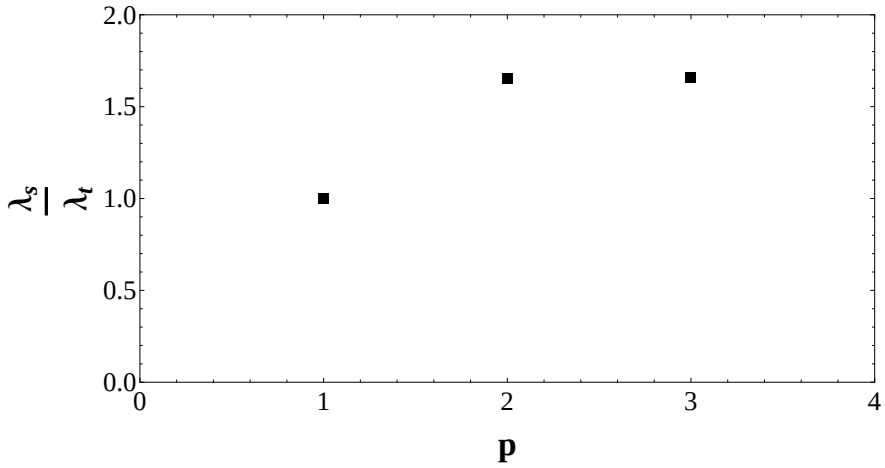


Figure 5.3: ratio of the thermal conductance of the chain with spatial noise (λ_s) and the thermal conductance of the same chain with colored noise (λ_t) as a function of the number sites in contact with each heat bath (p).

5.3.2 Two dimensional Sheet of functionalized Graphene

In this application we consider the functionalized sheet of graphene shown in fig.5.4. The hexagonal sheet is made of 54 carbon atoms bonded together in a honeycomb structure. The chains are alkanes covalently bonded to opposite boundaries of the graphene and to two heat baths at respective temperatures T_+ and T_-. The alkane chains are n-pentane. The Tersoff-Berner (TB) force field is used to describe the interactions among the atoms in the graphene sheet. The Nath, Escobedo, and Pablo revised (NERD) potential is used to describe the interactions in the chains and the bond between the chains and the graphene. We assume the characteristic length of the noise to be of the same order as the distance between adjacent sites, so that there is correlation with the nearest site in contact with the same heat bath. We use the method outlined in the previous section and calculate the thermal conductance of the functionalized graphene with (λ_s) and without (λ_t) space correlation when the last two sites of each chain are heated for size chains ranging from $N = 5$ to $N = 7$. Fig.5.5 represents the ratio of both conductances (λ_s/λ_t), as illustrated, the thermal conductance has improved, in addition, the graphene configuration with n-hexane experienced by far the largest increase among the selected configurations. We also investigated the effect the space correlation in the noise have on the performance of odd and even chains. As illustrated in fig.5.6, the additional coupling between the heated sites due to this correlation compensated for the difference in stiffness between these chains and the thermal conductance is decreasing with increasing length, a result that can be interpreted as the limit of simply embedding the stiff material in a very soft, long matrix.

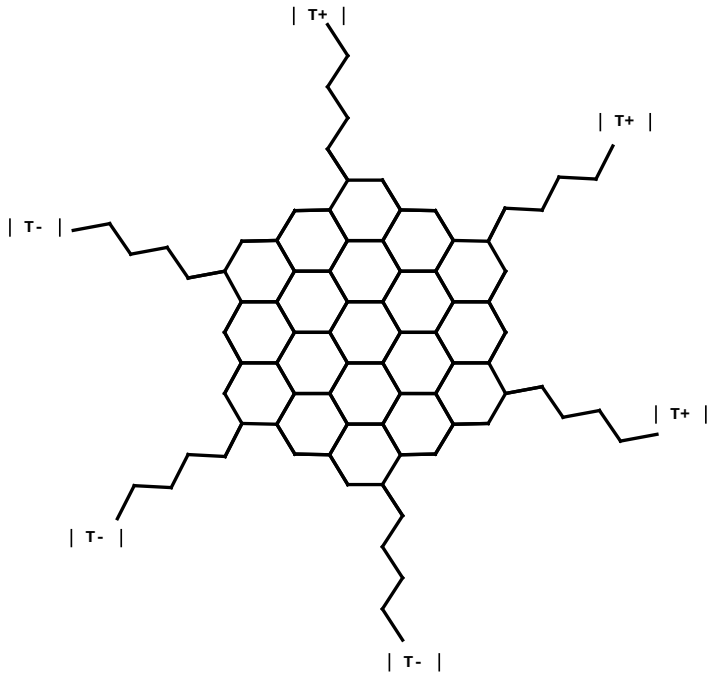


Figure 5.4: A pictorial representation of a functionalized sheet of graphene. The number of atoms in the graphene sheet is 54, The alkane chains are n-pentane. The end of the chains interact with two thermal reservoirs working at different temperatures T_+ and T_-.

5.4 Conclusion

In this chapter we investigated the effect of spatial correlation in the noise on the dynamical behavior of a system of interacting particles in contact with a heat bath. The noise which represent the effect of many degrees of freedom may have a characteristic length comparable to the distance between the system particles, as a result the noise in one site may affect the noise in other sites. It was shown that the additional correlations manifest as additional coupling and damping constants between the system particles. As an application we investigated the effect this correlation could possibly have on the heat flux throughout a linear chain and a sheet of functionalized graphene. It was shown that the additional coupling due to the noise spatial dependence improved the overall thermal conduction of heat throughout the system. In addition to the energy from the random stochastic force, some of the energy lost due to momentum exchange, is recovered because

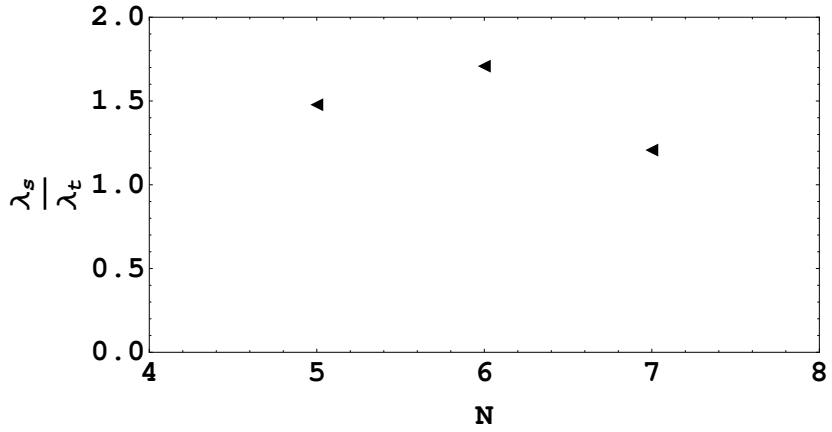


Figure 5.5: Ratio of the thermal conductance of functionalized graphene with space correlated noise λ_s and colored noise λ_t for size chains from $N = 5$ to $N = 7$. The last two sites of each chain are in contact with heat baths.

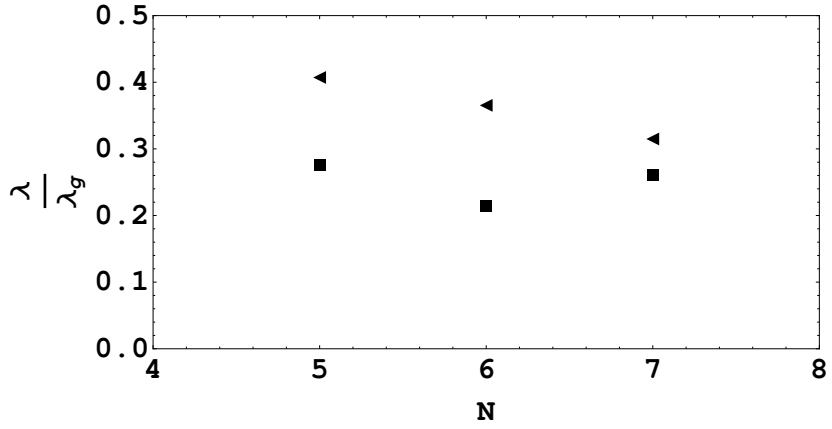


Figure 5.6: The ratio of the Thermal conductances of functionalized graphene λ and that of graphene λ_g as a function of chain length N. (solid square): heating one site, (solid triagle): heating two sites

of the additional coupling between system particles, this explains the improved thermal conduction.

We are developing simple models to be used in optimizing thermal conductivity, models that do not attempt to simulate the full dynamics of a molecules in a matrix. This method allows us to include correlation effects in the heat bath. It is not clear how much correlation we must include to best optimize real physical systems.

Chapter 6

Conclusion

Our first major result was the derivation of the generalized Langevin equations for a system interacting with heat baths in both the classical and quasi-classical approximations. We modeled the bath as an infinite ensemble of weakly interacting particles, and assumed the coupling between each particle of the system and the rest of the particles in the bath to be linear. We showed that the effect of the bath particles can be summarized into a set of drag and random stochastic forces that are related through the fluctuation-dissipation theorem.

Our second major result is the use of the system's normal modes as a tool to differentiate between the thermal efficiency of a variety of system configurations. We assumed the bath noise to be white then calculated the thermal conductance of the system and showed the close connection between the heat flux and the participation ratios of the different normal modes. We applied this technique to a graphene nanosheet functionalized with side chains of different sizes and showed that alkanes with odd number of sites perform better than those with even number of sites.

White noise assumes that the thermal fluctuations occur at a time scale that is much shorter than that of the system particles. This however is never exactly realized, and the time scales of both the system and fluctuations must be taken into account. Our third major result was the use of colored noise to analyze the heat transport throughout functionalized macromolecules in general and graphene nano-sheets as a case study. The close relation between the participation ratios of the normal modes and the thermal conduction allowed us to differentiate between several choices of functionalization and to identify the one that best conduct heat to the graphene. It was shown that stiffer but lighter

chains strongly couples to the graphene and produce higher thermal conductivities. Branching the functional groups may enhance the thermal conduction but not the coupling to the graphene.

We ignored non-linear correction up to this point and assumed the lattice interactions to be purely harmonic. We were interested in determining the major bottlenecks to thermal conductivity at the interface, and of course these are present even in the linear approximation. The question however was weather or not these Non-linear corrections alter the principles of optimization. Our fourth major result was to check the correspondence between the normal mode approach and the actual behavior of the system. To this end we simulated the average net heat flux and the temperature difference at the interface for several graphene configurations. We concluded that Non-linear corrections do alter the magnitude of the results, but not the essential principles for optimization.

Colored noise takes into account the time scales of both the system and bath, but assumes spatial independence of thermal fluctuations. Our fifth major result was to investigate the effects of spatial correlations in the noise on the dynamical behavior of a system of interacting particles in general and a nano-sheet of functionalized graphene as a case study. Because colored noises are completely uncorrelated the thermal conduction is minimal. Including spatial dependence in the noise reinforces the coupling between the system particles and enhances the overall thermal conductivity.

We obviously have not addressed all the relevant aspects pertaining to heat transport in functionalized macromolecules. We chose to develop simple models to help optimize thermal conductivity, models that do not attempt to simulate the full dynamics of a molecules in a matrix. There are many ways this approach can be expanded. For ease of application we chose to only functionalize the edges of a single graphene sheet. This can be expanded to include various forms

of functionalization including multi-wall and multi-sheet systems. Moreover, to improve our predictions we need to include more accurate spatial correlations that pertain to a given medium. Finally, with improved predictions, we can go a step further and design real molecule interfaces that improve coupling and minimize interfacial resistance.

Bibliography

[1] G. H. M. van der Heijden. A. P. Korte. *J. Phys.: Condens. Matter.*, 21(495301), 2009.

[2] S.; Bao W.; Calizo I.; Teweldebrhan D.; Miao F.; Lau C. N. Balandin, A. A.; Ghosh. *Nano Lett.*, 8(902), 2008.

[3] G.D.Harp B.Berne. *On the Calculation of Time Correlation Functions*. New York: John Wiley & Sons, Inc, 1st edition, 1970.

[4] Kwon Y.K. Tomanek D. Berber, S. Unusually high thermal conductivity of carbon nanotubes. *Phys. Rev. Lett.*, 84(4613), 2000.

[5] Llahuno M.C. Radosavljevic M. Hyun J.K. Jonson A.T. Biercuk, M.J. Carbon nanotubes composites for thermal management. *Applied physics letters.*, 80(2767-2769), 2002.

[6] K. J.; Jiang Z.; Klima M.; Fudenberg G.; Hone J.; Kim P.; Stormer H.L. Bolotin, K. I.; Sikes. *Solid State Commun.*, 146(351), 2008.

[7] T. Goddard W.A. Che, J. Cagin. Thermal conductivity of carbon nanotubes. *Nanotechnology*, 11(65), 2000.

[8] P. Zoller C.W.Gardiner. *Quantum Noise*. Springer, 3rd edition, 2004.

[9] A. Striolo. D. Konatham. Molecular design of stable graphene nanosheets dispersions. *Nano. Lett.*, 8(4630-4641), 2008.

[10] P. MAZUR. G. W. Ford, M. KAc. Statistical mechanics of assemblies of coupled oscillators. *J. Math. Phys.*, 6(4), 1964.

[11] I.; Teweldebrhan D.; Pokatilov E. P.; Nika D. L.; Balandin A. A.; Bao W.; Miao F.; Lau C. N. Ghosh, S.; Calizo. Carbon nanotubes composites for thermal management. *Appl. Phys.Lett.*, 92(151911), 2008.

[12] E. Hershkovitz. A fourth-order numerical integrator for stochastic langevin equations. *J. Chem. Phys.*, 108(22), 1998.

[13] Batlogg B. Benes Z. Johnson A.T. Fisher J.E. Home, J. Quantized phonon spectrum of single-wall carbon nanotubes. 289(1730), 2000.

[14] T.Frank. H.Risken. *The Fokker-Planck Equation: Methods of Solutions and Applications*. Springer Series in Synergetics, 1st edition, 1996.

[15] D. A. Bernard-Brunel. J. J, Potoff. Mie potentials for phase equilibria calculations. *J. Phys. Chem. B.*, 113(14725-14731), 2009.

[16] B.C.Bailey J.D.Patterson. *Solid state physics. Introduction to the theory.* Springer, 1st edition, 2007.

[17] P.L. Kapitza. *Zh. Eksp. Teor. Fiz.*, 11(1), 1941.

[18] P.L. Kapitza. *Sov. J. Phys. JETP.*, 4(121), 1941.

[19] T. J.; Baus M.; Kurz H. Lemme, M. C.; Echtermeyer. *IEEE Electron DeVice Lett.*, 28(282), 2007.

[20] X.; Zhang Li; Lee S; Dai. Li, X.; Wang. *H Science.*, 319(1229), 2008.

[21] Chung D.D.L. Lin, L. Thermally conducting polymer-matrix composites containing both ain particles and sic whiskers. *Journal of Electronic Materials.*, 23(6), 1994.

[22] J. Luczka. Non-markovian stochastic processes: Colored noise. *CHAOS.*, 15(026107), 2005.

[23] R. Zwanzig. M. Bixon. Nonlinear generalized langevin equations. *J. Stat. Phys.*, 3(3), 1971.

[24] F.; Elias D. C.; Jaszczak J. A.; Geim A. K. Morozov S. V.; Novoselov K. S.; Katsnelson, M. I.; Schedin. Unusually high thermal conductivity of carbon nanotubes. *Phys. Rev. Lett.*, 51(744), 2008.

[25] K. Yakubo K. W. Yu J. M.Zheng, M. Goda. Anomalous size dependence of inverse participation ratio of eigenfunctions in graded elastic lattices. *J. Phys. Soc. Japan.*, 77(094601), 2008.

[26] T. Pang. *An introduction to computational physics.* Cambridge University Press, 1st edition, 1997.

[27] E. Platen P.E. Kloeden. *Numerical solution of stochastic differential equations.* Springer, 1st edition, 1999.

[28] R. M. Reilly. Carbon nanotubes: Potential benefits and risks of nanotechnology in nuclear medicine. *J Nucl Med.*, 48(7 1039 - 1042), 1970.

[29] R. Khare. S. K. Nath. New forcefield parameters for branched hydrocarbons. *J. Chem. Phy.*, 115(23), 2001.

[30] W. A. Goddard III G. Caldwell R. B. Ross S. S. Jang, M. Blanco. The source of helicity in perfluorinated n-alkanes. *J. Chem. Phy.*, 36(5331-5341), 2003.

[31] Alain Joye. Stephane Attal. The langevin equation for a quantum heat bath. *Journal of Functional Analysis.*, 247(253), 2007.

[32] R.E. Steuer. *Multiple Criteria Optimization: Theory, Computations, and Application*. New York: John Wiley & Sons, Inc, 1st edition, 1986.

[33] J. Tersoff. New empirical approach for the structure and energy of covalent systems. *Phys. ReV. B.*, 37(69917000), 1988.

[34] J. Tersoff. Modeling solid-state chemistry: Interatomic potentials for multicomponent systems. *Phys. ReV. B.*, 39(55665568), 1989.

[35] M.; Ajiki H.; Sigrist M. Wakabayashi, K.; Fujita. Electronic and magnetic properties of nanographite ribbons. *Phys. ReV. B.*, 59(8271), 1999.

[36] Jian-Sheng Wang. Quantum thermal transport from classical molecular dynamics. *Phy. Rev. Lett.*, 99(160601), 2007.

[37] Y. Satake1 Y. Yokoyama1 R.Okada T. Nakayama M. Sasaki T. Kondo J. Oh J. Nakamura W.WHayes Y. Yamada1, C. Sugawara1. He/ar-atom scattering from molecular monolayers: C60/pt(111) and graphene/pt(111). *J. Phys.: Condens. Matter.*, 22(304010), 2010.

[38] Dou X. Rouhanipour A. Zhi L. Rader H. J. Mullen K. Yang, X. Two-dimensional graphene nanoribbons. *J. Am. Chem. Soc.*, 130(4216), 2008.

[39] Liem H. Yung, K.C. Enhanced thermal conductivity of boron nitride epoxy-matrix composite through multi-modal particle size mixing. *Journal of applied polymer science.*, 106(3587-3591), 207.

[40] R. Zwanzig. Nonlinear 8eneralized langevin equations. *J. Stat. Phys.*, 9(3), 1973.

Appendix A

Thermal Properties

A.1 Flux: White Noise

The goals of this section is to give a definition of the heat flux in terms of quantities we can calculate. The heat flux $\vec{j}(\vec{r},t)$ at time t in the spatial position $\vec{r}$ is nothing but the energy current, implicitly defined by the continuity equation.

$$\frac{dh(\vec{r},t)}{dt} + \nabla \cdot \vec{j} = 0 \tag{A.1}$$

Where $h(\vec{r},t)$ is the energy density.

With reference to an ensemble of interacting particles, we can write the microscopic energy density as the sum of the isolated contributions located in the instantaneous position of each particle.

$$h(\vec{r},t) = \sum_i h_i \; \delta(\vec{r} - \vec{r}_i) \tag{A.2}$$

Where $\delta(\vec{r})$ is the Dirac distribution and

$$h_i(\vec{r},t) = \frac{p_i^2}{2m_i} + \frac{1}{2}\sum_{j \neq i} V_{ij} \tag{A.3}$$

is the energy contribution of the i^{th} particle. The first term correspond to the kinetic energy. The last term amounts to half of the potential energy of the pairwise interactions with the neighboring particles to avoid double counting. In a similar way we can write the heat flux as the sum of the localized contributions.

$$\vec{j}(\vec{r},t) = \sum_i \vec{j}_i \; \delta(\vec{r} - \vec{r}_i) \tag{A.4}$$

the problem amounts therefore to give a definition of the local heat flux $j_i(\vec{r},t)$.

In the limit of small oscillations around the equilibrium position, density fluctuation can be neglected and $h_i(\vec{r},t)$ is proportional to the energy density.

The time derivative of $h_i(\vec{r},t)$ is

$$\begin{aligned}\frac{dh_i(\vec{r},t)}{dt} = -\frac{1}{2}\sum_{j\neq i}\left(\frac{\partial V_{ij}}{\partial x_i}\ \dot{x}_i + \frac{\partial V_{ij}}{\partial y_i}\ \dot{y}_i + \frac{\partial V_{ij}}{\partial z_i}\ \dot{z}_i\right) + \\ \frac{1}{2}\sum_{j\neq i}\left(\frac{\partial V_{ij}}{\partial x_j}\ \dot{x}_j + \frac{\partial V_{ij}}{\partial y_j}\ \dot{y}_j + \frac{\partial V_{ij}}{\partial z_j}\ \dot{z}_j\right)\end{aligned} \tag{A.5}$$

This equation can in turn be written as

$$\frac{dh_i}{dt} = -\sum_j \frac{j_{ij}}{a} \tag{A.6}$$

where a is the distance to the nearest neighbor. The local heat flux j_{ij} is such that

$$\begin{aligned}aj_{ij} = \frac{\partial V_{ij}}{\partial x_i}\ \dot{x}_i + \frac{\partial V_{ij}}{\partial y_i}\ \dot{y}_i + \frac{\partial V_{ij}}{\partial z_i}\ \dot{z}_i \\ -\frac{\partial V_{ij}}{\partial x_j}\ \dot{x}_j - \frac{\partial V_{ij}}{\partial y_j}\ \dot{y}_j - \frac{\partial V_{ij}}{\partial z_j}\ \dot{z}_j\end{aligned} \tag{A.7}$$

The total heat flux j is the sum of all the isolated contributions located in the instantaneous positions of each particle in the system

$$j = \sum_{ij} j_{ij} \tag{A.8}$$

A.2 Flux: Colored Noise

The heat flux through a system of interacting particles in the steady state can be computed in several equivalent ways one in fact is demonstrated in appendix.A.1. In the next analysis however we use a simpler expression that we extract from the time derivative of the system's total energy. Starting with eq.3.1 we multiply both sides by $\dot{x}_i$

$$m_i\ \ddot{x}_i\dot{x}_i = -\frac{\partial U}{\partial x_i}\dot{x}_i + \left(-\dot{x}_i\int_0^t dt' K_i(t')\dot{x}(t-t') + F_i(t)\dot{x}_i\right)\ (\delta_{i,1}+\delta_{i,N}) \quad \text{(A.9)}$$

Summing over all i's we get

$$\begin{aligned}\frac{dE}{dt} = \frac{d}{dt}\left(\frac{1}{2}\sum_i m_i\ \dot{x_i}^2 + U[x(t)]\right) &= -\sum_i \dot{x}_i(t)y_i(t)\ (\delta_{i,1}+\delta_{i,N}) \\ &\quad + \sum_i F_i(t)\dot{x}_i(t)\ (\delta_{i,1}+\delta_{i,N}) \\ &= \sum_i (F_i(t)-y_i(t))\dot{x}_i(t)\ \delta_{i,1} + \sum_i (F_i(t)-y_i(t))\dot{x}_i(t)\ \delta_{i,N}\end{aligned} \quad \text{(A.10)}$$

We identify the first term in eq.A.10 as the heat flux from the hot bath (J_h) and the second term in the same equation as the one delivered to the cold heat bath (J_c).

$$\begin{aligned}J_h &= \sum_i (F_i(t)-y_i(t))\dot{x}_i(t)\ \delta_{i,1} \\ J_c &= \sum_i (F_i(t)-y_i(t))\dot{x}_i(t)\ \delta_{i,N}\end{aligned} \quad \text{(A.11)}$$

A.3 Flux: Space/Time Correlated Noise

In this section we shall derive an expression for the heat flux for the space/time correlated noise. Starting with eq.3.1 we multiply both sides by $\dot{x}_i$

$$m_{s_i}\ \ddot{q_{s_i}}(t) = -\frac{\partial U}{\partial q_{s_i}}\dot{q}_{s_i} - \sum_j \widetilde{E}_{ij}\ q_{s_j}\ \dot{q}_{s_i} - \sum_j \widetilde{S}_{ij}\ \gamma_{ij}\ y_j\ \dot{q}_{s_i} + F_i(t)\ \dot{q}_{s_i} \quad \text{(A.12)}$$

where $\widetilde{S_{ij}} = 1$ if i and j are in contact with the same heat bath and zero if not.

Summing over all i's we get

$$\frac{dE}{dt} = \frac{d}{dt}\left(\frac{1}{2}\sum_i m_i\ \dot{q}_{s_i}^2 + U[q_s(t)]\right) = -\sum_{ij}\widetilde{E}_{ij}\ q_{s_j}\ \dot{q}_{s_i} - \sum_{ij}\widetilde{S}_{ij}\ \gamma_{ij}\ y_j\ \dot{q}_{s_i} + \sum_i F_i(t)\ \dot{q}_{s_i} \tag{A.13}$$

In average

$$< \frac{dE}{dt} >= -\sum_{ij}\frac{\widetilde{S}_{ij}\ \gamma_{ij}}{m_{s_i}}\ < y_j\ p_{s_i} > + \sum_i \frac{1}{m_{s_i}}\ < F_i(t)\ p_{s_i} > \tag{A.14}$$

We identify the sum in eq.A.14 where (ij) in contact with the hot bath as the average heat flux from the hot bath (J_h). similarly for (ij) in contact with the cold bath as the one delivered to the cold heat bath (J_c).

$$\begin{aligned} J_h &= \sum_{ij}^{hot}\frac{\widetilde{S}_{ij}\ \gamma_{ij}}{m_{s_i}}\ < y_j\ p_{s_i} > + \sum_i^{hot}\frac{1}{m_{s_i}}\ < F_i(t)\ p_{s_i} > \\ J_c &= \sum_{ij}^{cold}\frac{\widetilde{S}_{ij}\ \gamma_{ij}}{m_{s_i}}\ < y_j\ p_{s_i} > + \sum_i^{cold}\frac{1}{m_{s_i}}\ < F_i(t)\ p_{s_i} > \end{aligned} \tag{A.15}$$

In the steady state regime, the averages in the first two sum take an expression similar to. The last term however can be expanded as follow

$$< S_{s_i}(t)\ F_i(t_1) >= \sum_{kl}\widetilde{\theta}_{ik}\ \widetilde{\theta}_{kl}^{-1}\ e^{a_k\ t}\ \left(\int_0^t d\tau_1\ e^{-a_k\ \tau_1}\ < \vec{\Pi}_l(\tau_1)\ F_i(t_1) >\right) \tag{A.16}$$

Knowing that

$$< F_i(t)F_j(t') >= \widetilde{S}_{ij} k_B T \widetilde{L}_{ij}(t-t') \tag{A.17}$$

eq.A.16 simplifies in the steady state regime to

$$< S_{s_i}(t)\ F_i(t_1) >= k_B T \sum_{kl} \widetilde{\theta}_{ik}\ \widetilde{\theta}^{-1}_{kl}\ \widetilde{S}_{li}\ \left(\frac{\gamma_{li}}{1-\tau\ a_k}\right) \tag{A.18}$$

A.4 Heat Capacity

The heat capacity of the macromolecule can be calculated from the steady state average total energy of the system. We assume that the heat baths are identical and at the same temperature (T).

$$\begin{aligned}
C_v &= \frac{\partial < E >}{\partial T} = \lim_{t\to\infty} \frac{\partial < E(t) >}{\partial T} \\
&= \lim_{t\to\infty} \frac{\partial}{\partial T}\left(< \sum_i \frac{p_i^2(t)}{2m_i} + \frac{1}{2}\sum_{ij} K_{ij} x_i(t) x_j(t) > \right) \\
&= \lim_{t\to\infty} \sum_i \frac{1}{2m_i}\frac{\partial}{\partial T}(< p_i(t)p_i(t) >) + \lim_{t\to\infty}\frac{1}{2}\sum_{ij} K_{ij}\frac{\partial}{\partial T}(< x_i(t)x_j(t) >) \\
&= \lim_{t\to\infty} \sum_{i=N+1}^{2N} \frac{1}{2m_i}\frac{\partial}{\partial T}(< S_i(t)S_i(t) >) + \lim_{t\to\infty}\frac{1}{2}\sum_{ij=1}^{N} K_{ij}\frac{\partial}{\partial T}(< S_i(t)S_j(t) >)
\end{aligned} \tag{A.19}$$

The terms inside the sums are temperature dependent, consequently the calculated specific heat will depend on temperature.

Appendix B

Force Field

B.1 The Tersoff-Brenner potential

The Tersoff-brenner (TB)[33, 34] potential was employed to describe the interactions among the atoms in the graphene sheet. In the TB force field, the potential energy is modeled as a sum of pair like interactions, where the coefficient of the attractive term in the pair like potential depends on the local environment, yielding an effective many-body potential.

The interatomic potential is taken to have the form

$$E = \sum_i E_i = \frac{1}{2} \sum_{i \neq j} Vij$$
$$V_{ij} = f_c(r_{ij}) \; [f_R(r_{ij}) + b_{ij} \; f_A(r_{ij})] \tag{B.1}$$

here E is the total energy of the system, which is decomposed into a site energy E_i and a bond energy V_{ij}. The indices i and j run over the atoms of the system, and r_{ij} is the distance from atom i to atom j.

The function f_R represent a repulsive pair potential which includes the orthogonalization energy when atomic wave functions overlap, and f_A represents an attractive pair potential associated with bonding. The extra term f_c is merely a smooth cutoff function, to limit the range of the potential, since for many applications like the one we are running short ranged functions permit a tremendous reduction in computational effort.

The function b_{ij} represents a measure of the bond order. All these functions

are taken to be of the following form:

$$
\begin{aligned}
f_R(r_{ij}) &= A\ \exp(-\lambda\ r_{ij}) \\
f_A(r_{ij}) &= B\ \exp(-\mu\ r_{ij}) \\
b_{ij} &= (1+\beta^n\ \zeta_{ij}^n)^{-1/2n} \\
\zeta_{ij} &= \sum_{k\neq i,j} f_c(r_{ij})\ g(\theta_{ijk})\ \exp[\lambda_3^3\ (r_{ij}-r_{ik})^3] \\
g(\theta) &= 1+\frac{c^2}{d^2}-\frac{c^2}{[d^2+(h-\cos(\theta))^2]}
\end{aligned}
\tag{B.2}
$$

where θ_{ijk} is the bond angle between bond ij and ik. The cutoff function is taken to be a step down function so to include only the first and next nearest neighbors to each site.

Parameters and more details necessary to implement the TB force field are listed in Table B.1

B.2 The NERD potential

A united atom representation of the alkanes is adopted throughout this work. The alkanes considered were n-pentane, n-heptane, and n-nonane. Within the united atom description, an n-alkane molecule is described as a flexible linear chain of methylene (CH_2) pseudo atoms terminating at both ends with methyl (CH_3) pseudo atoms. The parameters were taken from the NERD force field [15**?** , 29]. In this simulation we ignore the potential due to interactions between sites, which are separated by more than three bonds as well as interactions between sites that belong to different molecules. A complete listing of all of the intermolecular potential parameters for saturated alkanes in the NERD force field is given in

Table B.1: TB parameters for Carbon

A(eV)	1.3936×10^3
B(eV)	3.467×10^2
$\lambda(\mathring{A}^{-1})$	3.4879
$\mu(\mathring{A}^{-1})$	2.2119
β	1.5724×10^{-7}
n	7.2751×10^{-1}
c	3.8049×10^4
d	4.384×10^0
h	-5.7058×10^{-1}
$R(\mathring{A})$	1.95
$S(\mathring{A})$	0.15

Table.B.2.

The potential in the branched alkane chains is divided between bond stretching potential U_r, bond bending potential U_θ and a torsional potential U_ϕ where

$$U_r = \frac{1}{2}\ k_r\ (r - r_o)^2$$
$$U_\theta = \frac{1}{2}\ k_\theta\ (\theta - \theta_o)^2 \tag{B.3}$$

and r_o and θ_o denote the equilibrium bond length and bond angle, respectively.

$$U_\phi = V_o + V_1\ (1 + \cos(\phi)) + V_2\ (1 - \cos(2\ \phi)) + V_3\ (1 + \cos(3\ \phi)) \tag{B.4}$$

Table B.2: Intramolecular potential energy parameters

Bond stretching potential:

	$b_{eq}(\mathring{A})$	k_r/k_B $(K/\mathring{A}^2)$
$CH_x - CH_y$	1.54	96500

Bond bending potential:

	$\theta_0(^o)$	k_θ/k_B (K)
$CH_x - (CH_2) - CH_y$	114.0	62500
$CH_x - (CH) - CH_y$	109.47	62500
$CH_x - (C) - CH_y$	109.47	62500

Torsional potential:

(K)	V_o/k_B	V_1/k_B	V_2/k_B	V_3/k_B
$CH_x - CH_2 - CH_2 - CH_y$	0	355.04	-68.19	791.32
$CH_x - CH_2 - CH - CH_y$	1416.3	398.3	139.12	-901.2
$CH_x - CH - CH - CH_y$	0	0	0	1635.7
$CH_x - CH_z - C - CH_y$	0	0	0	1635.7

B.3 Force Field for perfluoralkanes molecules

A united atom representation of the perfluoralkanes is adopted throughout this work. Within the united atom description, an n-perfluoralkanes molecule is described as a flexible linear chain of (CF_2) pseudo atoms terminating at both ends with (CF_3) pseudo atoms. The parameters were taken from Dreiding force field [15**?**]. In this simulation we ignore the potential due to interactions between sites, which are separated by more than three bonds as well as interactions between sites that belong to different molecules. A complete listing of all of the intermolecular potential parameters for saturated perfluoralkanes in is given in Table. B.3.

The potential in the branched alkane chains is divided between bond stretching potential U_r, bond bending potential U_θ and a torsional potential U_ϕ where

$$U_r = \frac{1}{2}\ k_r\ (r - r_o)^2$$
$$U_\theta = \frac{1}{2}\ k_\theta\ (\theta - \theta_o)^2 \tag{B.5}$$

and r_o and θ_o denote the equilibrium bond length and bond angle, respectively.

$$U_\phi = V_o + V_1\ (1 + \cos(\phi)) + V_2\ (1 - \cos(2\ \phi)) + V_3\ (1 + \cos(3\ \phi)) + V_4\ (1 - \cos(4\ \phi)) \tag{B.6}$$

Table B.3: Intramolecular potential energy parameters

Bond stretching potential:

	$b_{eq}(\mathring{A})$	$k_r/k_B\ (K/\mathring{A}^2)$
$CF_x - CF_y$	1.54	96500

Bond bending potential:

	$\theta_0(^o)$	k_θ/k_B (K)
$CF_x - (CF_2) - CF_y$	114.0	62500

Torsional potential:

(K)	V_o/k_B	V_1/k_B	V_2/k_B	V_3/k_B	V_4/k_B
$CF_x - CF_2 - CF_2 - CF_x$	0	1666.25	247.60	-349.26	-532.94

Appendix C

Estimating the noise parameters

The eligibility of our normal mode analysis and the use of Langevin dynamics to estimate the thermal conduction and by that identifying the graphene configuration that best optimize the heat transport, rests on the evaluation of the noise parameters that best describe the type of heat bath. There is however, a simple method to identifying these parameters. In this section we outline the major steps of this technique.

Start with one of the molecules of the chain isolated from the rest of the chain, but held by a harmonic potential of spring constant k strong enough to hold the molecule in place while surrounded by the molecules of the medium. We assume the hot and cold bath to be identical but at different temperatures. We start with the particle at a temperature ΔT above the heat bath temperature. The heat will then expand from the particle to the rest of the molecules in the heat bath. In the langevin dynamics, the trajectory of the particle obeys the equation of motion:

$$m_i\,\ddot{x}(t) = -k\,x(t) - \int_0^t dt' K(t-t')\,\dot{x}(t') + F(t) = -\int_0^t dt'\,(K(t-t')+k)\;\dot{x}(t') + F(t) \tag{C.1}$$

where m, x,respectively are the mass and displacement of the particle, $F(t)$ is the Langevin force on the particle, the overhead dot refers to time derivative.

In the classical limit, the noise term $(F(t))$ is related to the memory kernel by the fluctuation-dissipation theorem

$$< F(t)F(t') >= k_B T K(t-t') \tag{C.2}$$

By multiplying both sides of the previous equation by $p^T(0)$, and taking an ensemble average, the previous equation reduces to

$$\frac{\partial C(t)}{\partial t} = -\int_0^t dt' \frac{K(t-t')+k}{m}\, C(t') \tag{C.3}$$

where $C(t) =< p(t)p^T(0) >$, the momentum autocorrelation function.

The idea is to use data from molecular dynamics (MD) simulations to calculate $C(t)$, then solve the previous equation for $K(t)$. As a matter of fact the integral equation eq.C.3 is known in the literature as Volterra Integral Equations of the Second Kind and can be solved for the memory kernel $K(t)$[3].